EPA-650/2-74-119-b

ENTRAINMENT SEPARATORS FOR SCRUBBERS - FINAL REPORT

by

Seymour Calvert, Shuichow Yung, and James Leung

A.P.T., Inc.
4901 Morena Boulevard
Suite 402
San Diego, California 92117

Contract No. 68-02-0637
ROAP No. 21ACX-086
Program Element No. 1AB013

EPA Project Officer: L. E. Sparks

Industrial Environmental Research Laboratory
Office of Energy, Minerals, and Industry
Research Triangle Park, North Carolina 27711

Prepared for

U.S. ENVIRONMENTAL PROTECTION AGENCY
Office of Research and Development
Washington, D.C. 20460

August 1975

EPA REVIEW NOTICE

This report has been reviewed by the National Environmental Research Center - Research Triangle Park, Office of Research and Development, EPA, and approved for publication. Approval does not signify that the contents necessarily reflect the views and policies of the Environmental Protection Agency, nor does mention of trade names or commercial products constitute endorsement or recommendation for use.

RESEARCH REPORTING SERIES

Research reports of the Office of Research and Development, U.S. Environmental Protection Agency, have been grouped into series. These broad categories were established to facilitate further development and application of environmental technology. Elimination of traditional grouping was consciously planned to foster technology transfer and maximum interface in related fields. These series are:

1. ENVIRONMENTAL HEALTH EFFECTS RESEARCH
2. ENVIRONMENTAL PROTECTION TECHNOLOGY
3. ECOLOGICAL RESEARCH
4. ENVIRONMENTAL MONITORING
5. SOCIOECONOMIC ENVIRONMENTAL STUDIES
6. SCIENTIFIC AND TECHNICAL ASSESSMENT REPORTS
9. MISCELLANEOUS

This report has been assigned to the ENVIRONMENTAL PROTECTION TECHNOLOGY series. This series describes research performed to develop and demonstrate instrumentation, equipment and methodology to repair or prevent environmental degradation from point and non-point sources of pollution. This work provides the new or improved technology required for the control and treatment of pollution sources to meet environmental quality standards.

This document is available to the public for sale through the National Technical Information Service, Springfield, Virginia 22161.

Publication No. EPA-650/2-74-119-b

TECHNICAL REPORT DATA *(Please read Instructions on the reverse before completing)*		
1. REPORT NO. EPA-650/2-74-119-b	2.	3. RECIPIENT'S ACCESSION NO.
4. TITLE AND SUBTITLE Entrainment Separators for Scrubbers-- Final Report		5. REPORT DATE August 1975 6. PERFORMING ORGANIZATION CODE
7. AUTHOR(S) Seymour Calvert, Shuichow Yung, and James Leung		8. PERFORMING ORGANIZATION REPORT NO.
9. PERFORMING ORGANIZATION NAME AND ADDRESS A.P.T., Inc. 4901 Morena Blvd., Suite 402 San Diego, CA 92117		10. PROGRAM ELEMENT NO. 1AB013; ROAP 21ACX-086 11. CONTRACT/GRANT NO. 68-02-0637
12. SPONSORING AGENCY NAME AND ADDRESS EPA, Office of Research and Development Industrial Environmental Research Laboratory Research Triangle Park, NC 27711		13. TYPE OF REPORT AND PERIOD COVERED Final: 10/73 - 6/75 14. SPONSORING AGENCY CODE
15. SUPPLEMENTARY NOTES		

16. ABSTRACT The report gives results of an analytical and experimental study of the use of entrainment separation to remove the liquid mist carried out of a scrubber by the effluent gas. It includes an evaluation of current technology, results of experimental studies of entrainment separator characteristics, and theoretical analyses. Zigzag baffle, knitted mesh, tube bank, packed bed, and cyclone devices were tested. Collection efficiency and reentrainment were measured and related to drop size and separator geometry. Pressure drop as a function of gas flow rate is also reported. The effects of suspended solids on collection efficiency and the nature and extent of solids deposition were also investigated. An auxiliary experiment was employed to help determine solid deposition mechanisms. Mathematical models are given for predicting primary collection efficiency and pressure drop.

17. KEY WORDS AND DOCUMENT ANALYSIS		
a. DESCRIPTORS	b. IDENTIFIERS/OPEN ENDED TERMS	c. COSATI Field/Group
Air Pollution	Air Pollution Control	13B
Scrubbers	Stationary Sources	07A
Entrainment	Entrainment Separators	07D
Efficiency	Collection Efficiency	14A
Mathematical Models	Liquid Mist	12A
Exhaust Gases	Suspended Solids	21B
18. DISTRIBUTION STATEMENT Unlimited	19. SECURITY CLASS (This Report) Unclassified	21. NO. OF PAGES 219
	20. SECURITY CLASS (This page) Unclassified	22. PRICE 7.75

EPA Form 2220-1 (9-73)

ACKNOWLEDGEMENT

A.P.T., Inc. wishes to express its appreciation for excellent technical coordination and for very helpful assistance in support of our technical effort to Dr. Leslie Sparks, E.P.A. Project Officer.

TABLE OF CONTENTS Page

LIST OF FIGURES

LIST OF TABLES

NOMENCLATURE

Latin

A = cyclone inlet area, cm^2

A_p = total projected area of baffles per row in the direction of inlet air flow, cm^2

A_t = duct cross-sectional area, cm^2

a = cyclone inlet duct height, cm

= acceleration due to centrifugal force, cm/sec^2

a' = cross-sectional area of all the tubes in one row, cm^2

a_2 = specific area of mesh; surface area of wires per unit volume of mesh pad, cm^2/cm^3

a_3 = constant

a_7 = constant

b = distance between baffles normal to gas flow, cm

= cyclone inlet duct width, cm

= jet orifice width, cm

= channel width, cm

C_D = drag coefficient

C' = Cunningham slip factor

c_1 = constant defined by equation (4-1)

c_2 = constant defined by equation (4-1)

d_o = duct width or channel width, cm

d_c = cyclone diameter, cm

= collector diameter, cm

= packing diameter, cm

d_d = drop diameter, cm

d_e = exit pipe diameter of the cyclone, cm

d_{eq} = equivalent (hydraulic) diameter of liquid film, cm

d_h = hole diameter,cm

d_l = drop attachment length

d_{mm} = mass median drop diameter, cm

d_{pg} = inlet mass median drop diameter, cm

d_s = Sauter mean diameter, cm

E = primary collection efficiency, fraction

F = centrifugal force, dyne

= packing factor, cm^2/cm^3

F_l = foam density

F_w = column wall curvature correction factor

f = friction factor

f_D = drag coefficient

f_h = fraction of the perforated open area in the plate

f_G = friction factor in the absence of liquid phase

f_i = interfacial friction factor

G = mass flow rate of gas, Kg/m^2-sec

g = acceleration of gravity, cm/sec^2

H_d = fractional liquid hold-up in the bed

h_{dp} = dry plate head loss

h_{ow} = head over weir

h_r = residual pressure drop

h_s = height of vertical cylinder of cyclone, cm

h_w = weir height, cm

j = ratio of channel width to packing diameter

L = mass flow rate of liquid, Kg/m^2-sec

= natural length of the cyclone

L/A = superficial liquid velocity, cm/min

ℓ = length of baffle, cm

= distance between orifice and impingement plane

= length of settler

ℓ_2 = length of mesh pad in the direction of flow, cm

m = mass of drop, g

N = number of stages in the tube bank

$N_{Re,D}$ = drop Reynolds number
$N_{Re,G}$ = gas Reynolds number
$N_{Re,L}$ = liquid Reynolds number
n = number of rows of baffles or tubes
= vortex exponent
n_i = number of semicircular bends
n_j = collection efficiency for a given particle diameter in one stage of rectangular jet impingement
P = pressure, dyne/cm^2
Pt = fractional penetration
Δp = pressure drop, cm W.C.
Δp_{dry} = pressure drop in absence of liquid, cm W.C.
Δp_L = pressure drop due to presence of liquid, cm W.C.
Q_G = volumetric flow rate of gas, m^3/sec
Q_L = volumetric flow rate of liquid, m^3/sec
R = universal gas constant
= radius at the water line along the particle surface made by remaining water
= radius of the circle, cm
R_s = solid deposition rate, mg/cm^2-sec
r = distance from vertical axis of the cyclone
r' = radius of curvature between the particle surface
r_c = collection wall radius, cm
r_p = drop radius, cm
S = height of exit pipe inside cyclone, cm
T = absolute temperature, °K
t = mean residence time, sec
= drop travelling time, sec
U_f = flooding gas velocity, m/sec
u_G = superficial gas velocity, based on empty duct, cm/sec

u_{Gb} = gas velocity through channel, cm/sec
u'_G = actual gas velocity, cm/sec
u_t = drop terminal velocity, cm/sec
u_{tc} = drop terminal centrifugal velocity, cm/sec
u_{tg} = tangential velocity, cm/sec
v_{ave} = geometric average of the gas velocity at the cyclone inlet and outlet, cm/sec
Ve = effective volume of the cyclone, m^3
v_h = velocity of gas through hole, cm/sec
V_1 = annular shaped volume above exit duct inlet to mid-level of entrance duct, m^3
V_2 = volume of cyclone below exit duct inlet to the natural length of the cyclone, m^3
W = weight fraction of solid in slurry
w = baffle width, cm
w_1 = weir length, m
Z = bed length, cm

Greek

α = angle made between suspension surface and contact angle of the medium against the particle
β = parameter defined by equation 7-1
δ = liquid film thickness, cm
ψ = mole of entrained liquid per mole of gross downflowing liquid
= ratio of water density to entrained liquid density
ρ_d = drop density, g/cm^3
ρ_G = gas density, g/cm^3
ρ_L = liquid density, g/cm^3
ρ_{water} = density of water, g/cm^3
σ = liquid surface tension, dyne/cm
σ_g = geometric standard deviation

η = collection efficiency, fraction

μ_G = gas viscosity, poise

μ_L = liquid viscosity, poise

τ_i = interfacial shear stress, g/cm-sec^2

ε = porosity

ν_L = kinematic viscosity of liquid, cm^2/sec

θ = angle of inclination of the baffle to the flow path, degree

ϕ = slurry flux, mg/cm^2-sec

Subscripts

a = air

i = interfacial

G = gas

L = liquid

p = drop

w = water

ABSTRACT

Entrainment separation, which is used to remove the liquid mist carried out of a scrubber by the effluent gas, has been studied in the analytical and experimental program described in this report. Included in the report are an evaluation of current technology, the results of experimental studies of entrainment separator characteristics, and theoretical analyses.

Zigzag baffle, knitted mesh, tube bank, packed bed, and cyclone devices were tested. Collection efficiency and reentrainment were measured and related to drop size and separator geometry. Pressure drop as a function of gas flow rate, the effects of suspended solids on collection efficiency, and the nature and extent of solids deposition were also investigated. An auxiliary experiment was employed to help determine solid deposition mechanisms. Mathematical models for predicting primary collection efficiency and pressure drop were developed.

CHAPTER 1
INTRODUCTION

A scrubber is designed to promote good contact between the gas and liquid and a frequent consequence is that small drops of liquid are formed and carried out with the gas. To make matters worse, it is also common to find that the gas flow rate is increased as much as possible in order to attain more capacity with a given piece of equipment. This will cause both a higher rate of drop formation and a greater tendency for drops to be swept out with the gas.

The liquid entrainment or mist, as it is commonly referred to, will generally contain both suspended and dissolved solids. The suspended solids can be due to the particles collected by the scrubber, substances introduced into the scrubbing liquid, or products of chemical reaction occurring within the scrubber. Dissolved solids may similarly come from the impurities in the gas, reagents introduced into the scrubber liquid, or products of reaction.

Entrainment carryover can cause a variety of problems both within the air pollution control system and in the ambient atmosphere after the effluent has been emitted. Drops can collect on the fan blades where they may either dry out or deposit solids causing vibration and consequent failure of the fan blades, housing, or supporting structure. The entrainment also can cause corrosion or erosion of the fan blades or housing. Liquid or residual solid entrainment can also be deposited in the ductwork and smoke stack, causing eventual plugging and

possible corrosion, depending on the chemical nature of the system and the materials of construction. In cases where the scrubber effluent is reheated, entrainment can collect on the heat exchange surfaces of the reheater where it can cause eventual plugging and/or corrosion. Plugging will cause an increase in resistance to gas flow and therefore an increase in pressure drop through the system. This will in turn cause increased power consumption and possible overloading of the fan motor. Entrainment which finally emerges from the stack can cause problems in the area immediately surrounding the point of emission due to "rain-out" of liquid drops. In cases where a reheater has been used, the emission will include the solid residues of the dried out entrainment drops and in some cases the quantity of material can even exceed the quantity of particulate matter which entered the scrubber. The composition of the particulate matter can be quite different than that of the particulate which entered the scrubber, especially where reactive solutions or slurries are used for gas scrubbing. Thus, a bizarre consequence of excessive entrainment from a scrubber system can be that more pollutant is emitted either in total or within a certain size range than entered the scrubber.

In many cases the occurrence of excessive entrainment will impose a limitation upon the capacity of the scrubber. That is, while the scrubber itself might be capable of handling a larger gas flow rate, the generation of entrainment would be considered excessive at some point and this criterion will dictate a maximum gas flow rate which could be handled with a given piece of equipment.

All scrubber systems include an entrainment separator, either as an integral part of the scrubber configuration or as a separate, clearly identifiable device. Some entrainment separation will occur by gravitational settling or due to centrifugal forces caused by a change in gas flow direction within the exit region of the scrubber. For example, plate type scrubbers are routinely designed with a definite amount of clear space for disengaging entrainment above the top plate. Scrubber geometry may or may not be such that the entrainment, once it has been removed from the gas, is permitted to drain back into the scrubber rather than being swept along the walls of the scrubber into the outlet gas.

There are a number of devices which are commonly used as entrainment separators (or mist eliminators) which are added either within the scrubber body or in another vessel. Zigzag baffles, knitted mesh, packed beds, cyclone separators, and guide vanes causing rotation of the gas stream are frequently used for this purpose. While entrainment separators have been used for many years, their major application had been in relatively clean systems, such as chemical processing equipment. Consequently, the performance of the entrainment separators was not too critical and the duty not very severe. Where entrainment separators were used in air pollution control systems, there was often a lack of awareness of the importance of the entrainment separator unless the problems encountered were especially severe or the air pollution control requirements were unusually restrictive.

The situation at the time that the research program being reported here was initiated could be characterized as one in which increasing demands on air pollution control

systems had forced the recognition of many of the shortcomings and problems associated with existing entrainment separators. For one thing, the collection efficiency of the entrainment separator for the incoming entrainment was limited and very likely unknown. The nature of the entrainment,in terms of drop size, was also unknown for most situations. Once the drops are captured, there is the problem of removing them from the entrainment separator without their being reentrained. This liquid handling capacity was another cause of a limitation in the capacity of the entrainment separator. Where solids were present, the entrainment separators were susceptible to plugging, caused by solids deposition and this in turn would cause increased pressure drop and possible corrosion of the materials.

In general, the characteristics of the entrainment separators were not known well enough to permit good designs and specifications to be made. Consequently, the entrainment separator might be sized either too large or too small and its cost might be too high or not realistically high enough. The materials of construction could be inappropriate for coping with the corrosive effects of moist deposited solids. Maintenance might not be convenient or even possible. And in many cases, the type of entrainment separator might be totally inappropriate, causing a higher pressure drop than would actually be required to perform the necessary function.

The program which is reported here was undertaken in order to develop better information on the characteristics of existing entrainment separators and to point the way to the development of improved entrainment separators. The objectives and scope of the research are presented in the following section.

SCOPE OF WORK

The scope of work carried out in this program included the following:

Evaluate Technology

The status of present technology relating to wet scrubber entrainment separators was evaluated and included:

1. Review and assessment of the published literature and available unpublished information, including, where appropriate, information acquired through private communication with manufacturers, designers and users of entrainment separators.
2. Determination of the availability and adequacy of operational and design data for entrainment separators.
3. Determination and evaluation of the adequacy of existing theoretical models and design methods for predicting the performance of entrainment separators.
4. Review and evaluation of the performance of all major types of entrainment separators currently available. Assessment of advantages, disadvantages and limitations for each type of equipment.
5. Identification of specific operating and maintenance problems associated with entrainment separators. Particular attention was paid to the problems encountered in SO_2 scrubbing systems under development in E.P.A. programs.

Experimental Study

An experimental study of gas-water systems was aimed at simulating the performance of various types of entrainment separators in the presence of soluble and insoluble particulate matter. The experimental study investigated such variables as efficiency, pressure drop, reentrainment velocity, plugging and related problems.

Selection and Design

Improved engineering equations and methods were developed for entrainment separator selection and design.

Recommendations

Specific research and development recommendations for improving wet scrubber entrainment separators were developed.

GUIDE TO REPORT

The primary objective of this study is to review and evaluate the performance of all major types of entrainment separators currently available and to identify specific operating and maintenance problems associated with entrainment separators. This report is written in the hope that it will be helpful to the process engineer in the selection and design of entrainment separators for scrubbers.

Chapter 3 gives an overall view of all the entrainment separators available. The mechanisms of drop collection and drop formation are defined, and the performance of each entrainment separator, as regards to inlet drop size, primary collection efficiency, reentrainment, and pressure drop are compared. The last part of Chapter 3 also gives an account of the operational problems frequently encountered in entrainment separators.

Chapters 5 through 9 give an account of the design equations in predicting primary collection efficiency, pressure drop and reentrainment of the five common types of entrainment separators, namely, wire mesh, packed bed, tube bank, cyclone and zigzag baffles. The experimental results are compared to the mathematical models for each type of entrainment separator tested.

Chapter 10 studies the effect of solids in entrained drops on the performance of cyclone and zigzag baffles.

In Chapter 11, the problems dealing with solids deposition on an entrainment separator are investigated. The mechanisms of solids deposition are defined and an equation to predict the deposition trend on a baffle surface is developed.

Chapter 12 summarizes the design methods and information developed and identified in this study. It is intended to guide the engineer in the design or selection of an entrainment separator.

Chapter 13 defines the areas in which future research and development are needed.

Page Intentionally Blank

CHAPTER 2

SUMMARY AND CONCLUSIONS

This program involves the experimental and theoretical investigation of wet scrubber entrainment separation.

The objectives of this study are to (1) Evaluate present technology, (2) Conduct an experimental study of air-water systems aimed at simulating the performance of various types of entrainment separators, (3) Develop improved engineering equations and methods for entrainment separator selection, (4) Develop and evaluate on a small pilot basis new entrainment separator design, and (5) Develop specific research and development recommendations.

EVALUATE PRESENT TECHNOLOGY

A literature search was carried out to evaluate the technology on wet scrubber entrainment separators. Manufacturers of entrainment separators were contacted by mail and asked for information. Visits were made to E.P.A. and T.V.A. facilities to identify the specific operating and maintenance problems associated with entrainment separators.

The study indicates that presently available entrainment separators suffer from various shortcomings. Examples are: overdesign, which necessitates large equipment size; low operating velocities due to flooding or reentrainment; unpredictable performance due to lack of reliable industrial operating data; and plugging by solids.

The existing theoretical and empirical models which predict the performance of the entrainment separators were evaluated. The criteria for this evaluation were soundness of derivation and closeness of comparison with actual performance.

EXPERIMENTAL STUDY

A pilot plant to study wet scrubber entrainment separators was built. It has a gas flow capacity of 85 m^3/min (3,000 CFM) and it consists of prefilter, blower, heater, spray section, observation sections, test section, various supply and catch tanks, and auxiliary equipment. Five types of entrainment separators, namely, mesh, tube bank, packed bed, cyclone, and baffles were studied. The experiments were done with air and water, with and without suspended solids in the water. Observations included collection efficiency, pressure drop, reentrainment, flooding, drainage, drop size distribution, solid deposition, and other variables.

SELECTION AND DESIGN

Mathematical models for determining the following were developed in the present study:

1. Primary collection efficiency in zigzag baffle type entrainment separators.
2. Pressure drop in zigzag baffle type separators.
3. Primary collection based on either complete turbulent mixing or no mixing.
4. Reentrainment in vertical zigzag baffles.
5. Reentrainment in horizontal zigzag baffles.
6. Reentrainment in a cyclone.
7. Solid deposition in zigzag baffle.

CONCLUSIONS

The principal objectives of this study were achieved. The following conclusions can be drawn, based on evaluation of experimental results.

Primary Collection Efficiency

1. At low gas velocities (under industrially used conditions), primary collection efficiency of

knitted mesh, packed bed, tube bank, and cyclone can be predicted reasonably well by means of mathematical models presented in the literature.

2. Theoretical models were developed in the present study for zigzag baffles. One model, based on turbulent mixing, reaches 100% efficiency as an assymtote with increasing gas velocity. On the other hand the model, based on no mixing, reaches 100% efficiency as a straight line on efficiency versus gas velocity curve. The assumption of turbulent mixing gives better agreement with actual performance of entrainment separators.
3. The primary collection efficiency can be quickly predicted by means of a graphical correlation of cut diameter with pressure drop for some typical zigzag baffles, packed bed, tube bank, and knitted mesh. The same correlation can be used for other separator types.
4. The efficiency is not affected by the presence of solids in the entrainment as long as the solids deposited do not change the separator geometry significantly.
5. The orientation of separator mounting method has no effect on primary collection efficiency despite its effect on the liquid drainage capability and onset of reentrainment.

Capacity

The capacity of an entrainment separator is limited by reentrainment which is a function of gas velocity, entrainment flow rate, and drainage. Thus, capacity can be defined in terms of these variables.

1. Maximum gas velocity and liquid flow for negligible

reentrainment has been determined experimentally for knitted mesh tube, packed bed, and zigzag baffles. A correlation given by Chien and Ibele is recommended for determining the onset of reentrainment in a cyclone.

2. Liquid drainage capability of an entrainment separator has great effect on reentrainment velocity. Cross flow configuration with horizontal gas flow has the highest drainage capability and thus the highest reentrainment velocity.
3. Relationships between quantity of reentrainment and flow rates of gas and liquid have been experimentally determined for all five types of separators used in this program.

Nature of Reentrainment

1. At high gas velocities, reentrainment is a definite problem. Reentrainment may take place by various mechanisms such as: a) Transition from separated flow to separated-entrained flow, b) Rupture of bubbles, c) Creeping of liquid on the entrainment separator surface, and d) Shattering of liquid drops resulting from splashing.
2. Transition from separated flow to separated-entrained flow depends upon gas velocity, liquid Reynolds number and liquid properties. The transition does not depend upon the duct dimensions. The drop size distribution is independent of the duct dimensions. The average drop diameter resulting from this transition is about 250 μm. The reentrainment velocity is considerably reduced if jets of air stream strike the liquid film at an angle. Therefore, sharp angles should be reduced to avoid reentrainment.

3. The mechanism of reentrainment is zigzag baffles is tearing of the liquid sheets caused by high gas velocities and shattering of liquid drops. Reentrainment in cross flow baffles with horizontal gas flow should be less than in baffles with vertical gas flow. Zigzag baffles inclined at 30° from gas flow direction should have less reentrainment than baffles inclined at 45° from horizontal gas flow direction.
4. The reentrainment mechanisms in packed bed and mesh pad are shattering of drops and rupture of bubbles. Reentrainment resulting from small drops (less than 40 μm) due to rupture of bubbles is insignificant.
5. The mass median drop diameter due to reentrainment was determined to vary between 80 μm and 750 μm. Large drops (above 200 μm) are present due to shattering of drops.
6. Sampling of liquid drops and entrainment needs careful consideration. Due to large drop size in the reentrainment, a sedimentation effect is present.

Pressure Drop

1. Zigzag baffles- The pressure drop in zigzag baffles can be determined from drag coefficients for inclined plates held in the flow. The effect of liquid load on pressure drop is small. Wet pressure drop for vertical gas flow can also be predicted from generalized pressure drop correlation for packed beds.
2. Tube bank - Pressure drop is predictable by means of correlations available from the published literature relating to heat exchanger tube bundles.
3. Packed bed - Generalized pressure drop correlation predicts a higher pressure drop across the bed

than that measured in this study.

4. Cyclone - The experimental data can be correlated by an equation which has the same form as that given by Shepherd and Lapple. The only difference between these two equations is that the constant in the equation of present study is 2.7 times smaller than that in Shepherd and Lapple's equation.
5. Mesh - Pressure drop depends on liquid velocity and gas velocity. It varies according to $u_G^{1.65}$.
6. The orientation of the separator has little effect on pressure drop and except for knitted mesh, the presence of liquid entrainment only increases the pressure drop slightly.

Solid Deposition

Based on the results of solids deposition experiments, it appears that:

1. The solids deposition rate depends largely on drop size and entrainment flow rate. Small drops cause a higher deposition rate than large drops. Increasing the liquid flow rate will increase the liquid film thickness and thus increase the scouring action of the liquid collected on the surface.
2. Deposition rate is higher on an inclined surface due to increased settling rate of the suspended solids.
3. The empirical correlation on solid deposition rate, derived from small scale experiments, agrees fairly well with observations made on baffles.

Future Research

Entrainment separator design or specifications by means of rational methods is possible to a useful degree.

Several important areas require further study before the state of knowledge will be adequate for the reasonably through and accurate design of an entrainment separator. Some of these are:

1. Reentrainment mechanism and loading for separators under various operating conditions.
2. Entrainment loading and drop size distribution from various scrubbers under different operating conditions.
3. Solid depositions and factors affect the deposition rate.
4. Effective separator washing method and flow rate of washing liquid.

Page Intentionally Blank

CHAPTER 3

BASIC CONCEPTS

Liquid entrainment can be defined as the carrying over of liquid particles by a carrier gas or vapor which moves at too high a velocity to permit the quick settling out of the droplets by gravity. Liquid entrainment can result in serious loss of liquid or contamination of the atmosphere. For this reason, entrained drops of liquid must be separated from the gas. Thus, entrainment separators are frequently employed to separate the liquid from gas.

The design and operation of most entrainment separators are governed by three factors:

1. Pressure drop
2. Collection efficiency
3. Reentrainment velocity and reentrainment rate

Knowledge of the pressure drop through a separation system is important in calculating the energy loss incurred and in selecting the proper pumps and other auxiliary equipment to overcome that energy loss.

Collection efficiency or overall collection efficiency is defined as the fractional collection of the droplets by the separator, i.e.

$$\eta = \left(1 - \frac{\text{effluent concentration}}{\text{influent concentration}}\right) \qquad (3\text{-}1)$$

When the gas velocity in the entrainment separator is high, some separated droplets in the separator will be reentrained in the gas stream. Because of this reentrainment, the observed collection efficiency of the separator

is less than the primary collection efficiency which is defined as the efficiency an entrainment separator would have if reentrainment were not present.

Reentrainment velocity is the gas velocity at which drops are first observed to become reentrained in the gas. The onset of reentrainment will vary for different kinds of entrainment separators and different operating conditions. Reentrainment velocity determines the maximum allowable gas velocity in the separator. Reentrainment rate and drop size distribution are needed for the prediction of emissions from the system.

Once design equations predicting the primary efficiency, pressure drop, and reentrainment are available, operating characteristics of the entrainment separator can be established.

ENTRAINED LIQUID INFORMATION

In order to design a proper entrainment separator, or to predict the collection efficiency of an entrainment separator, certain entrainment liquid information is needed. This includes:

1. Entrainment drop and size distribution.
2. Quantity or inlet loading.

An extremely important factor in chosing and designing an entrainment separator is drop size distribution. Different entrainment separators are limited to certain drop diameters, below which their efficiency falls off sharply. The size of the drops depends upon the way they were formed. Basic mechanisms of drop formation are described later in the section on reentrainment.

Little information is available on the drop size distribution of entrainment from scrubbers. More attention

seems to have been given to the quantity of entrainment, although the published data on this are also very limited. The data found in this study are presented below and are organized according to the scrubber type.

Plates

Figure 3-1 shows a correlation of the available data for entrainment in bubble-cap and sieve plate gas liquid contacting columns, (Perry, 1973). The entrainment is expressed in "ψ", moles of entrained liquid per mole of gross downflowing liquid (net flow plus return of entrainment). For gas-water contacting the mole ratio is the same as the mass ratio so "ψ" is the mass rate of entrainment per unit of water mass flow rate. The parameter "percent of flood" is the actual vapor velocity divided by the flooding vapor velocity at the same L/G. Entrainment increases with decreasing tray spacing and this effect is accounted for in Figure 3-1 because the flooding velocity is a function of tray spacing.

Figure 3-2 represents a correlation of flooding velocities for sieve and bubble cap plates with several fluid flow rate and property parameters. As shown, the flooding velocity increases with plate spacing; therefore, the entrainment ratio decreases with plate spacing. Because this correlation was developed to describe the entrainment from plate-to-plate, the rate given by Figure 3-1 is that which would be measured at a distance of one plate spacing above the top plate. Scrubbers usually have more clear space above the top plate so the entrainment rate leaving the scrubber would be less than predicted by Figure 3-1.

Other studies, such as by Hunt, et.al.(1955), Atteridge et.al. (1956), Brooks et.al. (1955) and Jones and Pyle (1955) indicate lower entrainment ratios than

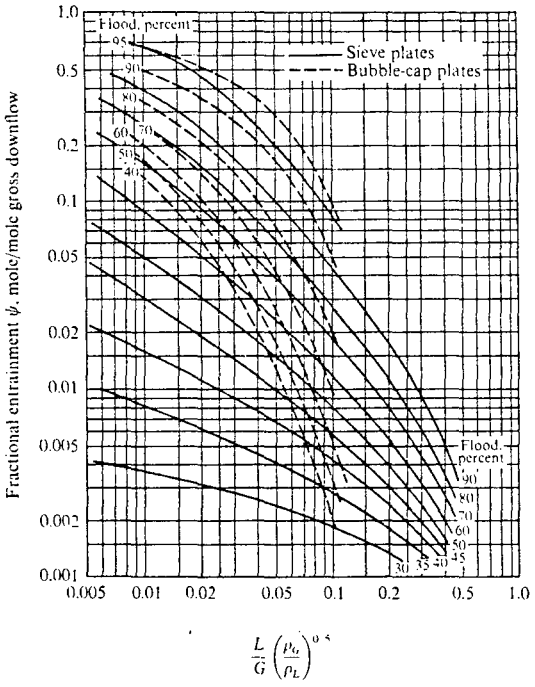

Figure 3-1 - Entrainment Correlation for Plates

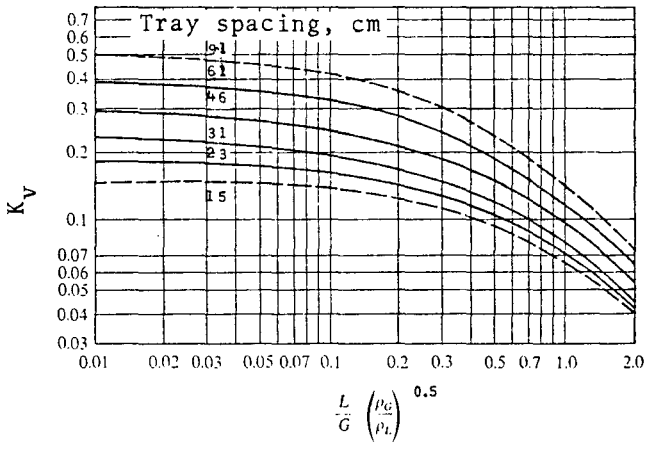

Figure 3-2 - Flooding limits for bubble caps and perforated plates.

$$K_V \equiv 3.28\ U_f \left(\frac{20.0}{\sigma}\right)^{0.2} \left(\frac{\rho_G}{\rho_L - \rho_G}\right)^{0.5}$$

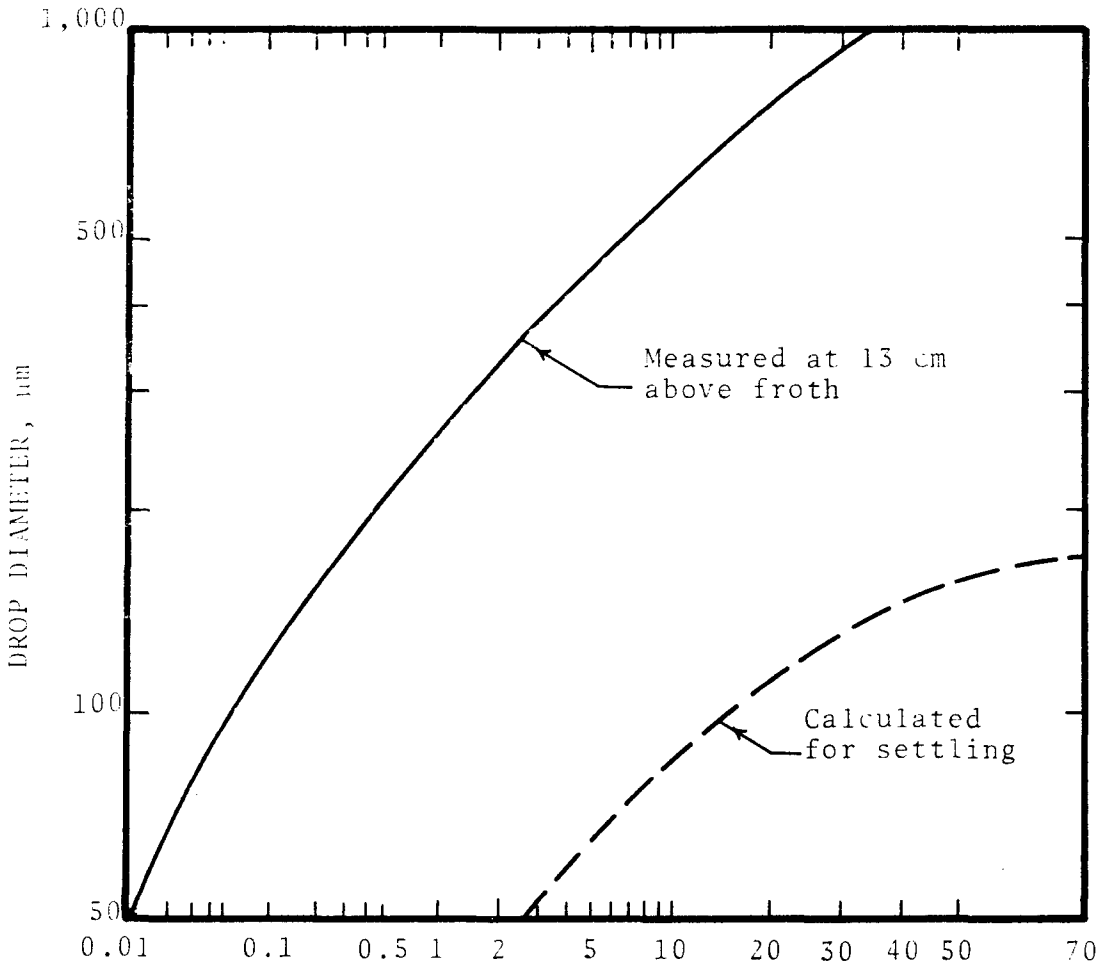

Figure 3-3. Sieve plate entrainment size distribution

given by Figure 3-1. Therefore designs based on Figure 3-1 will be conservatively large.

For illustration, we may note that for a water to gas ratio of 1.34 ℓ/m^3 (10 gal/MCF) the mass ratio, L/G = 1.1 Kg/Kg. If the plate spacing is 46 cm (18") the flooding velocity evaluated for standard air and water properties from Figure 3-2 is about 2 m/sec. At 50% of flooding (i.e., 1 m/sec superficial gas velocity), the entrainment ratios from bubble cap and sieve plates are given by Figure 3-1 as 0.024 and 0.018 mol/mol (or Kg/Kg), respectively. This means that the predicted liquid entrainment measured 46 cm above the top plate would be 0.03 ℓ/m^3 and 0.024 ℓ/m^3 for cap and sieve plates, respectively. At 91 cm above the top plate the entrainment would correspond to that for 91 cm plate spacing which for a sieve plate would be 0.0033 Kg/Kg.

Drop size distribution data for entrainment measured 13 cm above a sieve plate are reported in Perry (1973) as shown in Figure 3-3, a log-probability plot. The facts that the superficial air velocity at which these data were taken was 61 cm/sec and the terminal settling velocity of a 180 μm dia water drop is about 61 cm/sec (see Figure 3-7) enable us to see the influence of sampling point elevation. Figure 3-3 shows that 99.6% of the liquid volume was larger than 180 μm and would settle out of the air stream if the height above the plate were sufficient. If the drops larger than 180 μm were removed, the remaining size distribution, as shown by the dashed curve, would have a mass median diameter of roughly 150 μm and a σ_g of 1.8 (based on the small diameter end of the curve).

Gas Atomized Sprays

Entrainment rate and size distribution data for gas atomized spray scrubbers such as venturis have not been reported. Estimates can be made, as discussed below, but they are very rough because of uncertainties in predicting the characteristics of the initial atomization and the drop separation occurring within the venturi diffuser and similar flow elements.

Drop diameter can be predicted by means of the correlation by Nukiyama and Tanasawa (1938-40). For air and water at standard conditions the N+T correlation for Sauter mean diameter is:

$$d_s(\text{cm}) = \frac{50.0}{U_g(\text{cm/sec})} + 92.0 \left(\frac{Q_L}{Q_G}\right)^{1.5} \qquad (3\text{-}2)$$

where:

d_s = Sauter (volume-surface) mean diameter of drops, cm

U_g = air velocity relative to drops, cm/sec

Q_L = water flow rate, m^3/sec

Q_G = air flow rate, m^3/sec

According to Steinmeyer in Perry (1973), the Sauter mean diameter is typically 70% to 90% of the mass median diameter. This implies that the geometric standard deviation, σ_g, runs about 1.6 for 90% and 2.3 for 70%.

To illustrate the application of the above to the prediction of entrainment characteristics for a venturi scrubber, we can consider the case of a throat air velocity of 100 m/sec and water to air ratio of 1 ℓ/m^3 ($10^{-3} m^3/m^3$).

The gas pressure drop would be about 100 cm W.C. and the Sauter mean diameter computed from eq. (3-2) is 79 μm. From the typical ratios of mass median to Sauter diameter, we would expect the mass median drop diameter to range from 88 to 113 μm, with σ_g from 1.6 to 2.3, respectively. One would therefore predict that the cumulative entrainment concentration would be related to drop size within the range of high and low values tabulated below.

Drop diameter, μm	4	5	10	15	20
High concentration, cm^3/m^3	0.035	0.11	2	8	20
Low concentration, cm^3/m^3	-	-	0.0025	0.06	0.6

If the entrainment contained 10% solids by weight, the residual particle concentrations after evaporation would be such that if one wanted to limit the particle loading due to entrainment to 0.01 g/m^3(0.0044 gr/ft^3) it would require the separation of all entrainment larger than 5 μm diameter for the high estimate and 16 μm diameter for the low. Since particle loadings of this magnitude can be significant for plume opacity, the example shows the efficiency with which entrainment must be controlled and the necessity for good data on entrainment size distribution and concentration.

Mobile Bed

Calvert et. al. (1975) measured the entrainment flow rate and size distribution from a mobile bed (T.C.A. type) scrubber. Data were taken at a location about 76 cm above the top grid of the mobile bed. Figure 3-4 is a plot of entrainment flow rate versus liquid to gas ratio with superficial gas velocity as parameter. Figure 3-5 is a plot of mass median drop diameter of the entrainment as a function of liquid to gas ratio with superficial gas velocity as parameter. The geometric standard deviation, σ_g, for all operating conditions is approximately equal to 1.8.

COLLECTION MECHANISMS

Knowledge of the basic mechanisms of drop collection is fundamental to an understanding of entrainment separators. The separation mechanisms which have been used for entrainment are:

1. Inertial impaction
2. Sedimentation
3. Centrifugation
4. Interception
5. Diffusion
6. Electrostatic precipitation

Sub-micron drops are present in very small quantity in the entrainment generated by scrubbers so diffusional collection is not important. Cost considerations generally weigh against the use of electrostatic precipitators for entrainment separation. The design and operating conditions of separators thus favor inertial impaction, sedimentation, and centrifugation as the principal mechanisms of collection.

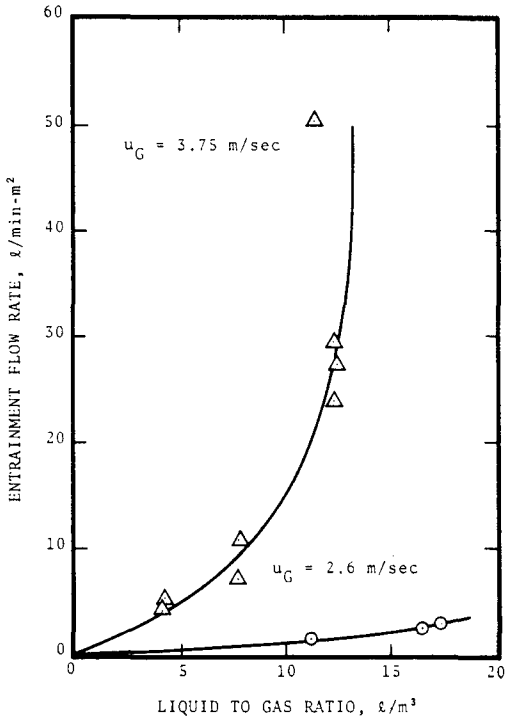

Figure 3-4. Entrainment flow rate versus liquid to gas ratio with superficial gas velocity as parameter for mobile bed.

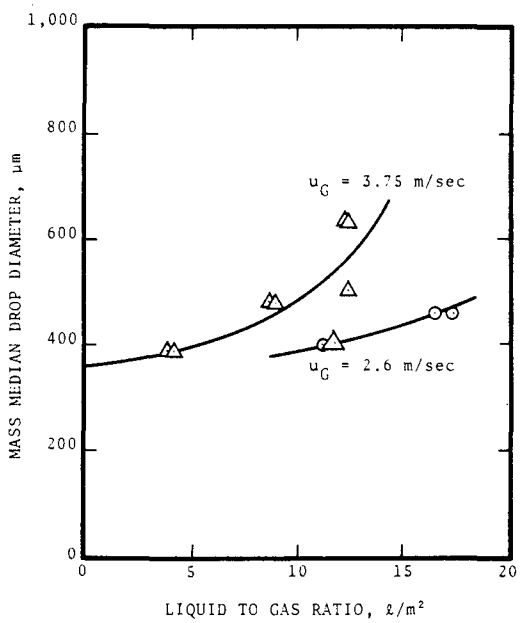

Figure 3-5. Entrainment drop diameter versus liquid to gas ratio with superficial gas velocity as parameter for mobile bed.

Inertial Impaction

Inertial impaction is the major collection mechanism in scrubber entrainment separators. When a fluid approaches an obstacle the fluid streamlines spread around it. At the same time inertial forces carry drops across the streamlines so that the drops hit and stick to the obstacle. It is assumed that all drops colliding with the obstacle adhere to it.

Two factors determine impaction collection efficiency. The first is the velocity distribution of the gas flowing by the collector, which varies with the Reynolds number of the gas with respect to the collector. The second factor is the drop trajectory, which depends on the mass of the drop, its air resistance, the size and shape of the collector, and the rate of flow of the gas stream.

Collection efficiency can be predicted from the equations of motion of a drop for a given gas flow pattern and a collection parameter. The "target" efficiency expresses the fraction of the particles in the entraining fluid, moving past an object in fluid, which impinge on the object. Figure 3-6 from Golovin and Putman (1962), gives theoretical "target" efficiency as a function of the inertial parameter for different targets.

Sedimentation

The second collection mechanism important in entrainment separators is sedimentation. Figure 3-7, from Fuchs (1964), is a plot of drop terminal settling velocity versus drop radius. Drop diameters encountered in wet scrubber entrainment may vary from 50 to 500 μm, and the terminal settling velocity for these drops will range from 0.1 to 2.0 m/sec. The gas velocities used in entrainment separators vary from 1.0 to 12.0 m/sec; however, except for

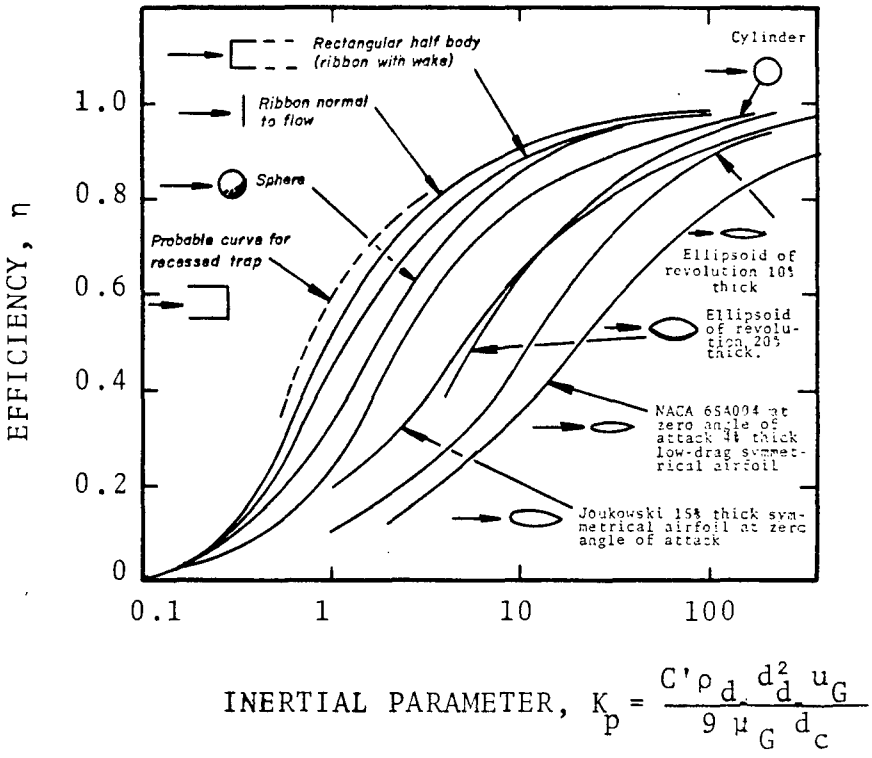

Figure 3-6 - Theoretical impaction efficiency as a function of inertial parameter for different targets.

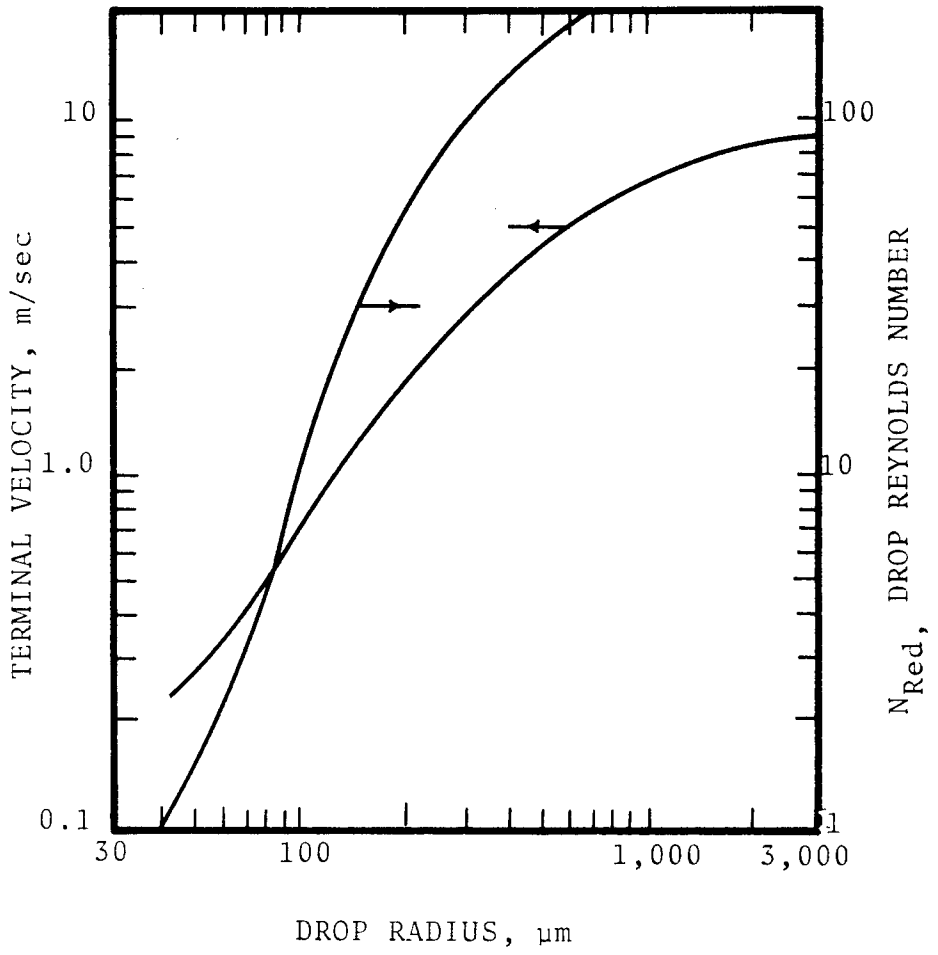

Figure 3-7. Terminal settling velocity and Reynolds number for water drops in air at 20°C and 760 mm Hg.

cyclone-type separators, which operate at very high velocities, most operate below 4.0 to 5.0 m/sec. Therefore, sedimentation can be expected to affect the separation of drops.

Centrifugation

When the entrainment laden gas is put into spinning motion, centrifugal force affects the droplets. The centrifugal force is much greater than gravity, therefore, droplets are thrown to the wall and collected.

If a gas stream moves round the arc of a circle, and it is assumed that the droplet has the same tangential velocity as the gas stream, then the centrifugal force on the droplet is given by:

$$F = m \frac{u_{tg}}{R} \qquad (3\text{-}3)$$

where F = centrifugal force
m = mass of the drop
u_{tg} = tangential component of the gas velocity
R = radius of the circle

If the droplets are sufficiently large and have high enough initial velocity, they are thrown to the wall close to the inlet. On the other hand, when liquid drops are small, they are carried by the gas flow part of the way before being thrown out to the wall by centrifugal force.

The time required for the drop-travel from the initial position "R" to the wall is

$$t = \frac{9\,\mu_G}{(n+1)\rho_d} \left(\frac{rc}{u_{tg} d_d}\right)^2 \left[1 - \left(\frac{R}{rc}\right)^{2n+2}\right] \qquad (3\text{-}3a)$$

where t = time elapsed, sec

ρ_d = drop density, g/cm^3

μ_G = gas viscosity, poise

d_d = drop diameter, cm

r_c = collector wall radius, cm

n = vortex component

= 0.5 - 0.7 for cyclones

If the time required is less than the residence time of the gas, the drop will be collected.

REENTRAINMENT

The overall collection efficiency of an entrainment separator is often found to be less than the primary efficiency because of reentrainment. Increasing overall efficiency means reducing reentrainment, the achievement of which requires a knowledge of the parameters important in determining the extent of reentrainment. Thus, engineering equations describing this process are vital to improved efficiency.

One cause of reentrainment is high gas velocity. To avoid this hazard, entrainment separators have been operated at lower gas velocities than necessary, resulting in the use of equipment which is larger and more expensive than needed.

Reentrainment from an entrainment separator may take place by any one of more of the following mechanisms:

1. Transition from separated to separated-entrained flow caused by high gas velocity.
2. Rupture of bubbles at the gas liquid interface and subsequent drop formation.
3. Creeping of the liquid along the solid surface and movement into the gas exit in the entrainment separator.

4. Shattering of liquid drops due to impaction.

The last three mechanisms of reentrainment depend upon the design of the entrainment separators. The first mechanism represents the upper limit of the operation of entrainment separators.

Transition from Separated to Separated-Entrained Flow

Reentrainment may occur at high gas velocities due to transition from separated to separated-entrained flow. In simple geometries such as straight tubes, the transition takes place at much higher velocities than those at which entrainment separators are operated. Yet reentrainment is observed in separators at the lower velocity. This is caused by such phenomena as the impingement of the gas stream onto the liquid at an angle and the presence of gas jets. Also the flow pattern in the entrainment separator is not so uniform as in circular tubes.

In the operation of entrainment separators, flows may be horizontal, vertically upward or downward, or inclined. The onset of reentrainment depends upon the flow direction, flow geometry and the fluid properties. The reentrainment models for simple geometries has been examined and given in the "Initial Report" (1974).

Effect of Impingement of Gas Jets - As mentioned earlier, the gas and liquid phases do not flow parallel in the entrainment separator. Jets of gas are present, which may impinge on the liquid film at various angles. The presence of gas jets, their impingement on the liquid film at various angles, etc. depend upon the entrainment separator design.

Wallis (1962) studied entrainment in ducts with various inlet designs. The reentrainment velocity varies with inlet design, from 18 m/sec to 24 m/sec. The data are shown in Figure 3-8.

Interfacial Waves - The study of interfacial wave behavior is important in the determination of transition from separated flow to separated-entrained flow. Experimental and theoretical studies of wave behavior and its influence on other phenomena are still at a very early stage of development. The most advanced theoretical studies have been concerned with the problem of the initial formation of waves, rather than their development and influence. However, the instability of the waves represents the physical phenomenon responsible for transition from separated to separated-entrained flow. Thus, to understand the physical phenomena responsible for reentrainment in entrainment separators, one should look at the interfacial waves, breaking of the waves, drag friction on the film due to gas flow, etc.

For vertical flow the only forces opposing these normal stresses are those due to surface tension. For a stable interface condition, the surface tension stresses exactly balance the effects of the normal stress. On the other hand, the wave will grow in amplitude when the sum of the local liquid and gas normal stresses exceeds the surface tension stress. It can be further deduced that the thinner the liquid film the greater the gas velocity needed to cause an increase in amplitude of a given size wave.

It may be expected that the effect of waves will be to increase the friction factor. To determine the liquid flow rate, it is necessary to have interfacial friction factor.

Roberts and Hartley (1961) found, on plotting friction factor as a function of liquid film thickness for a given gas velocity, that the friction factor did not begin to increase with film thickness until a certain value had been

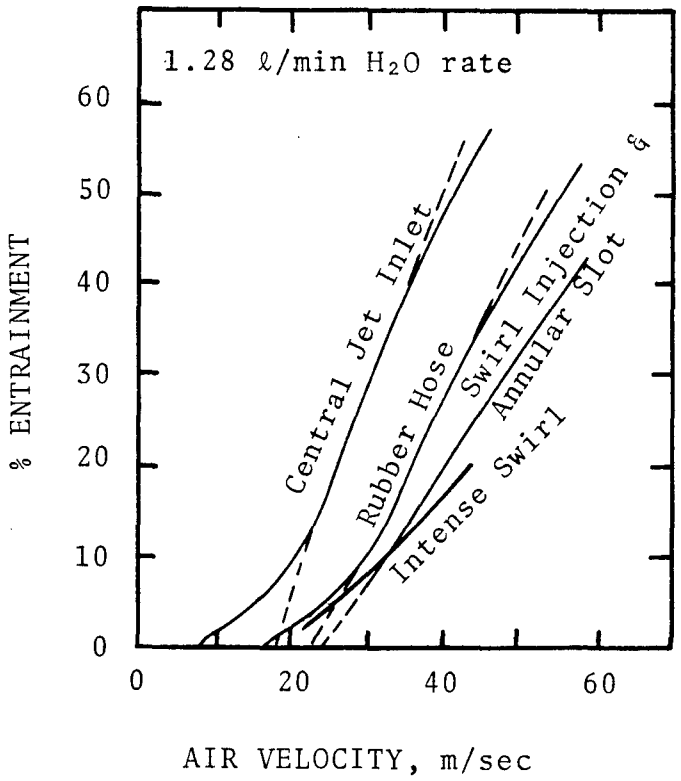

Figure 3-8 - Extrapolation method for determination of point of onset of entrainment for vertical downflow in 2.2 cm I.D. tube.

exceeded. They were able to correlate the difference between the interfacial friction factor and that for the same gas flow rate in the absence of the liquid phase, by the equation:

$$f_i = f_G + 1.5\left[\frac{\delta}{d_{eq}} - \frac{5}{N_{Re,G}}\left(\frac{2}{f_G}\right)^{0.5}\right] \qquad (3\text{-}4)$$

$$f_i = \tau_i \left(\frac{1}{2}\rho_G u_G'^2\right)^{-1} \qquad (3\text{-}5)$$

where f_i = interfacial friction factor

f_G = friction factor in the absence of liquid phase

δ = liquid film thickness, cm

d_{eq} = equivalent (hydraulic) diameter, cm

τ_i = interfacial shear stress, g/cm-sec^2

$N_{Re,G}$ = gas Reynolds number

Thus, for very thin liquid films there would be no significant waves on the interface and no effective roughness. For thicker films there would be a minimum instantaneous film thickness corresponding to the troughs of the waves on the surface.

A number of possible mechanisms have been suggested by which transfer of droplets can be effected by the waves, but at present there is no definite evidence to favor any particular one. Lane (1957) described the mechanism illustrated in Figure 3-9. The gas starts to "undercut" the wave and a round, open ended bubble begins to form. The bubble grows, leaving a thick-ringed filament around its base and eventually breaks up into droplets. Once the breakup occurs, the excess (dynamic) pressure inside the bubble gives rise to a rapid radial transport of the droplets.

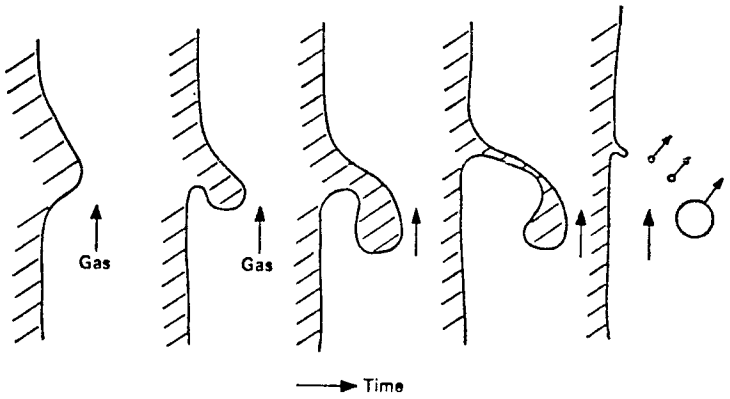

Figure 3-9

Breakdown of Disturbance Wave by Undercutting

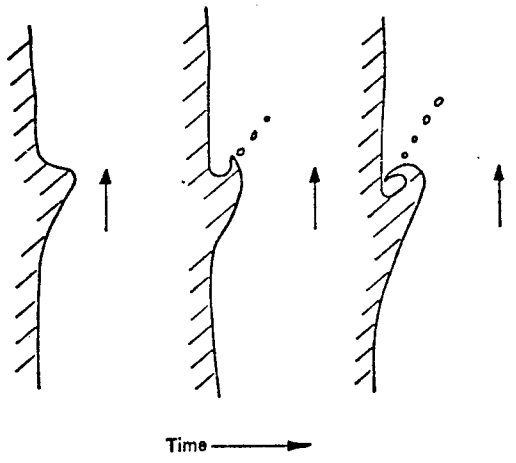

Figure 3-10

Breakdown of Disturbance Wave by Rolling

An alternative form of breakup is illustrated in Figure 3-10. A large amplitude wave on a shallow liquid layer tends to steepen at the front and then to form a breaking wave. If the gas velocity is very high, it might be expected that the tips of the waves would be drawn out into thin liquid sheets with subsequent breakup.

Reentrainment Due to Rupture of Bubbles

The second mechanism which leads to reentrainment is rupture of bubbles. This mechanism is the main cause of the reentrainment of liquid drops into the gas phase in devices such as sieve plate, bubble cap plate, packed bed, and mesh type separators. The collapse of a bubble when exiting from the liquid phase is associated with thinning of the liquid film starting at the top part of the bubble. The upper surface thins to the extent of becoming weak enough to rupture. Rupture of the upper part of the bubble film takes place when the film thickness is of the order of 0.1 μm, provided there are no external disturbance forces leading to the rupture of films (Kitchener, 1964; Jashnani, 1971). The collapse of the bubble at the interface leads to the release of surface tension energy which is converted into kinetic energy. The kinetic energy is sufficient to impart high velocities to liquid drops formed during this process.

Drop formation due to bubble burst occurs in three steps. The first step, the lifetime of the bubble at the interface, lasts on the order of 1/100th sec.or longer; the actual bubble burst, the second step, takes a few micro-seconds; and events subsequent to the bubble burst extend over a few milliseconds.

Creeping of Fluids

The presence of drag forces due to gas flow leads to creeping of liquid in the entrainment separator. Creeping may be prevented by providing a proper drainage system. If creeping is not prevented, reentrainment may occur.

Consider liquid and gas flowing in a vertical tube. The gas is flowing vertically upward and liquid is flowing as a film and therefore forming an annulus. The liquid film is subject to various forces: drag force due to gas flow in the vertically upward direction, gravity force in the downward direction and frictional force due to tube wall.

For gas velocity lower than the critical velocity the liquid near the wall flows downward due to gravity. As the gas velocity is increased the liquid at the interface reverses its flow direction and moves with the gas; as a result the liquid film begins to thicken. At a critical gas flow rate the liquid does not flow down any more, and the liquid film thickens rapidly.

Shattering of Drops

Reentrainment may take place due to shattering of drops in two ways:

1. Due to splashing of drops on the solid surface
2. Due to high relative velocity between gas and liquid drops.

Shattering of the drops due to high relative velocity between gas and liquid drops does not increase entrainment in the gas phase. However, small drops are more

liable to be carried away in the gas phase than large drops and therefore shattering of drops should be avoided.

ENTRAINMENT REMOVAL EQUIPMENT

We have already seen the principal mechanisms of entrainment separation. In many cases, actual equipment combines two or more of those mechanisms. The following section discusses each of the main equipment types.

Gravity Settlers

The gravity settler is one of the earliest and simplest types of equipment for separating particles from gases. The function of a gravity settler is to reduce the gas velocity, from one which permits entrainment down to a velocity that will permit gravity to remove the entrained droplets. There are two basic types, tranquil and stirred. The only effect of stirring is to maintain an even concentration throughout the separator. In most cases, it neither helps nor hinders the settling.

Primary Collection Efficiency - If the gas passes vertically upward through the settler, all particles having terminal velocities equal to or greater than the velocity of the gas stream will be removed. A 100 μm water particle has a terminal velocity in air of about 30 cm/sec. Thus, very low velocities and consequently large equipment sizes are required to remove particles which are 100 μm or less in diameter.

For complete removal to take place if the gas passes

horizontally through the settler, the drop terminal velocity multiplied by the residence time must equal the maximum settling height:

$$u_t = \frac{Q_G}{b\ell} \qquad (3\text{-}6)$$

where u_t = drop settling velocity, cm/sec
Q_G = volumetric gas flow rate, m^3/sec
b = width of settler, cm
ℓ = length of settler, cm.

When u_t is not equal to $Q_G/b\ell$, the removal efficiency becomes:

$$E = \frac{u_t b\ell}{Q_G} \qquad (3\text{-}7)$$

For droplets greater than ≈ 0.15 cm ($500 < N_{Re}$), Newton's law applies and,

$$u_t = 1.74\left(\frac{g d_d \rho_d}{\rho_G}\right)^{0.5} \qquad (3\text{-}8)$$

where g = gravitational acceleration
d_d = droplet diameter, cm
ρ_d = droplet density, g/cm^3
ρ_G = gas density, g/cm^3

When $d_d < 100$ μm, Stokes law applies:

$$u_t = \frac{d_d^2 \, g \rho_d}{18 \mu_G} \qquad (3\text{-}9)$$

where μ_G = gas viscosity, poise.

For drops larger than 100 μm in diameter and smaller than 0.15 cm, drop settling velocity can be taken from Figure 3-7.

Pressure Drop - The pressure drop across gravity settlers can be estimated reasonably well by the standard methods of calculating pressure drop in a conduit. It is usually very low (less than 1 cm W.C.), consisting primarily of entrance and exit losses.

Impingement Separators

For its removal qualities, the impingement type separator depends on particles colliding with a surface. Some typical impingement separators are shown in Figure 3-11. The most extensively used impingement type separators are:

1. Wire mesh
2. Packed bed
3. Vanes or baffles

In addition, tube bank (staggered rods) type separators appear to have useful characteristics even though they are not commonly used. These four types of impingement separators will be discussed in detail in Chapters 5,6,7 and 9 respectively.

Centrifugal Separators

The centrifugal separator is a device utilizing radial acceleration for separating the entrained particles from the carrier. Because of the liquid's greater density and momentum, the circular motion imparted to the fluid causes the entrained particles to separate from the carrier and impinge on the walls, then move downward by the vertical

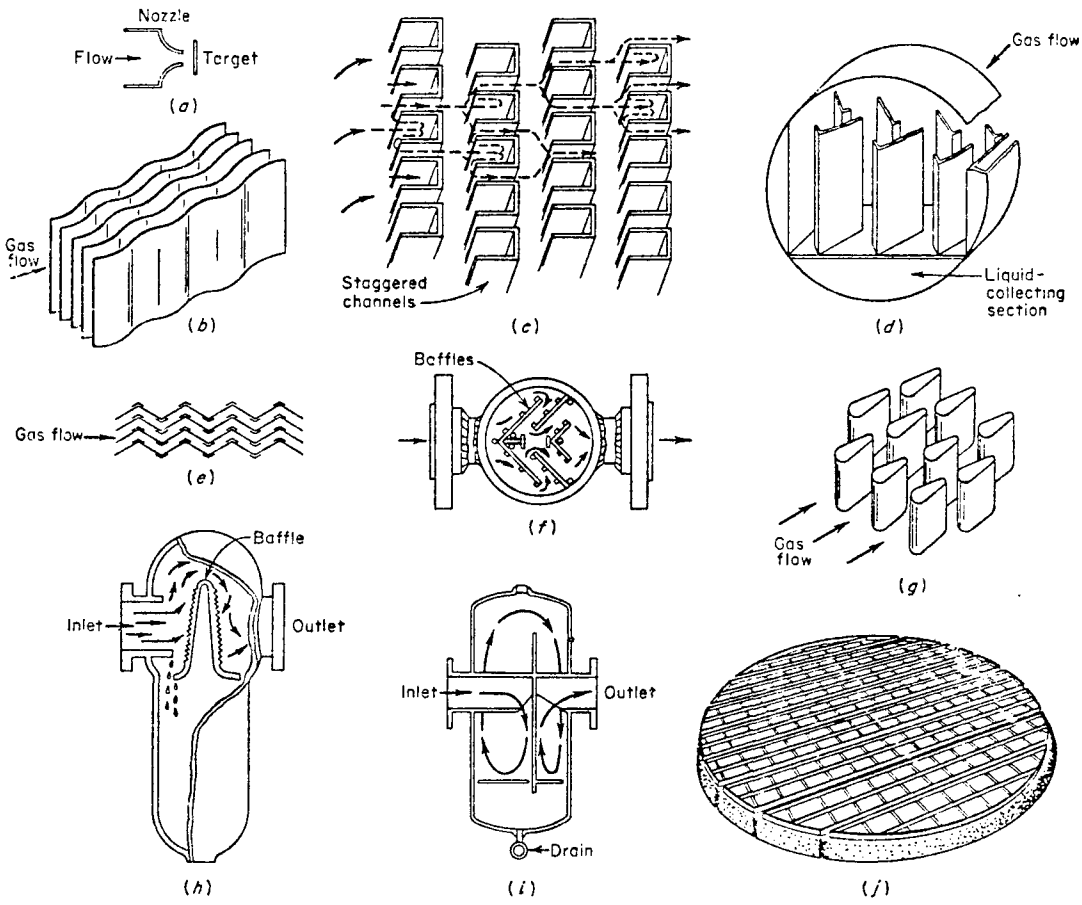

Figure 3-11 Typical Impingement Separators

(a) Jet impactor
(b) Wave plate
(c) Staggered channels
(d) Zigzag baffle
(e) Peerless line separator
(f) Strong separator
(g) Karbate line separator (staggered streamline rods)
(h) Type E horizontal separator
(i) PL separator
(j) Wire mesh

component of the force, as well as by gravitation. Figure3-12 shows some typical centrifugal separators.

The cyclone is undoubtedly the most commonly used type of centrifugal separator. This is due primarily to its simplicity of construction and low maintenance costs. Its efficiency is not as high as those of some other types of separators. Often, if higher removal efficiency is needed, they may be preceded or followed by supplementary separators. A droplet size of 5 to 10 μm is generally considered the lower size limit for particle removal.

The spinning motion can be applied to the gas stream in several ways and cyclone types can be classified accordingly. The gases can be drawn through curved vanes in a duct, in a unit called the "straight through cyclone" or "vortex air cleaner", or they can be spun in a special turbine. In the conventional or "reverse flow cyclone" the gases are admitted tangentially to a cylindrical upper section ; it contains a centrally placed exhaust pipe penetrating below the tangential inlet, while a conical lower section is connected to the dust hopper. The gases, in this case, spiral down towards the apex of the cone and then are reversed up again through the exit.

The primary collection efficiency, pressure drop, and reentrainment for cyclone separators are discussed in Chapter 8.

Other Types of Entrainment Separators

In general, any device that can be used to remove solid particulates can also be employed to remove entrainments. For example, scrubbers and electrostatic precipitators are commonly used to separate liquid mists.

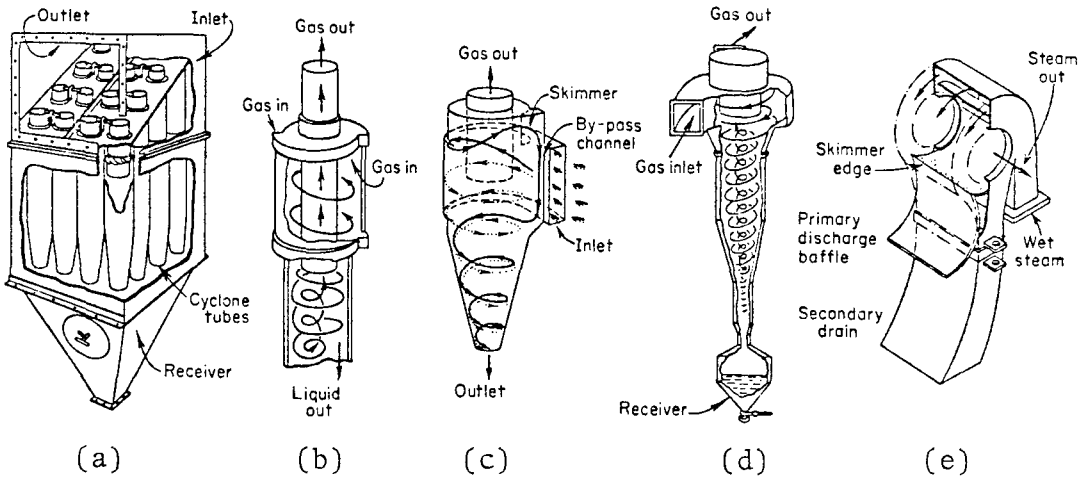

Figure 3-12 Typical Centrifugal Separators

(a) Multiclone
(b) Thermix ceramic tube
(c) Van Tongeren cyclone
(d) Sirocco type D collector
(e) Horizontal steam separator

Tray Towers - Tray towers are vertical channels in which the liquid and gas are contacted in stepwise fashion on trays or plates. The liquid enters at the top and flows downward by gravity. On the way, it flows across each tray and through a downspout to the tray below. The gas passes through openings in the tray, then bubbles through the liquid to form a froth, disengages from the froth, and passes onto the next tray above. There are various tray geometries. The sieve tray and bubble cap are the two most common types:

Sieve plates -

Primary efficiency - Taheri and Calvert (1968) derived an equation for sieve plate primary collection efficiency:

$$E = 1 - \exp\left(-40\, F_\ell^2\, K_p\right) \qquad (3\text{-}10)$$

where $0.30 < F_\ell < 0.65$,

$$K_p = \frac{\rho_d d_d^2 v_h}{9\mu_G d_h} \qquad (3\text{-}11)$$

where F_ℓ = foam density, ratio of clear liquid height to total foam height

v_h = velocity of gas through hole, cm/sec

d_h = hole diameter, cm

Pressure Drop - Perry (1963) has suggested that the pressure drop in sieve plates can be calculated according to:

$$\Delta P = h_w + h_{ow} + h_{dp} + h_r \qquad (3\text{-}12)$$

where,

h_w = weir height = 4-9 cm, assume 5 cm, if unknown

h_{ow} = head over the weir = $0.143\ F_w \frac{Q_L}{w_1}$

h_{dp} = dry plate head loss = $\frac{1}{c^2} \frac{\rho_G}{\rho_L} \frac{v_h}{2g}$

h_r = residual pressure drop = $0.013 \frac{\rho_{water}}{\rho_L}$

$$\frac{1}{c^2} = 1.14\ [0.4\ (1.25 - f_h) + (1 - f_h)^2] \quad (3\text{-}15)$$

where,

F_w = column wall curvature correction factor = 1.1
Q_L = liquid flow rate, here in m^3/hr
w_1 = weir length, m
f_h = fraction of the perforated open area in the plate

Bubble-cap Trays - Equations used to predict primary collection efficiency and pressure drop of sieve plates can also be applied to bubble-cap trays.

CHAPTER 4

EXPERIMENTAL PILOT PLANT

An experimental pilot plant for the study of entrainment separators was designed and built. The purpose of the pilot plant was to do the following:

1. To obtain reliable data over a wide range of operating variables in order to provide a basis for the improvement or development of new separators.
2. To check presently available design equations for entrainment separators
   A. Efficiency of separation
   B. Pressure drop
3. To determine the effect of higher gas velocity on reentrainment, bouncing of drops and impaction mechanism
4. To study liquid drainage and flooding
5. To study problems associated with entrainment separators
6. To study the effect of separator mounting methods on its performance.

DESCRIPTION OF THE PILOT PLANT

The maximum capacity of the wet scrubber entrainment separator is 85 m^3/min (3,000 CFM). The capacity was selected based on the following consideration. The entrainment separator cross-section was selected to be 30.5 cm x 61 cm. This section is sufficiently large to have minimal wall effects for separators and provides a fairly long (61 cm) collection element when cross-flow effects are important. Normally, the maximum air velocity in industrial separators is around 3.0 m/sec. If velocities 2.5 times higher are studied, the maximum air velocity will be 7.5 m/sec. This will give the maximum capacity of 85 m^3/min.

The sampling method and equipment used in studying the horizontal test sections have already been described in detail in the "Initial Report" and will not be repeated here. The equipment used in studying the vertical test section is given below.

EXPERIMENTAL SYSTEM

Figure 4-1 is a flow diagram of the experimental system. Liquid collected from the drain was recirculated. The amount of liquid recirculated into the system was recorded by water meter #1. Barrel #2 acted as a reservoir. The amount of liquid fed into the spray section was measured by water meter #2.

Air Inlet

The air flow to the test section was supplied by a Western Blower size 122 B1 and Class III. It has a capacity rating of 88 m^3/min at 30.5 cm W.C. (static pressure), a 7.5 kW (10 HP) motor, rotatable housing and an opposed blade discharge damper. The blower was supported on a hard rubber base to prevent vibrations and it was insulated with accoustical fiberglass and concrete blocks to reduce the noise level.

Spray Section

The spray section served to generate entrainment for the test section. It was equipped with various nozzles

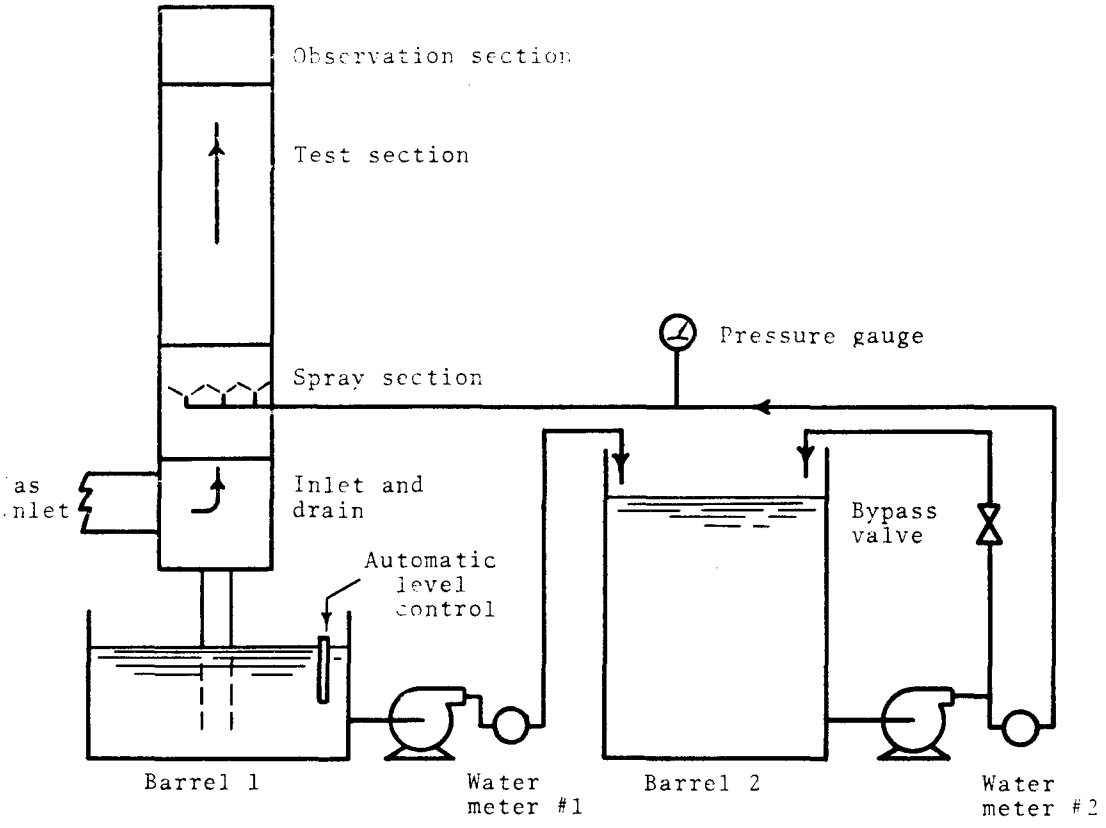

Figure 4-1. System flow diagram for vertical test section.

from Spraying Systems Co. The nozzle specifications are given in Table 4-1. In any section, the nozzles were equispaced as shown in Figure 4-2 to generate uniform flow.

The spray section was also equipped with a plexiglass door, so that the spray drop size could be measured. Also the spray nozzles could be changed without taking the whole test assembly apart.

Observation Section

The observation section had dimensions of 30.5 cm x 61 cm, cross-section and 50 cm length. Two plexiglass windows 30 cm x 30 cm, were installed on opposite sides on each observation section. A door was provided for sampling of entrainment drop diameters.

Liquid Catch and Liquid Supply Tanks

One 100 liter (30 gal) drum was used as the liquid catch tank. The tank was connected to a water meter and a pump with a liquid level controller for the recirculation of liquid.

The liquid supply tank was a 200 liter (55 gal) drum. The recirculated water from the liquid catch tank was fed back into the system through the liquid supply tank. On the outlet side were located water meters and rotameters for flow measurements. The flowrate and pressure into the system was controlled by the bypass valve.

Control Panel for Equipment

The control panel was equipped with the following:

1. Electrical connections
    A. Magnetic starter for blower
    B. Switches for pumps, heater, sampling pump,

Table 4-1. NOZZLES USED IN SPRAY SECTION

Type of Nozzle	Model # (Spray Systems)	Pressure atm	# of Nozzles	Flow rate cm^3/sec nozzle
Hollow cone	1/4 M6SS	13.6	12	14.2
Fogjet Nozzle	1-11 1/2 F18	2.7	1	1140
	1 1/2-11 1/2 F35	2.7	1	2200
Full Cone	1/8 GG3	2.7	12	63.0
Hollow Cone	1/4 M26	2.7	12	27.2

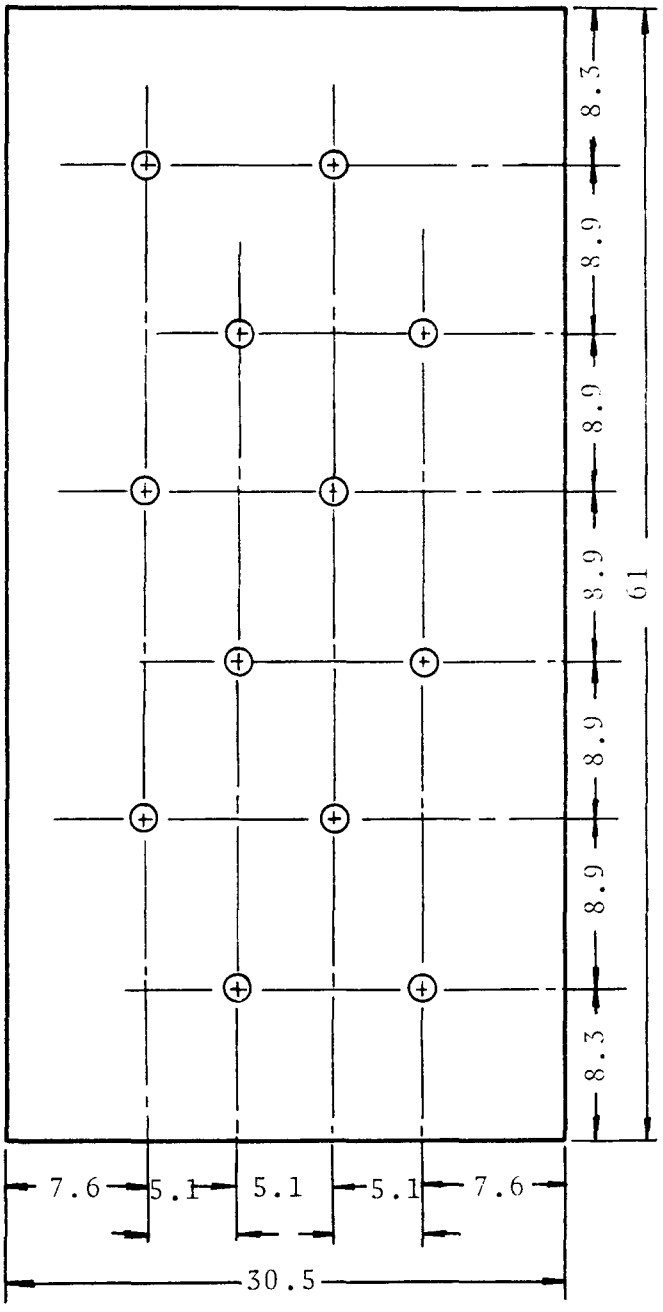

Figure 4-2 - Nozzle positions in the 30.5cmx61cm duct. All dimensions in cm.

observation lights, etc.

C. Temperature recorder

2. Non-electrical connections

A. Rotameters and water meters

B. Dry gas meter

C. Pressure gauges

D. Needle valve, diaphram valves, globe valves, and gate valves

E. Manometers to measure pressure drop

Electrical Supply Panel

A 110 V, 3 phase, 90 amp/phase electrical supply panel was installed near the equipment site.

Water Supply

Water supply to the spray nozzles:

Centrifugal pump - model 165U (Barnes Pump)

Maximum pressure - 3.4 atm (50 Psi)

Motor rpm - 3,450

Motor output - 1.1 kW (1.5 HP)

Flow rate at maximum pressure - 120 ℓ/min (31 GPM)

Test Section

Five different types of entrainment separators were tested:

1. Mesh
2. Packed bed
3. Tube bank
4. Cyclone
5. Zigzag baffles

The test sections for the mesh, packed bed, tube bank,

and zigzag baffles were the same as those used for the experiments with horizontal air flow. They were described in detail in the "Initial Report". The inclined baffle section was built for experiments with vertical air flow only. A brief description of each section is given as follows:

1. Mesh - ACS model 4CA mesh was used. The thickness of the mesh was 10 cm, with 0.028 cm diameter wires arranged in layers crimped in alternate directions. Voids occupied 98.2% of the total volume and the mesh surface area was 2.8 cm^2/cm^3. The mesh was located in the first 30 cm of the test section.
2. Packed bed - Packing - 2.5 cm pall rings. Specific surface = 1.9 cm^2/cm^3. Density = 0.088 g/cm^3. Material of construction = Polypropylene plastic. Bed length = 30 cm.
3. Tube Bank - Number of rows = 6. External diameter = 1.9 cm. Length = 61 cm. Tubes per row = 8. Tube spacing within row = 3.8 cm center - center spacing between rows = 2.13 cm c-c.
4. Cyclone - The cyclone is a cylinder 61 cm diameter x 243 cm overall height. The cyclone inlet is 30.5 cm high and 15 cm wide, giving a maximum inlet velocity of 3,000 cm/sec. Higher velocities were studied by using a vane in the inlet. The design is described by Stearman and Williamson (1972) and is a straight cylinder with flat bottom. Figure 4-3 shows the cyclone used in the present study.
5. Zigzag Baffles - Baffle dimension = 7.5 cm width x 61 cm height x 0.16 thickness. Number of rows = 6. Spacing between rows = 2.5 cm. Angle between baffle surface and air flow direction = 30°. Spacing between baffles in a row = 7.3 cm. Figure 4-4 shows the baffle arrangement.

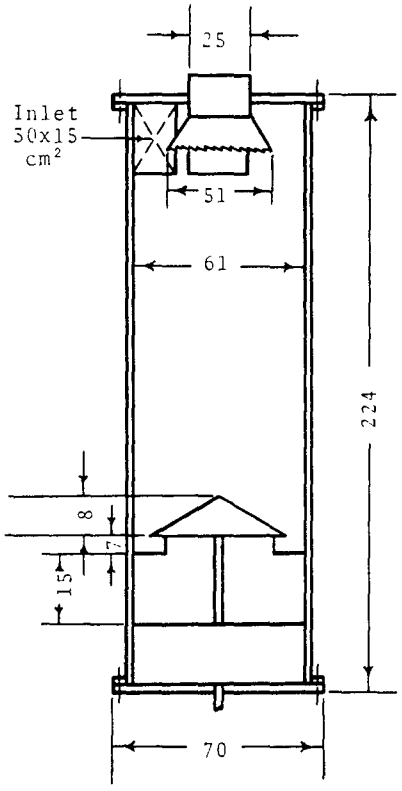

Figure 4-3. Cyclone assembly. All dimensions are in cm.

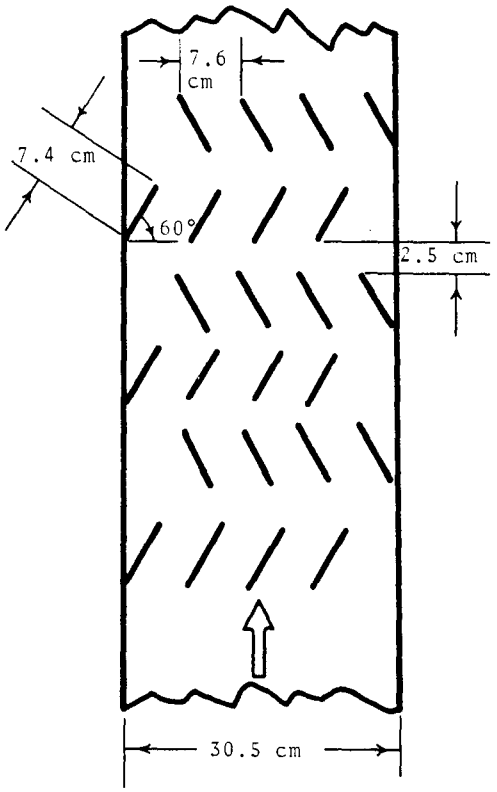

Figure 4-4. Top view of baffle arrangement.

6. Inclined Baffles - Two inclined baffle sections were built. One section with the baffle inclined 45° to the horizontal and the other section inclined 30°. Figure 4-5 shows the front view of the inclined baffle section and Figures 4-6 and 4-7 are dimensions of each baffle for 30° inclination and 45° inclination respectfully. The mounting method is the same as that shown in Figure 4-4.

Flow Measurements

Air flow rate was measured by a standard pilot tube located at the inlet air duct. Liquid flow to the spray section was metered with a calibrated water meter. Alternatively, the total amount of liquid flow to the spray section can be determined by the sum of the amount of liquid recycled and the amount of liquid lost after the experiment. The amount of liquid lost was given by the difference in liquid level in the two tanks (which were calibrated) before and after the experiment.

EXPERIMENTAL PROCEDURE

The major points of the experimental procedure are described below. The procedure was modified as required for individual runs.

1. All the tanks were emptied before starting the experiment in order to avoid rust in the water.
2. All the wet bulb thermometers were checked for

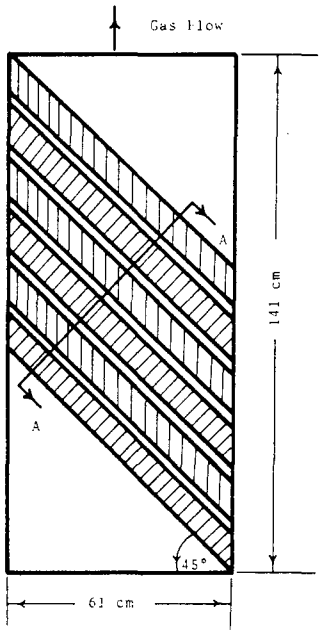

Figure 4-5. Front view of inclined baffle section - 45° inclination.

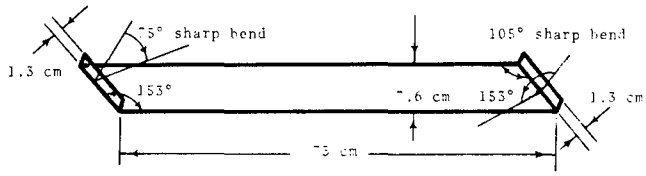

Figure 4-6. Dimensions for a 30° inclined baffle.

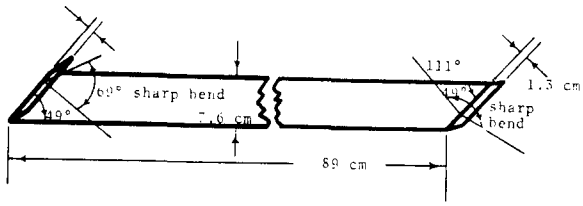

Figure 4-7. Dimensions for a 45° inclined baffle.

water.

3. All the valves were checked so that the required valves were kept opened and the rest closed.
4. All the recycle pumps were kept on to maintain the liquid level in the tanks between the upper and lower limits.
5. All the catch tanks were filled with liquid until the level was between the upper and lower controlled limits.
6. The feed supply tank was filled to the overflow line.
7. The zero position of the inclined manometer was adjusted.
8. Readings were noted for all the water meters and the liquid levels in the catch tanks.
9. The desired air flow was started.
10. Pressure drop across the test section was measured.
11. The desired water flow rate was started.
12. About 1-5 minutes were needed to reach steady state. The experiment was continued for 2 hours.
13. Air flow rate, water flow rate, etc., were checked every few minutes.
14. Visual observations of penetration, flooding, liquid drainage, bouncing of drops, liquid flow on elements of the entrainment separator, etc., were made for the duration of the experiment.
15. Readings were taken of temperature (each hour), entrainment drop size, pressure drop, entrainment loading, etc. (once during each run).

16. At the end of the experiment liquid and air flow were shut down. Readings were noted for water levels in the tanks and water meter readings.

INLET ENTRAINMENT DROP SIZE

Various nozzles were used in the experiments, although only one type of nozzle was used in any given experiment. A description of the nozzles is given in Table 4-1. A complex relationship among the characteristics of the individual spray nozzles, the interaction of multiple nozzles, the configuration of the experimental duct and the air velocity determines the inlet entrainment size distribution.

The spray generated from the M6 nozzles was analyzed under experimental conditions by filter papers coated with 1% potassium ferricyanide and ferrous ammonium sulfate as described in the initial report. The drop diameter generated from the other nozzles was greater than 100 μm. For these, the manufacturer's data were used to determine drop diameters.

The effect of gas velocity on mass median drop diameter generated from M6 nozzles is shown in Figure 4-8. There is no definite trend. The mass median diameter varies from 76 to 102 μm and averages 84 μm, with an average geometric standard deviation of 1.32. The minumum drop diameter found in the inlet was 30 μm.

Inlet entrainment measurements were made at a point 75 cm downstream of the spray nozzles and 30 cm upstream of the test section. The average water supply pressure was 13.6 atm. gauge (200 psig). The nozzles were oriented toward the downstream side and gave the drops an initial velocity

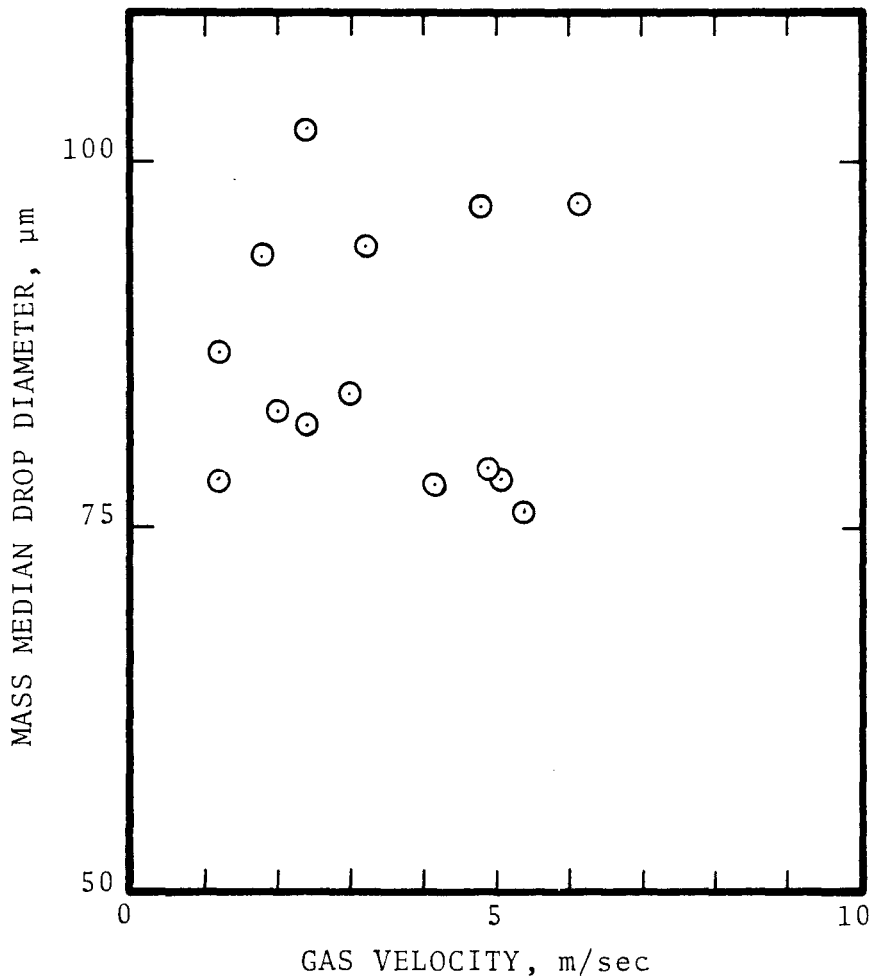

Figure 4-8. The effect of gas velocity on drop diameter for M6.

of 51 m/sec.

An analysis of the drop diameters created by each nozzle is given in Table 4-2 , and more detailed information concerning the size distribution curves, as provided by the manufacturers, is presented in Figures 4-9 through 4-11 These distributions were measured 30 cm from the nozzles.

In these experiments the M26 nozzles were operated at 2.7 atm pressure, but the drop size data provided by the manufacturer are for 6.8 atm and 10.2 atm. The mass median drop diameter produced by M26 nozzles was obtained from fitting the following relation for the effect of operating pressure on drop diameter:

$$d_{pg} = c_1 (\Delta P)^{c_2} \qquad (4\text{-}1)$$

where d_{pg} = mass median drop diameter, cm

ΔP = pressure drop at nozzle, atm

c_1, c_2 = constant

The mass median drop diameter for an operating pressure of 2.7 atm was 380 μm. The geometric standard deviation was 1.5 and did not significantly vary with operating pressure.

The nozzles often plugged, due to formation of rust in the water tanks. This resulted in a decreased water flow rate and also may have caused some variation in the drop diameter and standard deviation.

It was observed that the entrainment flow rate reaching the entrainment separator decreased with decreasing air velocity. This is due to an increase in collection by the walls of the spray section.

Table 4-2. DROP SIZE ANALYSIS

Source of Data	Type of Nozzle	Operating Pressure atm gauge	Mass Median Diameter, μm	Minimum Drop Diameter, μm	Geometric Standard Deviation
Manufacturer	M6	6.8	127	45*	1.5
Manufacturer	M6	10.2	110	45*	1.5
This Study	M6	13.6	84	30	1.3
Manufacturer	M26	6.8	295	110*	1.5
Manufacturer	M26	10.2	265	102*	1.5
Predicted From Equation (7-1)	M26	2.7	380	-	1.5
Manufacturer	GG3	2.7	1,230	450*	1.8

*2% of the drops are smaller than this diameter.

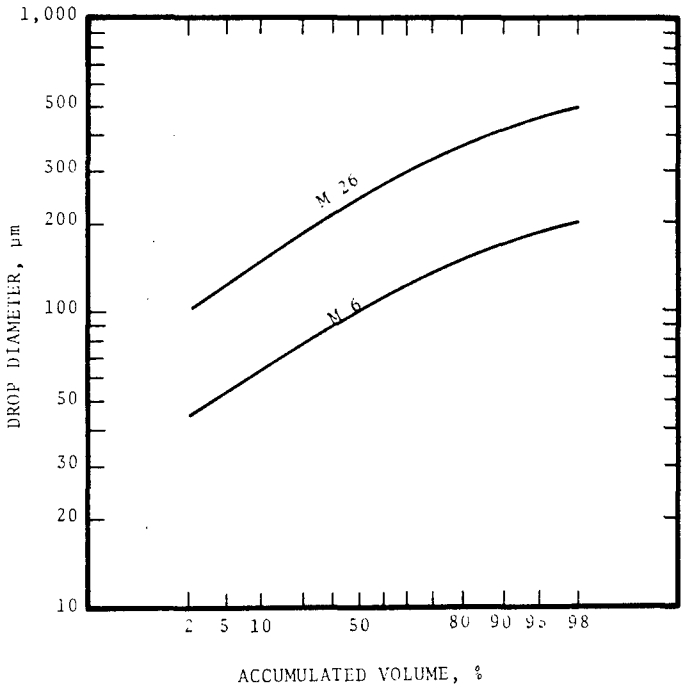

Figure 4-9. Drop diameter versus volume percentage for hollow cone nozzle spraying water at 10.2 atm gauge pressure (Manufacturer's data)

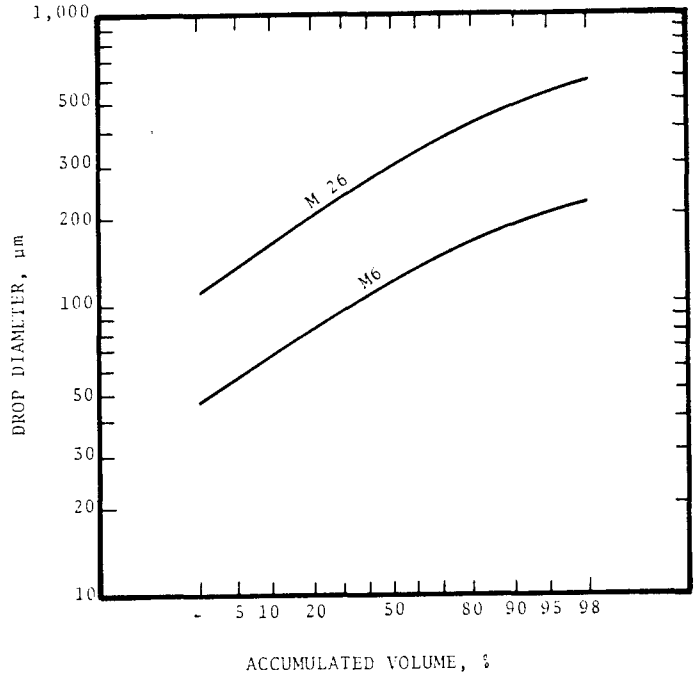

Figure 4-10. Drop diameter versus volume percentage for hollow cone nozzle spraying water at 6.8 atm gauge pressure. (Manufacturer's data)

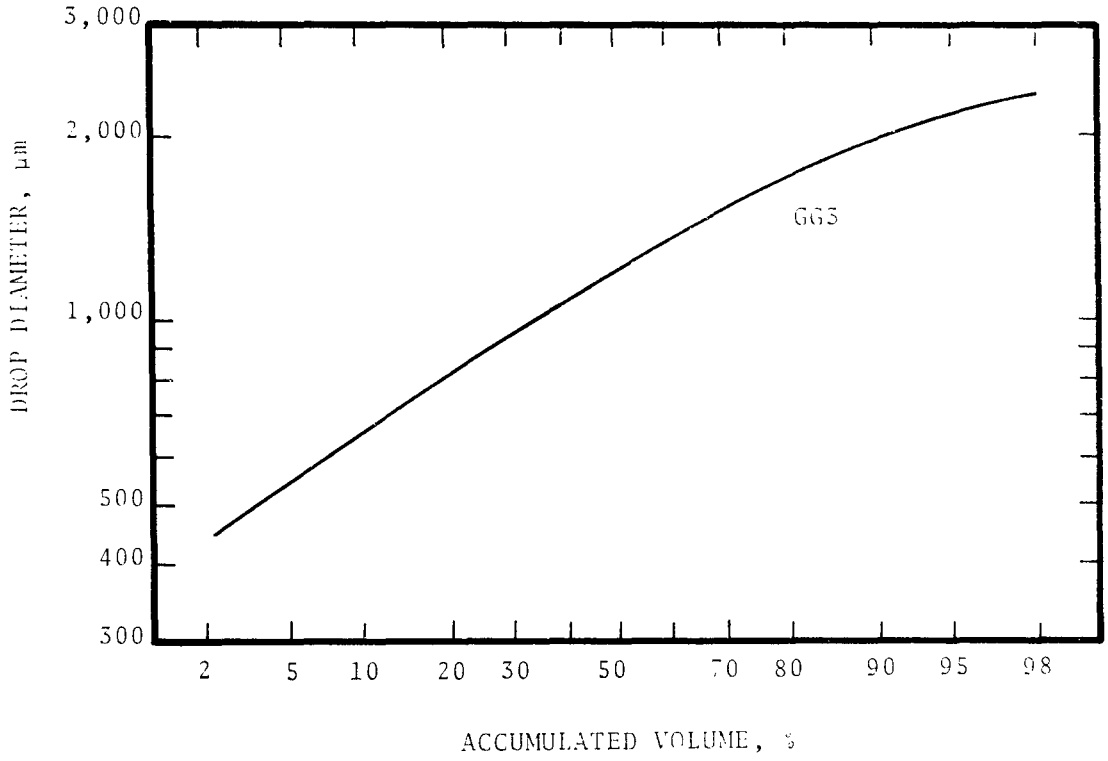

Figure 4-11. Drop diameter versus volume percentage for fulljet nozzles spraying water at 2.7 atm gauge pressure. (Manufacturer's data)

CHAPTER 5

MESH

Knitted mesh of varying density and voidage is widely used for entrainment separators. There are basically three different kinds of mesh: (1) Layers with crimp in the same direction - each layer is actually a nested double layer. (2) Layers with crimp in alternate directions - this results in an increase in voidage, reduced sheltering, a decrease in pressure drop per unit length and an increase in target efficiency per layer (3) Spirally wound layers - the pressure drop is lower by about 2/3 than in layers with crimp in the same direction, but the creeping of fluids, which contributes to reentrainment, is expected to be higher.

Standard mesh 10-15 cm thick having a density of about 0.15 g/cm^3 is used to remove drops larger than 5 μm in diameter. Gas velocities range from 0.3 to 5 m/sec and liquid flow rate is limited by the drainage capacity of the mesh to 2.5×10^{-3} $g/sec\ cm^2$ of mesh. A lower density mesh made of standard wires is used when 10-20% higher flow rates are desired.

Often two mesh type separators in series are used to remove drops in the 1-5 μm diameter range. The first mesh, normally made of fine wires, coalesces the small drops, and the second mesh, made of standard wires, removes them. The first mesh is operated beyond the flooding velocity and the second under flooding velocity. A major disadvantage with this arrangement is a pressure drop which may reach 25 cm W.C.

Some manufacturers use two or three stages of mesh, the first being coarser and the final being finer, to remove large and small drops successively.

A mesh type separator has the advantage that it can be made to fit vessels of any shape. Any material which can be drawn into the shape of a wire can be used for fabrication. However, mesh separators are limited in application because they plug easily. This can be avoided by upstream washing, which will decrease removal efficiency and increase pressure drop.

MATHEMATICAL MODELS

Primary Efficiency

Bradie and Dickson (1969) present the following expression for primary efficiency in mesh separators:

$$E = 1 - \exp\left(-\frac{2}{3}\pi\, a_2 \ell_2\, \eta\right) \qquad (5\text{-}1)$$

where a_2 = specific area of mesh, surface area of wires per unit volume of mesh pad, cm^2/cm^3

ℓ_2 = thickness of mesh pad in the direction of gas flow, cm

η = collection efficiency of cylindrical wire

The collection efficiency of cylindrical wire "η" can be obtained from Figure 3-6. The factor of 2/3 in the exponential was introduced by Carpenter and Othmer (1955) to correct for the fact that all the wires in the knitted mesh are not perpendicular to the flow. That factor is the ratio of the projected area of wires perpendicular to the flow to the cross-sectional area of wires along the wire length.

If the specific area, "a_2",is not specified, it can be determined from the mesh porosity, "ε", and the knitted mesh wire diameter, "d_c"

$$a_2 = \frac{4(1-\varepsilon)}{d_c} \qquad (5\text{-}2)$$

Pressure Drop

York and Poppele (1963) have suggested that the total pressure drop in the knitted mesh is the sum of the pressure drop in the dry knitted mesh and the pressure drop due to the presence of liquid:

$$\Delta P = \Delta P_{dry} + \Delta P_L \qquad (5\text{-}3)$$

where ΔP_{dry} = pressure drop in absence of liquid, cm W.C.
ΔP_L = pressure drop due to presence of liquid, cm W.C.

York and Poppele considered the mesh to be equivalent to numerous small circular channels and used the D'Arcy formula for pressure drop in a pipe to correlate the dry pressure drop through the mesh. York and Poppele's data for knitted mesh with crimps in alternated and in same direction are plotted in Figure 5-1. Their data are close to those obtained by Stasangee (1948) and Shuring (1946). Similar curves obtained by Bradie and Dickson (1969) for spiral-wound and layered mesh are also plotted in Figure 5-1. Figure 5-1 should be used in determining dry pressure drop, which is calculated from the expression

$$\Delta p_{dry} = \frac{f\, \ell_2 a_2\, \rho_G\, u_G^2}{\varepsilon^3} \qquad (5\text{-}4)$$

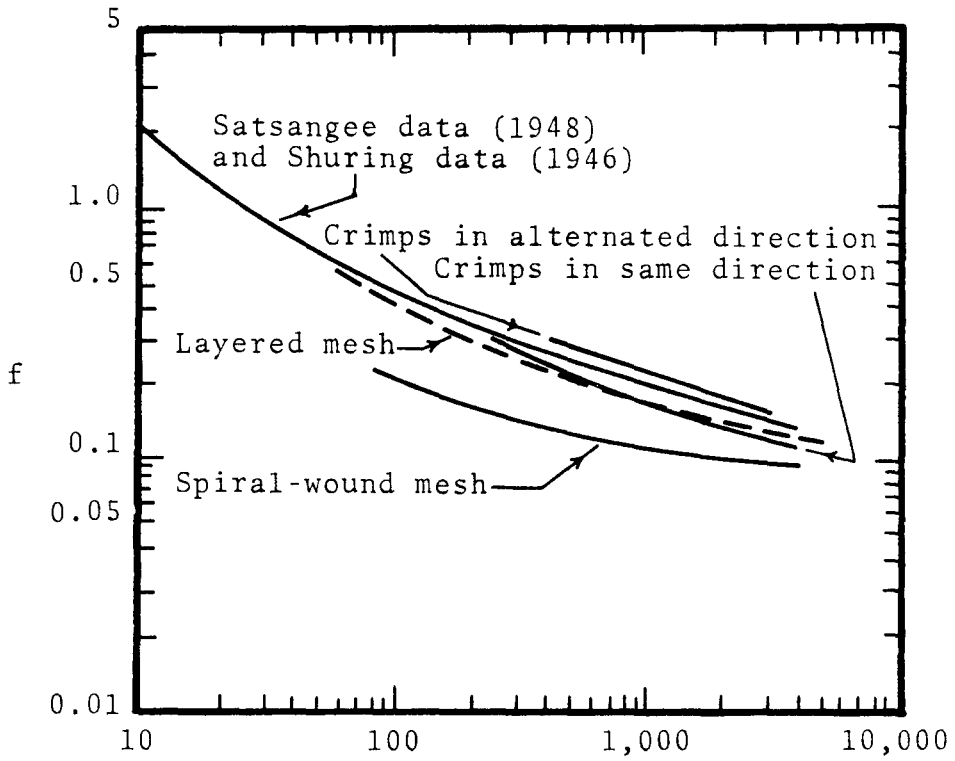

Figure 5-1. Friction Factor, f, versus Reynolds number, $N_{Re,G}$ for wire mesh entrainment separator with entrainment load.

The unit of "ΔP_{dry}" is in dynes/cm^2. It can be converted to cm W.C. by dividing it by 981.

Pressure drop data due to presence of liquid are not available for all operating conditions or for mesh of different styles. Values of "ΔP_L" obtained by York and Poppele are presented in Figures 5-2 and 5-3, with liquid velocity as the parameter. Liquid velocity is defined as $\frac{"L"}{A}$ where 'L' is the volumetric flow rate of liquid and 'A' is the cross-sectional of the mesh in liquid flow direction. The specifications of the knitted mesh used are shown in the two figures.

Maximum Allowable Gas Velocity

Several factors govern the allowable gas velocity through wire mesh for a given set of conditions:

1. ρ_L and ρ_G
2. liquid viscosity
3. specific surface
4. liquid entrainment loading
5. suspended solid content

Application of the Souders-Brown equation for the calculation of allowable vapor velocity for wire mesh mist eliminator based on gas and liquid densities has been suggested by York (1954).

$$u_{G\ max} = 30.5\ a_3 \left(\frac{\rho_L - \rho_G}{\rho_G} \right)^{0.5} \qquad (5\text{-}4)$$

where "a_3" varies with operating conditions and mesh design. For most cases, $a_3 = 0.35$. For air-water system, $u_{G\ max} = 3.1$ m/sec.

When liquid viscosity and entrainment loading are high, or the liquid very dirty, a reduced value of "a_3"

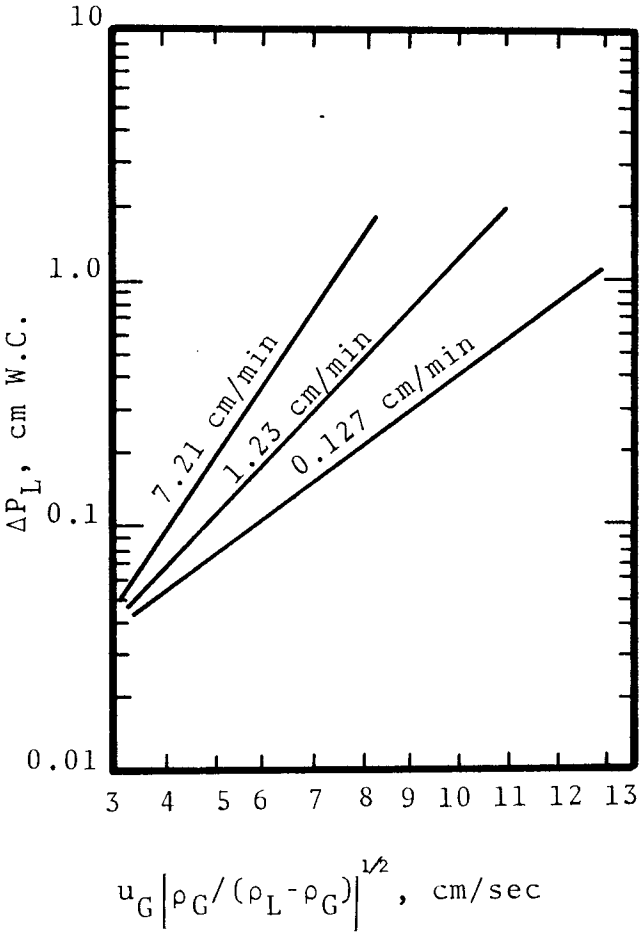

Fig. 5-2. Pressure drop due to presence of liquid in the knitted mesh with the crimps in the same direction.

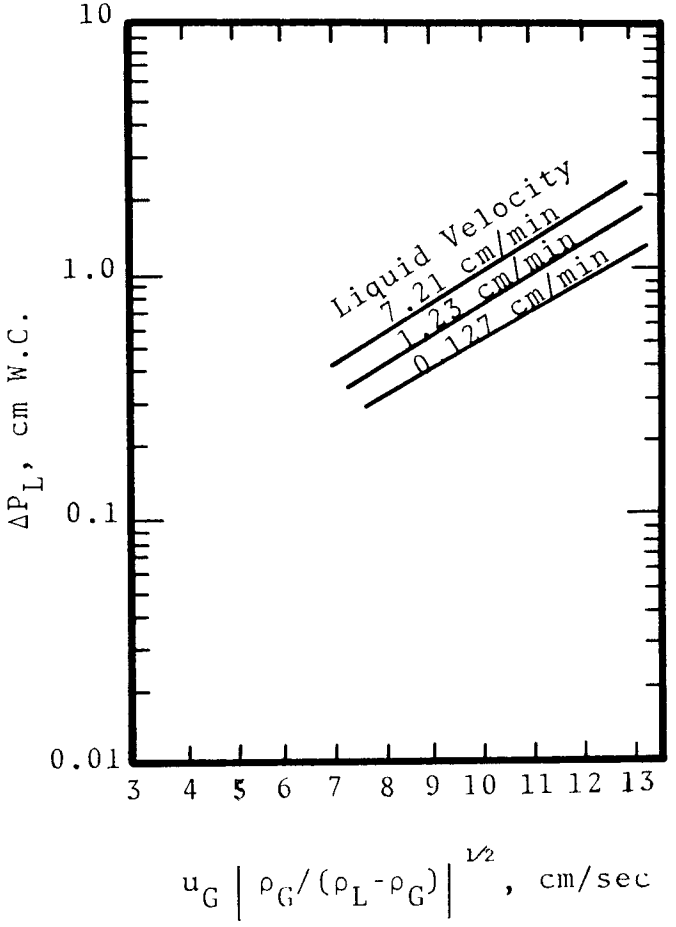

Fig. 5-3. Pressure drop due to presence of liquid in the knitted mesh with the crimps in the alternate direction.

must be used. The influence of liquid entrainment loading upon "a_3" has been investigated by Poppelle (1958) for an air-water system. The data for the incipient flooding are shown in Figure 5-4 together with the flooding velocity correlation by Sherwood (1938) for dumped rings. Also shown is a recommended design curve.

EXPERIMENTAL RESULTS AND DISCUSSION

Overall Efficiency

The overall collection efficiency data for horizontal flow through wire mesh are plotted in Figure 5-5. No penetration was observed in the experiments at low gas velocity, less than 3.0 m/sec. At higher velocities, penetration due to reentrainment was observed. The dotted line, predicting 100% efficiency, represents the theoretical curve based on equation (5-1).

The overall collection efficiency data for vertical flow through wire mesh is plotted in Figure 5-6. Water flow rate is used as a parameter. M6 nozzles were used in the experiments. The effect of higher water flow rate is to increase the penetration and decrease the onset of reentrainment velocity.

If the performance of entrainment separators with vertical air flow and horizontal air flow is compared, the experimental data lead to the following conclusions:

1. Reentrainment velocities are lower in the system with vertical gas flow than with horizontal gas flow. This is because vertically installed mesh provides better drainage.
2. The amount of reentrainment is higher in the system with vertical gas flow than with horizontal gas flow.

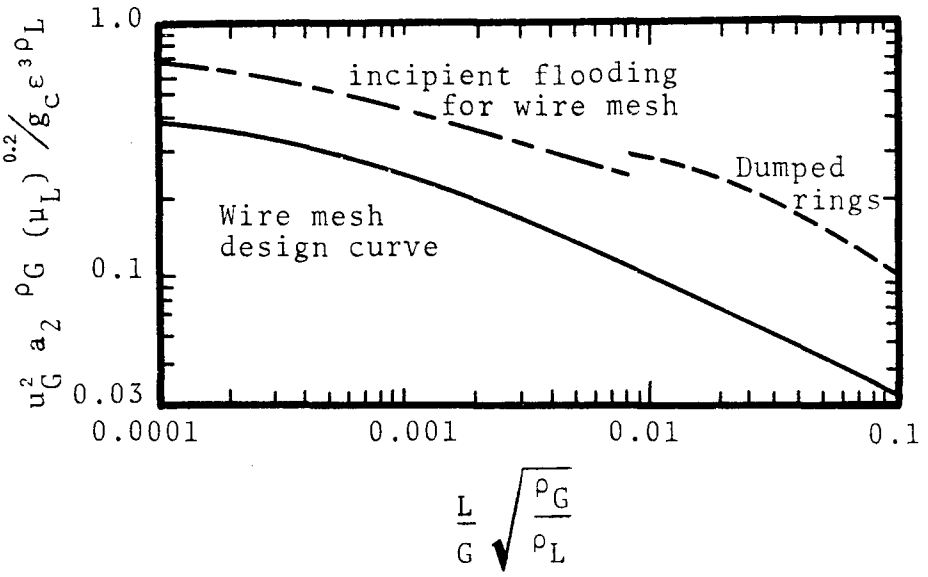

Figure 5-4. Effect of liquid entrainment load on allowable gas velocity.

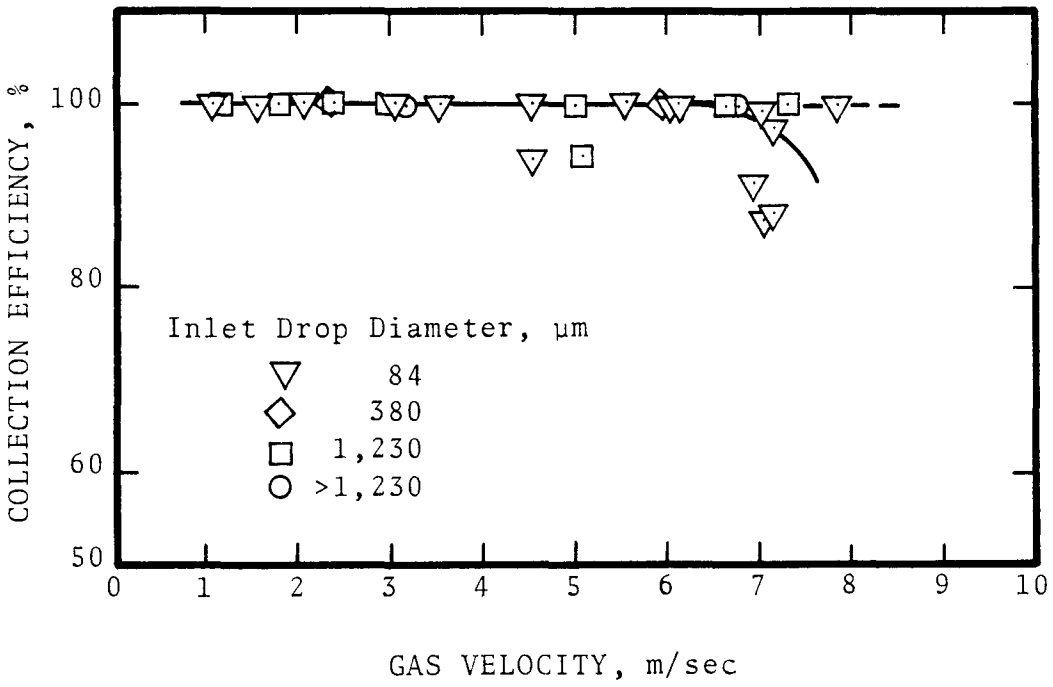

Figure 5-5. Experimental collection efficiency of wire mesh for horizontal gas flow.

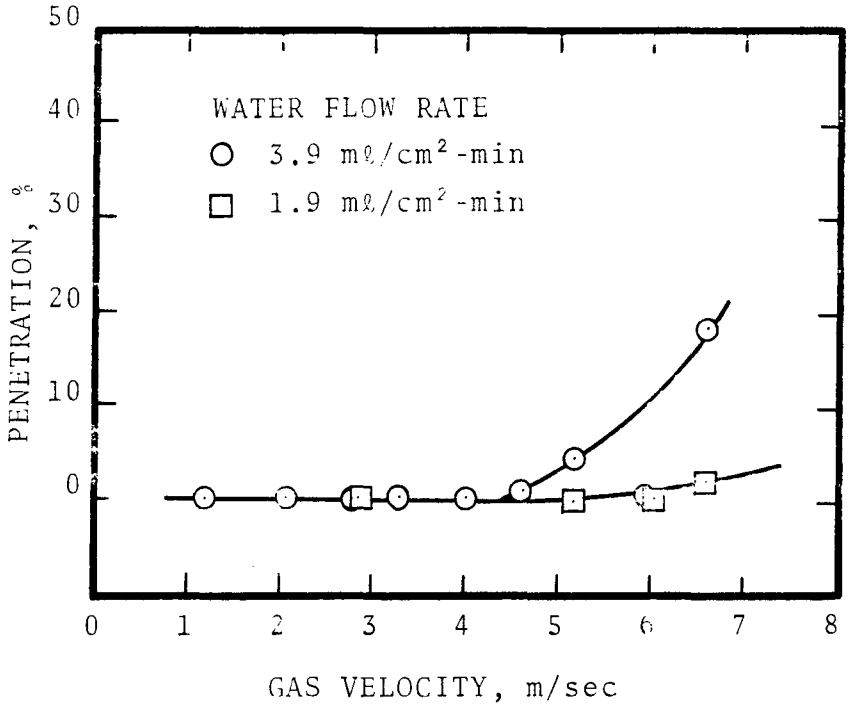

Figure 5-6. Experimental penetration for vertical gas flow up mesh.

Pressure Drop

The pressure drop in wire mesh is highly affected by the liquid load, as seen in Figure 5-7. The slope of the straight lines on the log-log plot is 1.65; thus "p" can be represented as a function of $u_G^{1.65}$. In Figure 5-6, L/A = 0, represents the dry pressure drop, "ΔP_{dry}", through the mesh. For $0 < L/A < 1$, the pressure drop is 1.5 ΔP_{dry} and for $1 < L/A < 5$, the pressure drop is 2.3 ΔP_{dry}.

Figure 5-8 shows the comparison between experimental and predicted dry pressure drop in mesh. As can be seen, the experimental dry pressure drop is about 1/3 of that calculated from Figure 5-1.

The pressure drop data for vertical flow are given in Figure 5-9. As can be seen, when comparing Figures 5-7 and 5-9, the pressure drop data are comparable for both horizontal and vertical air flows.

Reentrainment

The outlet mass median drop diameter as a function of horizontal gas velocity is plotted in Figure 5-10. Drop size samples were taken at a location 95 cm downstream from the mesh and at the center of the duct. Figure 5-10 shows there is a dependence of median drop diameter on gas velocity. This dependence is primarily due to drop settling. For low gas velocities, large drops were settled out before they could reach the sampling point. The maximum drop diameter that can occur at the sampling point can be predicted from drop terminal settling velocity (Figure 3-7).

Figure 5-11 shows a straight line correlation between geometric standard deviation and the mass median drop diameter in the outlet. If a secondary collection device is to be used to collect the reentrainment from the mesh,

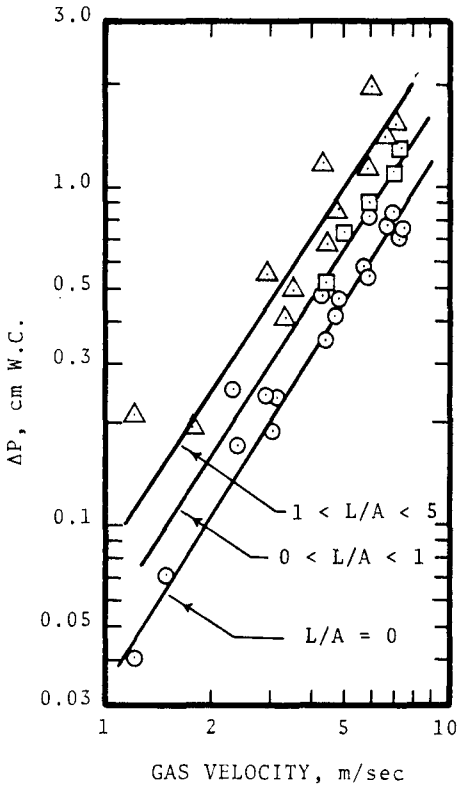

Figure 5-7. Pressure drop in wire mesh versus horizontal gas velocity with liquid load as parameter.

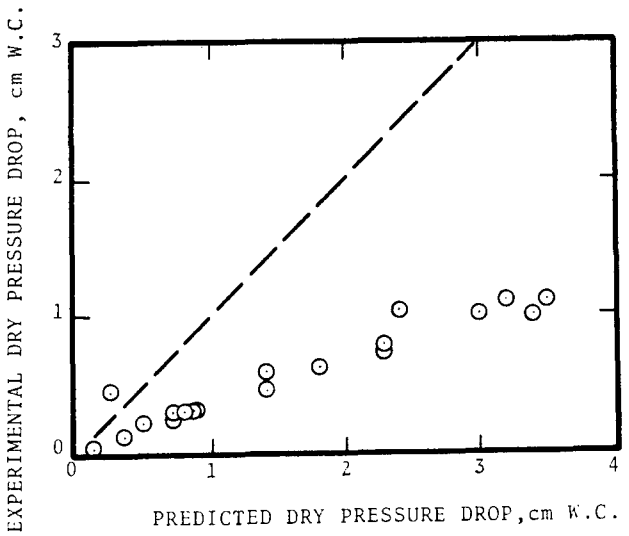

Figure 5-8. Comparison between experimental and predicted dry pressure drop for mesh.

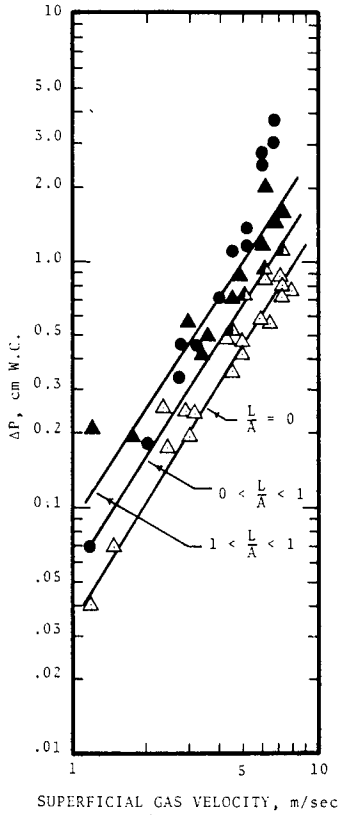

Figure 5-9. Pressure drop in knitted mesh versus vertical gas velocity with liquid load as parameter.

$\frac{L}{A}$ = Superficial liquid velocity, cm/min

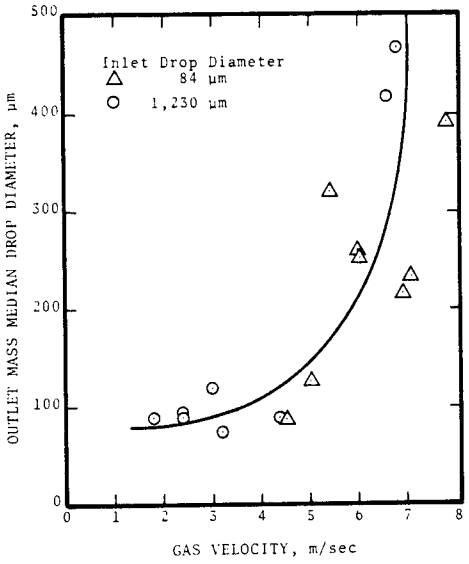

Figure 5-10. Outlet drop diameter for mesh separator with horizontal gas flow.

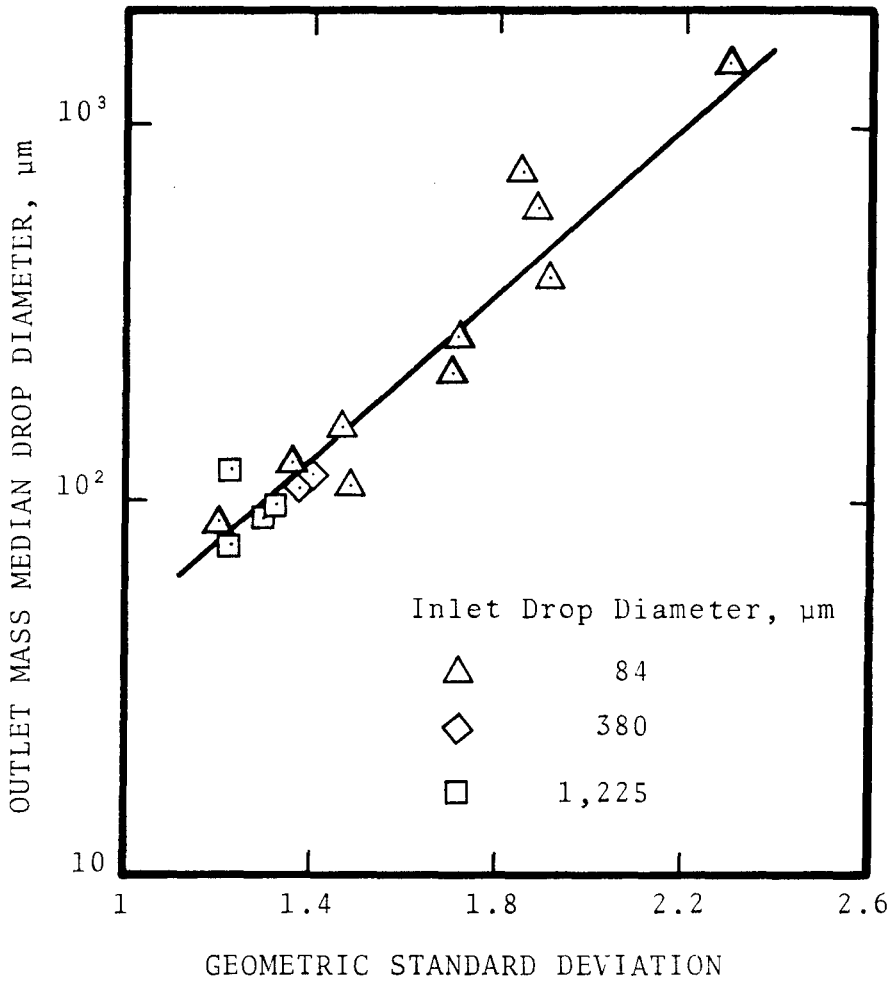

Figure 5-11. Drop diameter versus geometric standard deviation for mesh.

information presented in Figures 5-10 and 5-11 can be employed to make a proper selection of the device.

Figure 5-12 shows the effect of liquid to gas ratio on gas velocity for onset of reentrainment. The shaded area is the region where reentrainment was observed. Thus, the boundary line relates entrainment loading to maximum permissible gas velocity through mesh without causing re-entrainment.

Figure 5-13 compares the reentrainment onset velocity obtained in the present study with Poppele's data. The present study observed a higher reentrainment than the flooding velocity observed by Poppelle.

Buerkholz (1970) collected reentrainment data for sulfuric acid mist 150 cm downstream of a mesh separator. He found that reentrainment increased from 1.6 to 4.0% of collected liquid (0.3 to 1.3 mg/m^3) as the gas velocity was increased from 4.7 to 8.2 m/sec. The outlet mass median drop diameter also increased from 150 to 750 μm. Buerkholz' data, plotted in Figure 5-13, were collected on a 15 cm x 15 cm mesh with sedimentation present between the mesh and the sampling point. The solid line in Figure 5-14 is the onset of reentrainment curve obtained in the present study. The data show good agreement in determining the reentrainment velocity of 5 m/sec at very small liquid loads.

The reentrainment curve obtained from the manufacturer also appears in Figure 5-14. The manufacturer predicts higher reentrainment velocity than the present results.

Visual Observation of Reentrainment

Reentrainment in the mesh section was observed to take place in the following ways:

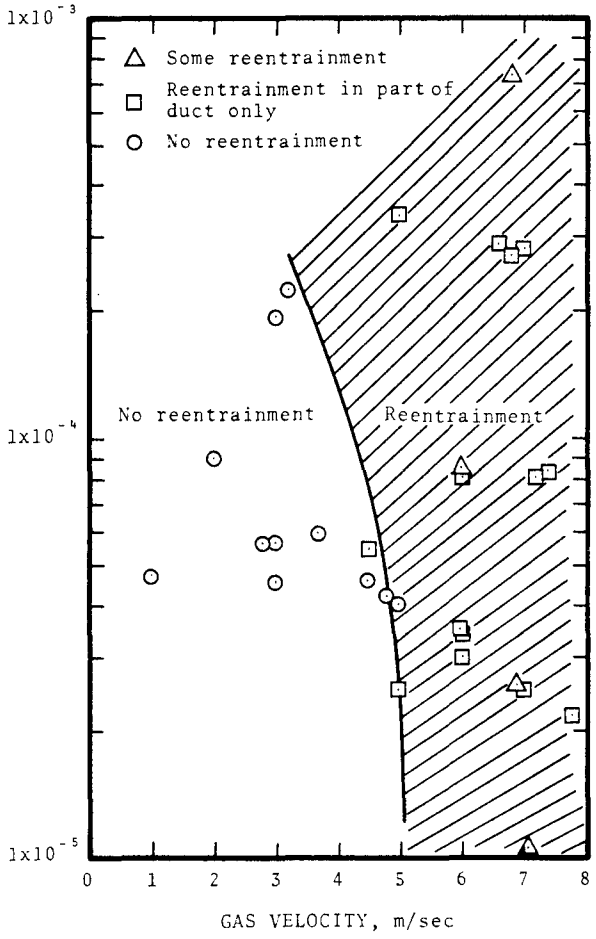

Figure 5-12. Effect of gas velocity and liquid load on performance of mesh.

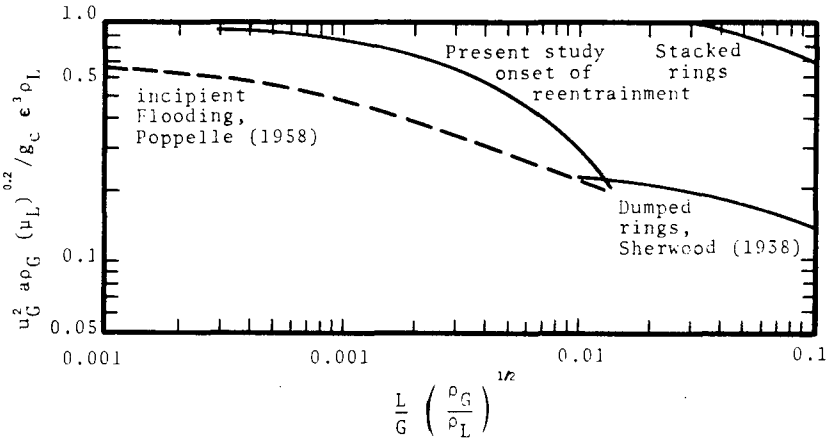

Figure 5-13. Effect of entrainment load on reentrainment onset velocity.

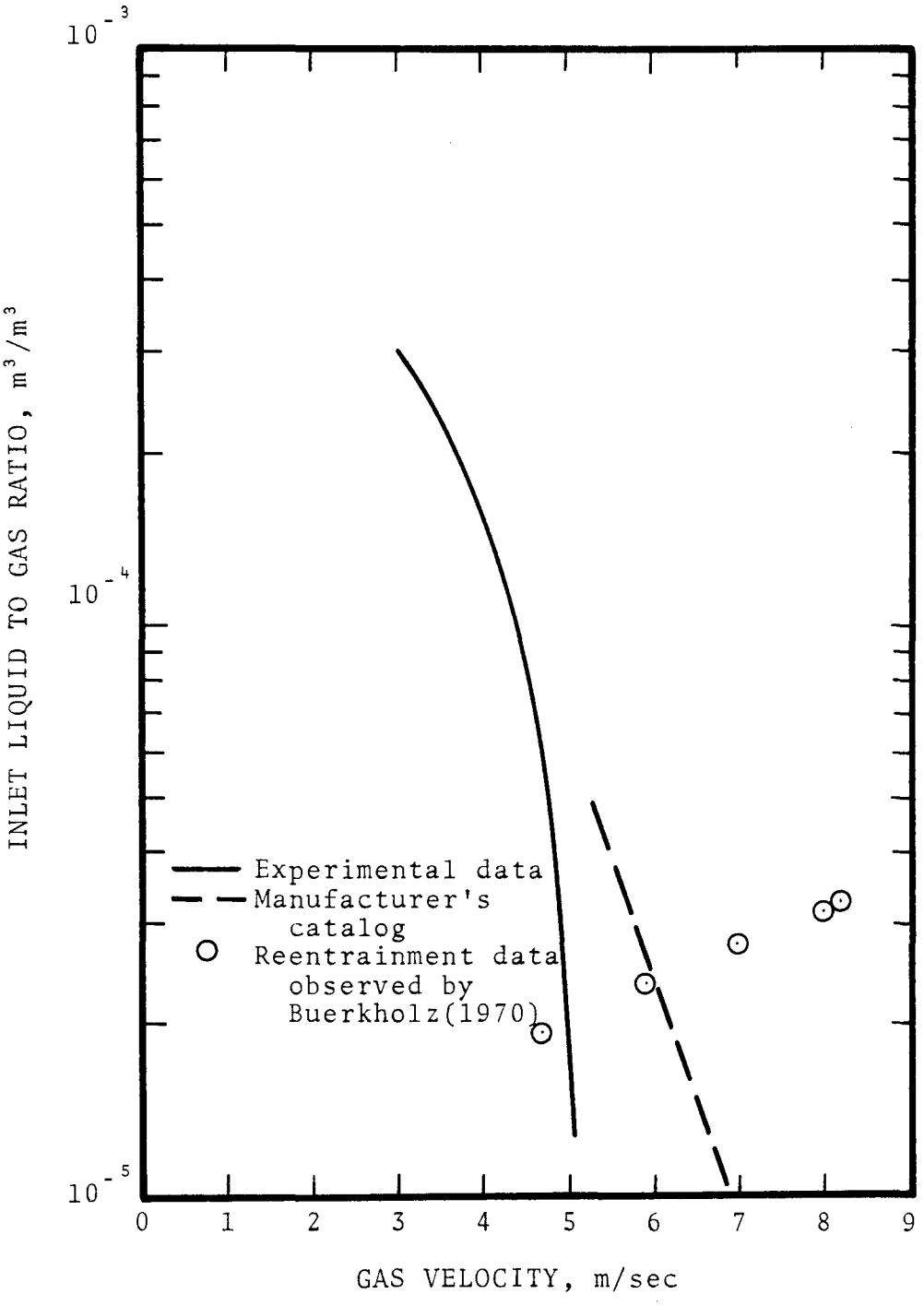

Figure 5-14. Onset of reentrainment velocity curves of mesh for horizontal gas flow.

1. At low liquid loads the mesh operated without flooding. Apparently, the drops that are collected on the mesh wires grew to 3-5 mm diameter before they drained down. If the air velocity is high, the path of the drop is not vertically downward. Some of these drops were airborne and struck the wires of the grid supporting the mesh.
   Normally, the drop shattered into one large drop slightly smaller than the original size and 2-4 satellite drops, which were reentrained.
   Some of the drops collected on the grid wire drained at once, whereas the rest drained after growing to a larger size. There were other drops which missed striking any wires and emerged from the mesh. These drops were collected at the downstream side of the mesh. The drops passing through the mesh without striking any wires were carried farther downstream of the mesh than others. All these reentrained drops were 4-5 mm in diameter and upon reaching the bottom, they shattered into a few (3-4) satellite drops. The rest of the liquid in the original drop was mixed with the liquid film at the bottom. These satellite drops flew into the air due to kinetic energy, and their initial trajectory formed a cone along a vertical axis. The angle of the cone was dependent upon initial drop velocity and was observed to range from 0° to 90°. Some of these satellite drops were reentrained while others fell down.
2. Some drops were reentrained inside the mesh, and the process of reentrainment could not be observed; it is assumed to be the same as described in the earlier part of the first method.

3. When the liquid load was high, partial flooding was observed. Reentrainment by methods 1 and 2 took place above the flooded zone. In the flooded section the air flow rate was low. The flooded section was partially covered by the falling drops from above on the downstream side of the mesh. The reentrainment mechanism was rupture of bubbles, but it could not be observed properly.

CONCLUSIONS

Based on the data obtained above, the following conclusions can be drawn:

1. Bradie and Dickson's expression in predicting primary efficiency agrees quite well with the experimental data.
2. Pressure drop data can be correlated by the expression

$$\Delta P = a_7 \, u_G^{1.65}$$

where "a_7" is a constant dependent on "L/A".

3. Pressure drop data are comparable for both horizontal and vertical air flows.
4. Reentrainment velocities are lower in the system with horizontal gas flows than with vertical gas flows.
5. The amount of reentrainment is higher in the system with vertical gas flow than with horizontal gas flow.

CHAPTER 6

PACKED BED

Packed beds of standard design with a capacity of up to 65 m^3/sec (140,000 CFM) are available. They can remove drops as small as 3 μm in diameter at 80-90% efficiency. Superficial gas velocities range from 75 to 250 cm/sec, and pressure drop is generally low, 0.05 - 0.1 cm W.C. per cm of bed length.

Cross flow beds are claimed to have high drainage efficiency and therefore are less prone to plugging. Upstream washing is recommended to avoid plugging if solids are present in the drops to be removed.

Packing in different materials, shapes and sizes is available. Various rings are claimed to have high collection efficiency and low pressure drop.

Packed beds are often used for mass transfer because of their high interfacial area. Thus they are sometimes employed when simultaneous mass transfer and entrainment separation are desired.

MATHEMATICAL MODELS

Primary Efficiency

Jackson and Calvert (1966) and Calvert (1968) have developed a theoretical relationship between particle collection efficiency and packed bed operating parameters. Their formulation included the following assumptions:

1. The drag force on the drop is given by Stokes Law.

2. The number of semicircular bends, "n_1", is related to the overall length, "Z", of the packed section of the bed, the packing diameter, "d_c", and the channel width, "b", where any consistent units may be used, by:

$$n_1 = \frac{Z}{d_c + b}$$

3. The gas velocity through the channels, u_{Gb} is inversely proportional to the free volume of the bed available for gas flow, where any consistent units may be used:

$$u_{Gb} = u_G \left(\frac{1}{\varepsilon - H_d} \right)$$

where u_G is the superficial gas velocity of the bed (volumetric flow rate divided by total cross sectional area of the shell), "ε" is the bed void fraction (porosity), and "H_d" is the liquid holdup within the bed, i.e. the fraction of the total bed volume taken up with liquid. Table 6-1 lists values of bed porosity, ε, for beds using various packing materials.

4. The width of the semicircular channels, b, can be described as a fraction, j, of the diameter of a single packing element:

$$b = j\, d_c$$

These assumptions lead to the following equation for predicting the particle penetration for a packed bed.

$$Pt = 1 - \exp\left[\frac{-\pi}{2(j + j^2)(\varepsilon - H_d)} \frac{Z}{d_c} K_p \right] \qquad (6\text{-}1)$$

$$K_p = \frac{\rho_d\, d_d^2\, u_G}{9\, \mu_G\, d_c}$$

where j = ratio of channel width to packing diameter
H_d = fractional liquid hold-up in the bed
ε = bed porosity
Z = bed length, cm
d_c = packing diameter, cm
u_G = superficial gas velocity, cm/sec
d_d = drop diameter, cm

The experimental data of Jackson (1964) were analyzed to determine appropriate values of "j" to use in Equation 6-1 with all quantities in the equation known except "j", which was calculated. The results are given in Table 6-2 which lists "j" values for various types and sizes of packing material. For the manufactured packing materials, "j" is fairly constant at about 0.16 - 0.19. The very low value of 0.03 for coke may be due to the small passages within the coke itself, which make each large piece of coke function effectively as a number of smaller pieces.

Pressure Drop

Perry (1963) gives a generalized pressure drop and flooding correlation plot which appears as Figure 6-1, where a dimensional group of function $\frac{G^2 F \Psi \mu_L^{0.2}}{\rho_G \rho_L g}$, (centipoise) $^{0.2}$, is plotted against a dimensionless group of function $\frac{L}{G}\left(\frac{\rho_G}{\rho_L}\right)^{1/2}$, where "G" and "L" refer to the gas and liquid mass flow rates respectively. "Ψ" is the ratio of water density to entrained liquid density. Values for the packing factor, "F", for dumped pieces, stacked pieces and grids are given in Tables 6-3 and 6-4. If "F" is not known, $\frac{a}{\varepsilon^3}$ may be used instead.

TABLE 6-1

BED POROSITY, ε, FOR VARIOUS PACKING MATERIALS

Name	Stoneware Raschig Rings	Carbon Raschig Rings	Steel Raschig Rings (1/16" thick)	Stoneware Berl Saddles	Stoneware Intalox Saddles	Steel Pall Rings
Size (cm)						
1.27	0.57*	0.71*	--	--	--	--
1.9	0.67	--	--	0.65	--	--
2.54	0.68	0.75	0.92	0.69	0.70	0.93
3.8	0.68	0.67	0.92	0.70	0.81	0.94
5.1	0.75	--	--	--	--	--

*Treyball (1955) All other data from Perry (1963)

TABLE 6-2

EXPERIMENTAL VALUES OF
j, CHANNEL WIDTH AS FRACTION OF PACKING DIAMETER

Size (cm)	Type of Packing	j
1.27	Berl Saddles, marbles, Raschig Rings, Intalox Saddles	0.192
2.54	Berl Saddles, Raschig Rings, Pall Rings	0.190
3.8	Berl Saddles, Raschig Rings Pall Rings	0.165
7.6 - 12.7	Coke	0.03

Adapted from Jackson (1964) and Calvert (1968)

Table 6-3. PACKING FACTORS, "F", FOR DUMPED PIECES (m^2/m^3)

	Nominal size of packing, cm										
	[0.64]	[0.95]	[1.27]	[1.59]	[1.9]	[2.5]	[3.2]	[3.8]	[5]	[8]	[10]
Raschig rings, ceramic											
.16 cm wall	5,250	3,280									
.32 cm wall						510					
.63 cm wall								430	210		
.95 cm wall										121	98
Raschig rings, carbon											
.16 cm wall	5,250		1,340								
.32 cm wall					920	525					
.63 cm wall								430	210		
.79 cm wall										118	
Raschig rings, metal											
.08 cm wall	2,300	1,280	980	560	510	380					
.16 cm wall			1,340	950	720	450	360	272	187	105	
Lessing rings, porcelain											
.32 cm wall						(800)					
.63 cm wall									(360)		
Lessing rings, metal											
.08 cm wall			(1,060)		(630)						
.16 cm wall						(472)	(387)	(295)	(200)		

Table 6-3. PACKING FACTORS, "F", FOR DUMPED PIECES (m^2/m^3) (continued)

	Nominal size of packing, cm										
	[0.64]	[0.95]	[1.27]	[1.59]	[1.9]	[2.5]	[3.2]	[3.8]	[5]	[8]	[10]
Partition rings										262	190
Pall rings, plastic				318		171		105	82		
Pall rings, metal				230		158		92	66		
Berl saddles	2,950		790		560	360		213	148		
Intalox saddles, ceramic	2,380	1,080	660		475	322		171	131	72	
Intalox saddles, plastic						108			69	52	
Super-Intalox, ceramic						200			100		
Tellerettes									150		

Parentheses denote a value of a/ε^3, rather than empirical F.

Table 6-4. PACKING FACTORS,"F", FOR GRIDS AND STACKED PIECES (m^2/m^3)

	Nominal size of packing, cm							
	2.5	3.8	5	8	10	13	14	15
Wood grid	20	11	8.2	5.9	4.9			
Metal grid	8.2							
Grid tiles						118		
Checker brick, ε=0.55							135	
Raschig rings, ceramic								
.63 cm wall			95	16				
.95 cm wall				36	12.8			
Raschig rings, metal				21				
Partition rings, diameter								
7.6 cm length				(1,200)	(725)			
10.2 cm length					(705)			(410)
15.2 cm length								(375)
Partition rings, square set								
7.6 cm length				(690)	(460)			
10.2 cm length					(450)			(275)
15.2 cm length								(260)

Parentheses denote a value of a/ε^3, rather than empirical F.

The operation of packed beds is limited by flooding. The flooding lines for dumped pieces, grids and stacked rings are shown in Figure 6-1. Pressure drop should be obtained by using the largest gas and liquid streams.

EXPERIMENTAL RESULTS AND DISCUSSION

Overall Efficiency

Efficiency data for horizontal gas flow through 30 cm of 2.5 cm Pall rings are presented in Figure 6-2. Runs at superficial gas velocities lower than 6.0 m/sec did not show any penetration. There were negligible reentrainment when gas velocity was higher than 6m/sec. The theory for primary collection efficiency, shown as a solid line, is based on equation 6-1 and predicts 100% primary efficiency over the range of gas velocities studied.

Overall efficiency data for vertical gas flow is plotted in Figure 6-3. Inlet liquid loading is used as a parameter. The mass median drop diameter of the inlet entrainment is 84 μm. It can be observed that the rate of reentrainment is increased as liquid loading is increased. Heavy reentrainment started at a gas velocity of 6m/sec.

The bed when installed in vertical direction (i.e. horizontal gas flow) has higher collection efficiency than the bed installed horizontally. This is because the vertical bed has a higher liquid drainage capability.

Pressure Drop

Figures 6-4 and 6-5 show the dry and wet pressure drops respectively for horizontal gas flow. There is no effect of liquid load on pressure drop for the liquid loading used in the present study. Figure 6-6 shows the wet pressure drop data for horizontal and vertical gas flows. It can be observed that the gas flow orientation has little effect on pressure drop.

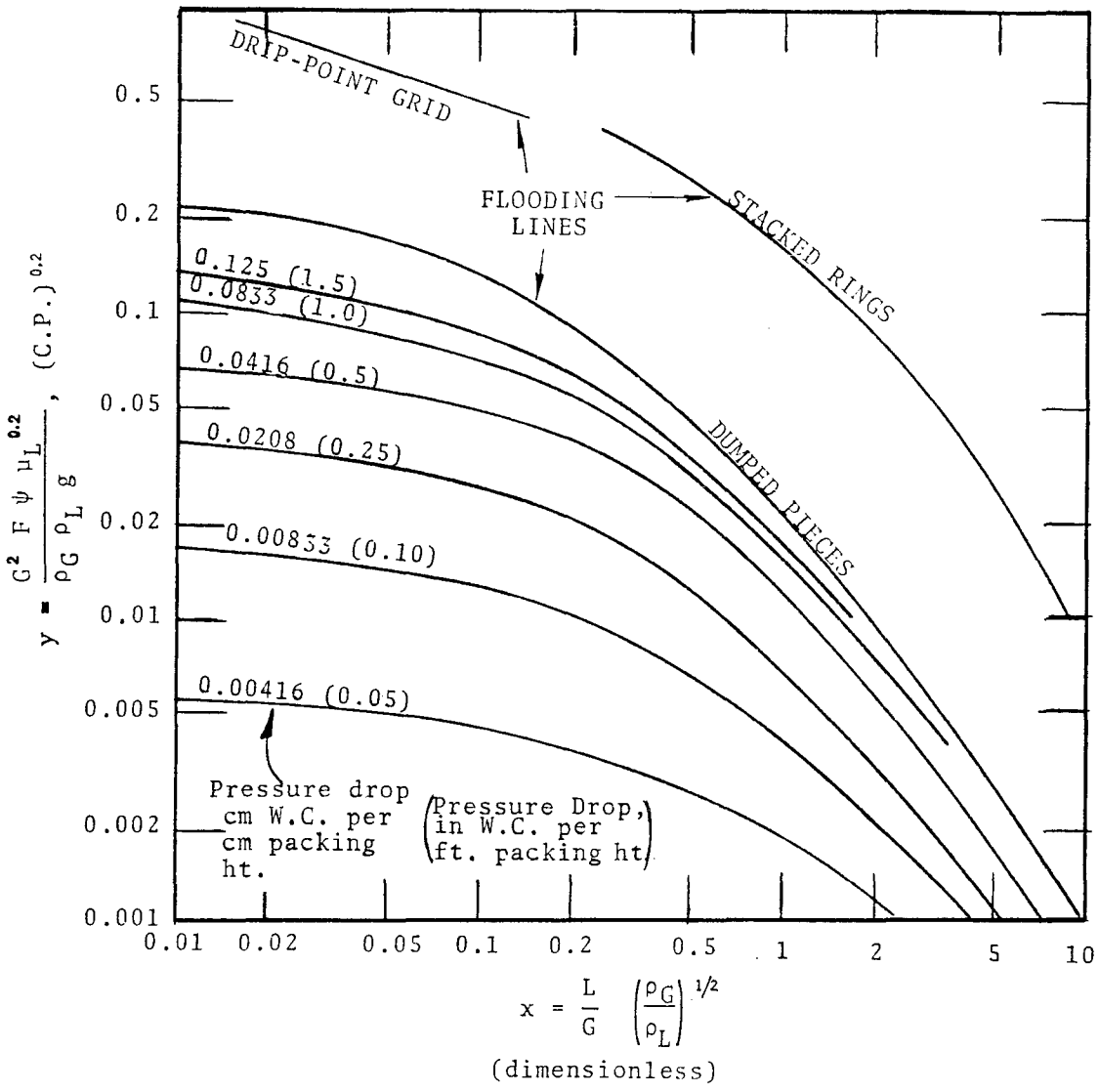

Figure 6-1 - Generalized flooding and pressure drop correlation for packed beds (Perry, 1963).

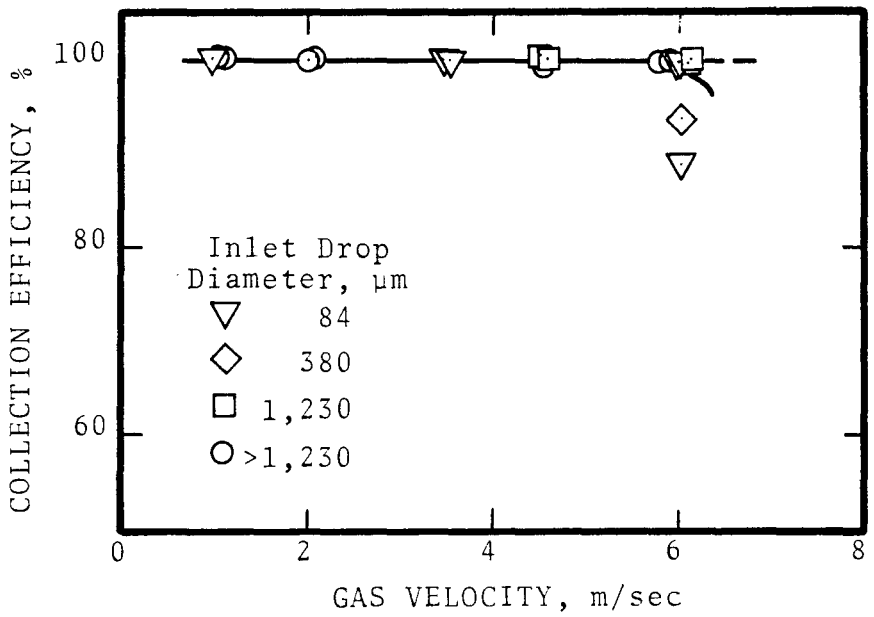

Figure 6-2. Experimental collection efficiency in packed bed, horizontal gas flow, Pall rings.

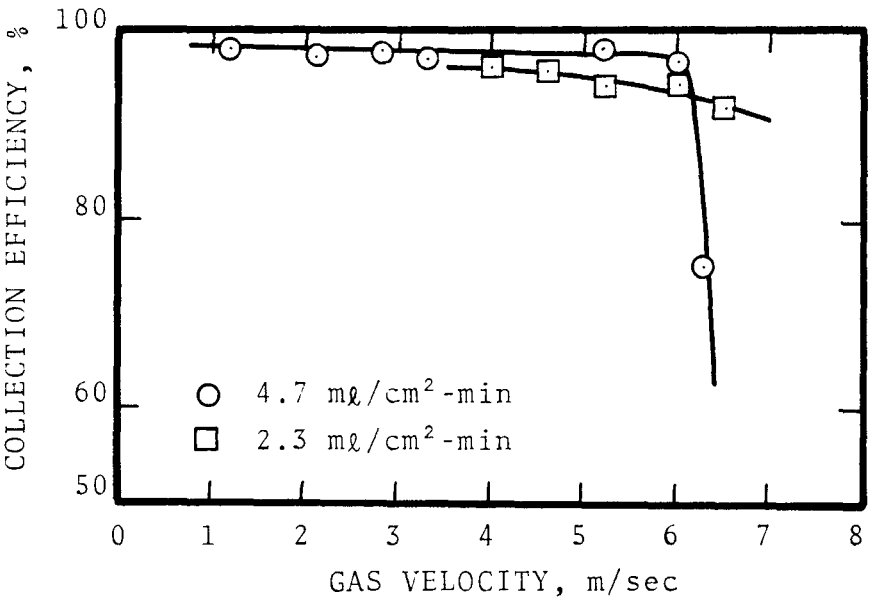

Figure 6-3. Collection efficiency in packed bed, vertical gas flow, Pall rings.

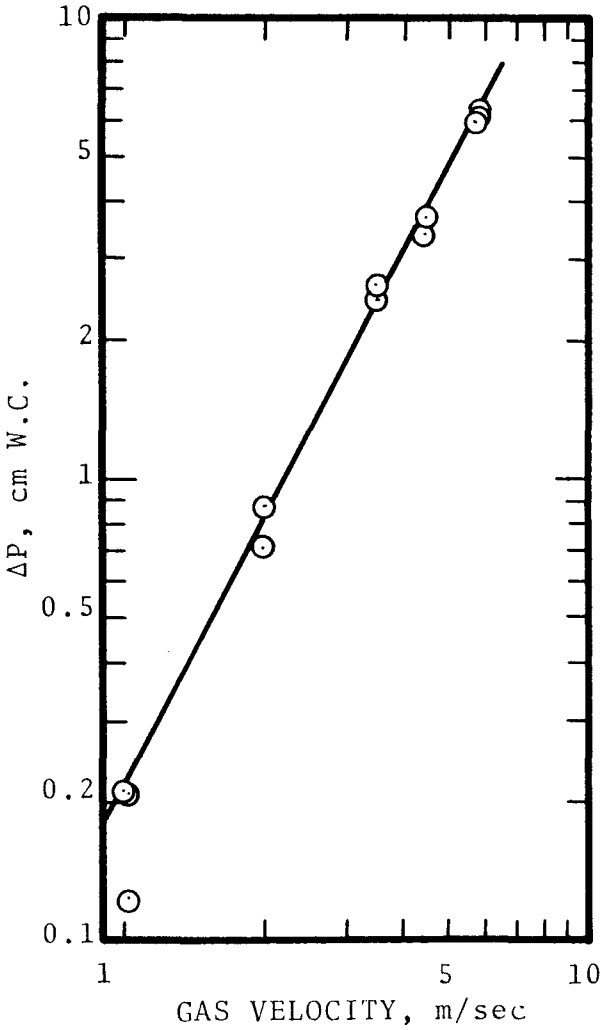

Figure 6-4. Dry pressure drop in packed bed, Pall rings.

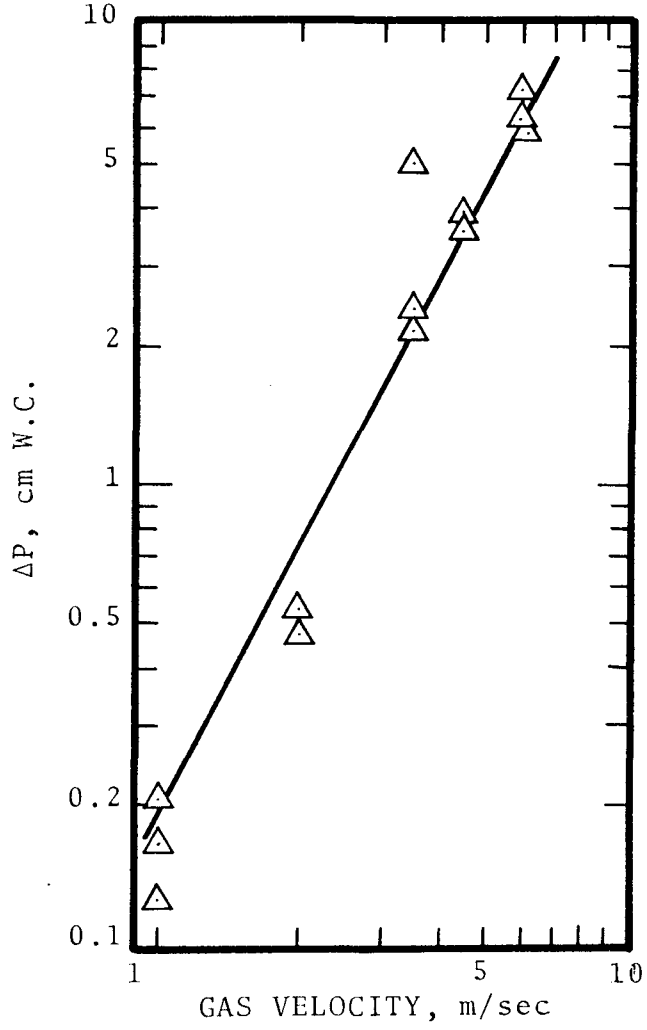

Figure 6-5. Wet pressure drop in packed bed, Pall rings.

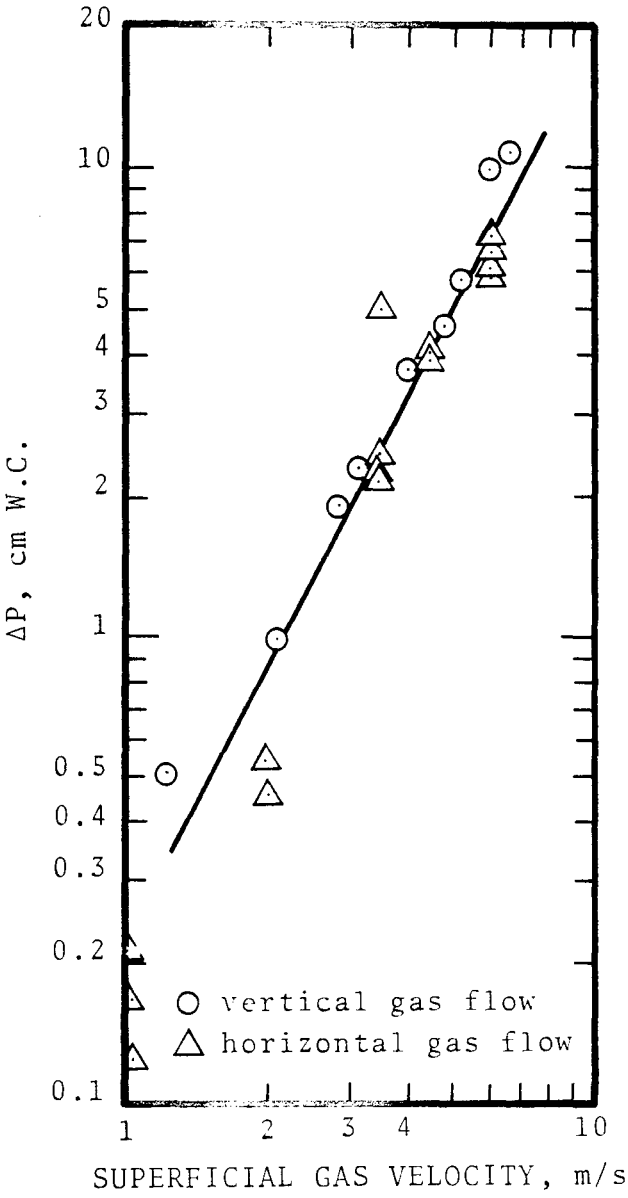

Figure 6-6. Wet pressure drop in packed bed, Pall rings.

Figure 6-7 compares the measured pressure drops with those predicted by the generalized correlation. As can be seen, the predicted pressure drop is higher than that measured in the present study. Thus the generalized correlation will give a conservative design.

Reentrainment

Reentrainment was observed to start when the bed became flooded. In the present study, for a liquid loading, L/G, ranging from 10^{-6} to 10^{-3}, reentrainment was observed to start at a superficial gas flow of 6 m/sec for a bed of 2.5 cm Pall rings when the bed was operated in cross flow. This reentrainment onset gas velocity is higher than the flooding velocity calculated from the generalized flooding correlation. Possibly this is due to cross flow bed offering better drainage capability. Figure 6-8 shows the correlation of reentrainment velocity along with flooding lines for dumped pieces, stacked rings and drip-point grid.

CONCLUSION

The following conclusions are drawn based on the above experimental results for a packed bed:

1. The model developed by Jackson and Calvert agrees well with experimental data in predicting primary collection efficiency.
2. The effect of gas flow orientation on overall efficiency in the packed bed is not significant.
3. Neither liquid load nor gas flow orientation has any significant effect on pressure drop provided there is good drainage.
4. The gas velocity for the onset of reentrainment from a cross flow bed of 2.5 cm Pall

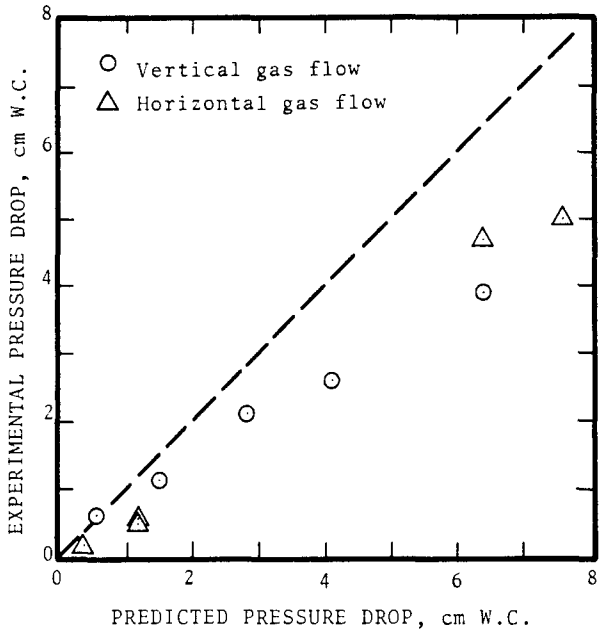

Figure 6-7. Experimental versus predicted pressure drop across 30 cm of 2.5 Pall rings.

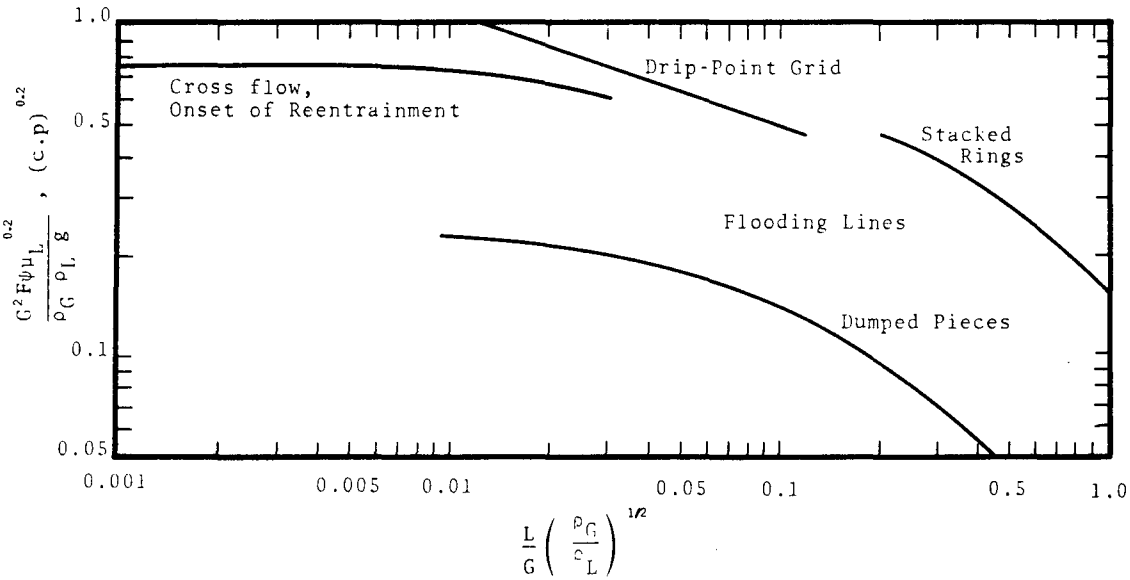

Figure 6-8. Correlation for onset of reentrainment in cross flow beds.

rings is 6 m/sec, and is not affected by liquid load.

5. Generalized pressure drop correlation (Figure 6-1) predicts a higher pressure drop across the bed than that measured in this study.

CHAPTER 7

TUBE BANK

Tube banks made of streamlined struts have been used as entrainment separators but no experience with round tubes has been reported. Particle collection efficiency and pressure drop for round tube banks have been studied and the characteristics appeared promising for entrainment separation application. Therefore, the performance of tube banks for use as entrainment separators was chosen for study as a possible basis for the development of improved devices

MATHEMATICAL MODELS

Primary Efficiency

Calvert and Lundgren (1970) found that the collection efficiency for closely packed rods is given by the equation for rectangular jet impaction. The collection efficiency of each stage of impaction can be found in Figure 7-1. Each row of tubes except the first represents one stage of impaction. "β" is used as a parameter in Figure 7-1 and is defined by:

$$\beta = 2\ \ell/b \qquad (7\text{-}1)$$

where b = jet orifice width

ℓ = distance between orifice and impingement plane

"K_p", the inertia parameter, is defined with drop radius, "r_p", rather than diameter as in Figure 3-3.

Efficiency for the bank of tubes is given by:

$$E = 1 - (1 - n_j)^N \qquad (7\text{-}2)$$

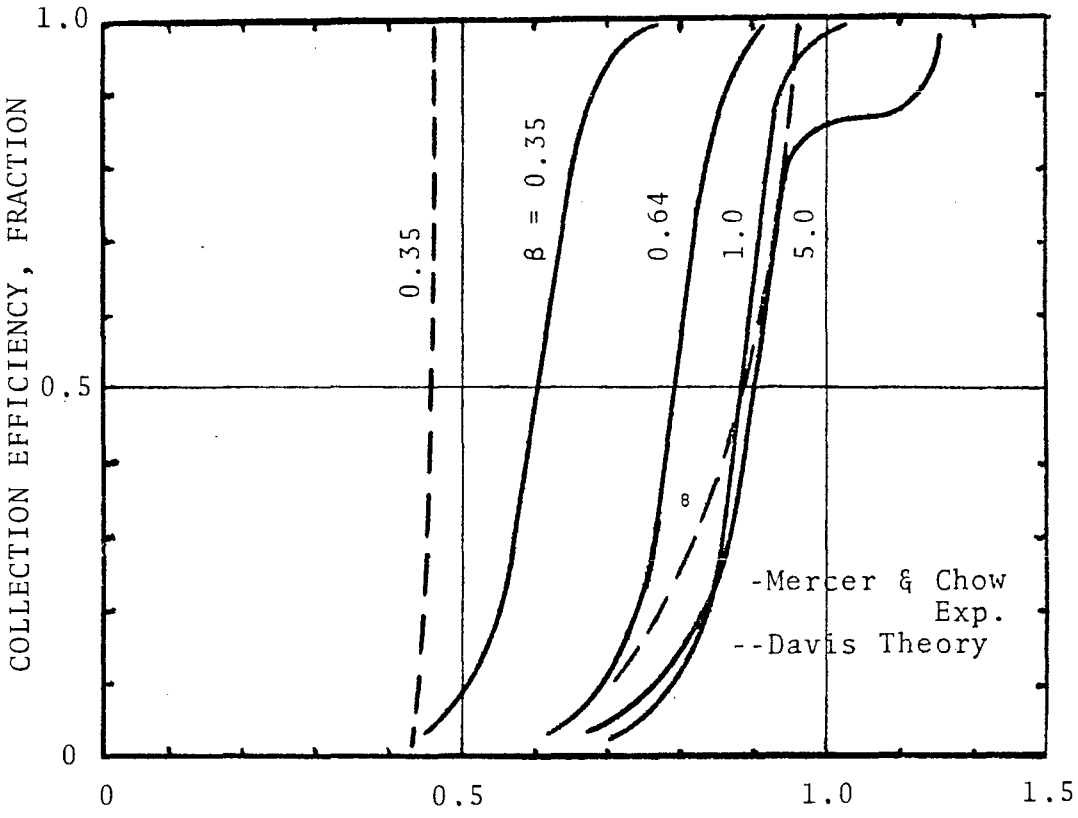

$$(K_p)^{1/2} = \left(\frac{2 \rho_p \, C' \, u_o}{9 \, \mu_G \, \frac{b}{2}} \right)^{1/2} r_p$$

Figure 7-1- Theoretical and experimental collection efficiencies of rectangular aerosol jets.

where n_j = collection efficiency for a given particle diameter in one stage of rectangular jet impingement

N = number of stages in the tube bank
= (number of rows) - 1

If the tubes are widely spaced, the target efficiency, "η", can be calculated from Figure 3-6. In this case the efficiency for the entire tube bank is:

$$E = 1 - (1 - \eta \frac{a'}{A})^n \qquad (7\text{-}3)$$

where a' = cross-sectional area of all the tubes in one row

A = total flow area

n = number of rows

Pressure Drop

Pressure drop for gas flow normal to banks of round tubes can be predicted by means of Grimison's correlations (Perry, 1973). As an approximation, Lapple (Perry, 1973) suggests that 0.72 velocity heads are lost per row of tubes in arrangements of the kind commonly used in heat exchangers Calvert and Lundgren (1970) found that for closely spaced tube banks Lapple's approximation agreed satisfactorily with experimentally determined pressure drops.

Houghton and Radford (1939) studied streamline strut banks and found that for a center-to-center spacing of 2 strut widths (i.e. open space = strut width) the pressure drop was about 0.16 velocity heads per row. This can be expressed as:

$$\Delta P = 0.16\ N\ \rho_G (5.3 \times 10^{-4}) (u'_G)^2 \text{ cm W.C.} \qquad (7\text{-}4)$$

where u'_G is the actual gas velocity

Reentrainment

Ullock (1956) determined the reentrainment velocity experimentally for streamlined struts. He found that the reentrainment velocity was a direct function of the surface tension and specific gravity of the liquid on the tube and an inverse function of the density of the gas flowing around the tubes. The empirical equation for reentrainment velocity was

$$u'_G = 35.6 \frac{\sigma^{0.127} \rho_L^{1.27}}{\rho_G^{0.5}} \qquad (7\text{-}5)$$

where the velocity is in cm/sec, "σ" the surface tension in dyne/cm and"ρ_L" and "ρ_G" are the liquid and gas densities in g/cm^3.

EXPERIMENTAL RESULTS AND DISCUSSION

Overall Collection Efficiency

Collection efficiency versus gas velocity data for horizontal flow through tube banks are plotted in Figures 7-2 through 7-4 for various inlet drop diameters. Penetration due to primary efficiency of less than 100% was observed for velocities lower than 3.0 m/sec. Figure 7-5 is a plot of overall collection efficiency versus gas velocity data for vertical flow through tube banks. Liquid load was used as a parameter. It can be observed that the onset of reentrainment velocity is as low as 3 m/sec.

Houghton and Radford's (1938) data for strut separators are also plotted in Figure 7-3. They found a constant collection efficiency of 96.2% for gas velocities from 1.25 to 17.5 m/sec. The inlet entrainment contained drops as small as 1 μm. However, no increase in penetration at lower velocities or reentrainment at higher velo-

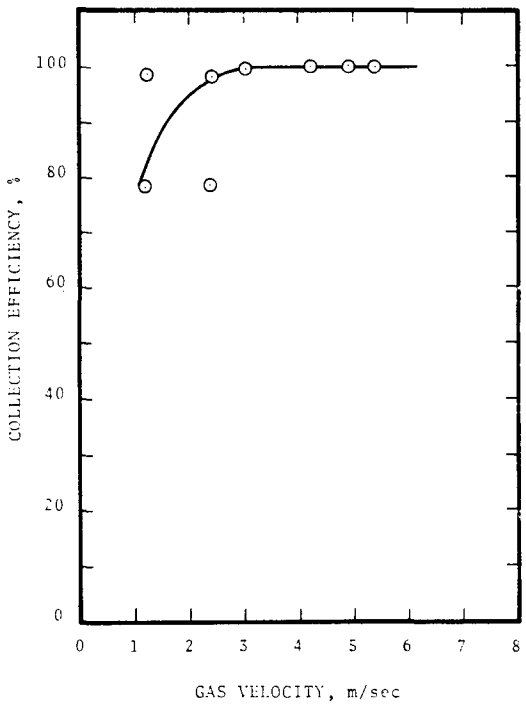

Figure 7-2. Collection efficiency versus gas velocity in tube bank with n = 6, d_{pg} = 84 μm and σ_g = 1.32.

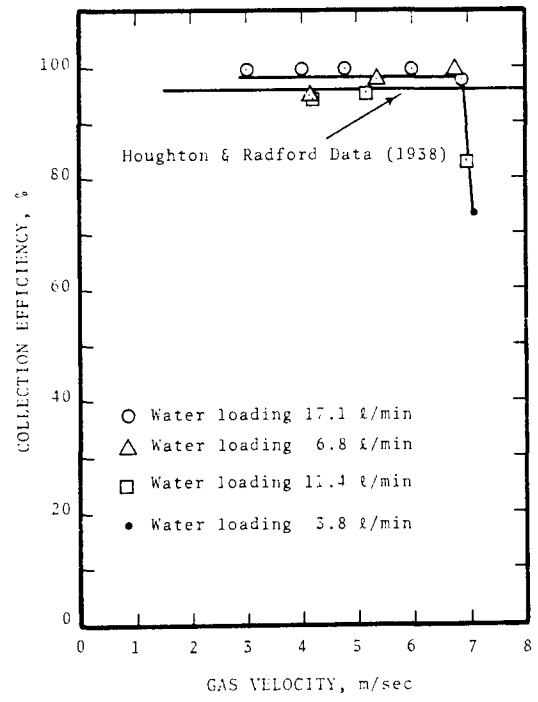

Figure 7-3. Collection efficiency versus gas velocity in tube bank with d_{pg} = 380 μm and σ_g = 1.5

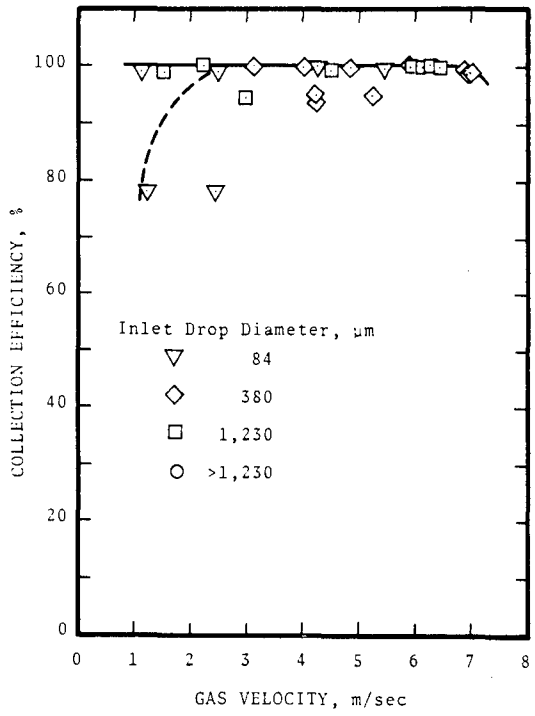

Figure 7-4. Collection efficiency versus gas velocity in tube bank. Solid line represents theory.

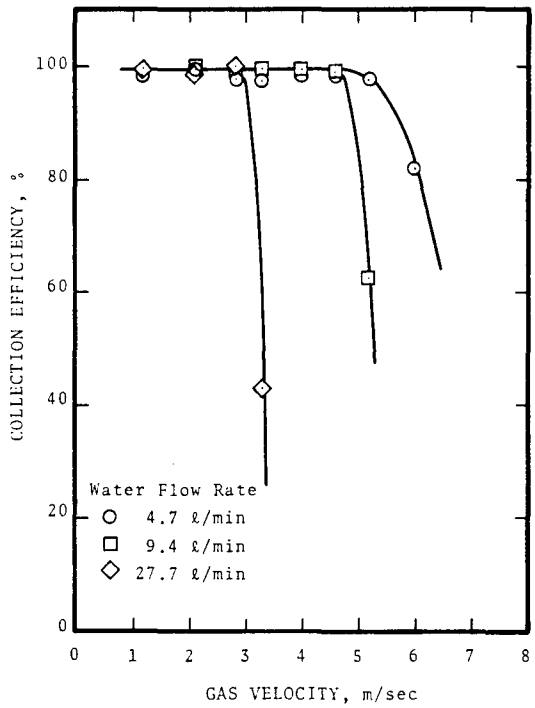

Figure 7-5. Collection efficiency versus gas velocity in vertical direction in bank of tubes.

cities was observed. A comparison between the configuration used in the present study and that of Houghton and Radford is given in Table 7-1.

Pressure Drop

Dry and wet pressure drops through the tube bank are plotted in Figures 7-6, 7-7, and 7-8. There is little effect of liquid load and air flow orientation on the pressure drop although there is an increase of pressure drop with gas velocity for vertical gas flow. This is in keeping with the increase in liquid holdup which would be expected. The pressure drops are about 1.0 velocity head for 6 rows, which is in agreement with equation (7-4). Thus, for standard air the experimental dry pressure drops are given by:

$$\Delta P \simeq 1.0 \times 10^{-7} N(u'_G)^2 \text{ cm W.C.} \qquad (7\text{-}6)$$

Reentrainment

Figure 7-9 depicts the value of gas velocity and liquid load observed as being necessary for reentrainment from tube banks in cross-flow arrangement. The shaded area is the operating condition at which drops were observed to tear off the tube by the gas, i.e. reentrained. However, most of these reenetrained droplets settled out in the observation section ahead of the sampling point. Below the shaded area, reentrainment was not present. Above the shaded area, although reentrainment was detected at the sampling point (90 cm from the separator) its quantity was negligible. Heavy reentrainment started at a superficial gas velocity of 7 m/sec. This velocity did not depend on the liquid loading. This velocity is lower than that predicted by equation 7-5 (8.9 m/sec based on this

Table 7-1 . COMPARISON OF TUBE BANKS

	Present Study	Houghton & Radford (1938)
Tube (minor-major axis) diameter, cm	1.9	1.25x3.2
Spacing between tubes, center to center, cm	3.8	2.5
Spacing between rows, center to center, cm	3.3	5
Number of rows	6	6
Material of tubes	Al	

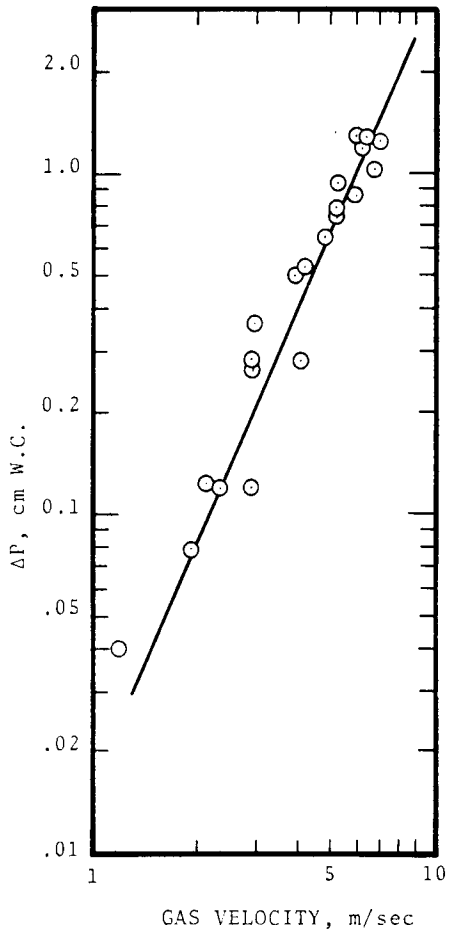

Figure 7-6. Dry pressure drop in tube bank versus gas velocity.

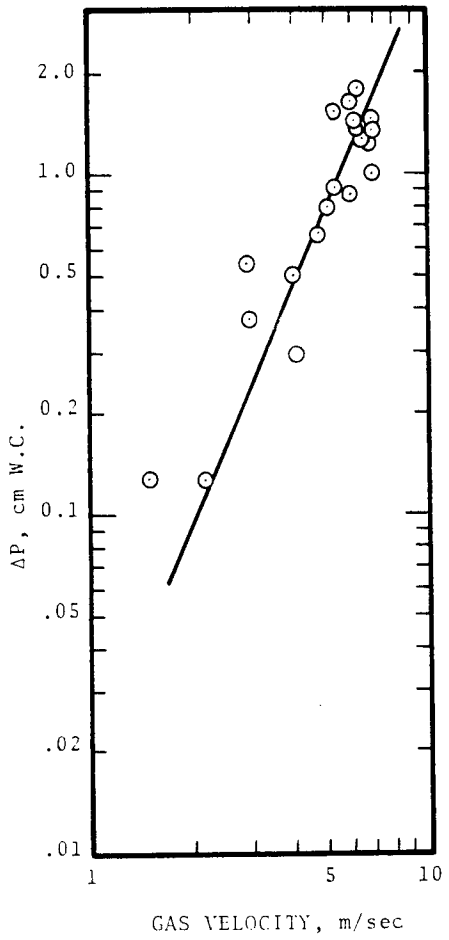

Figure 7-7. Wet pressure drop in tube bank versus gas velocity

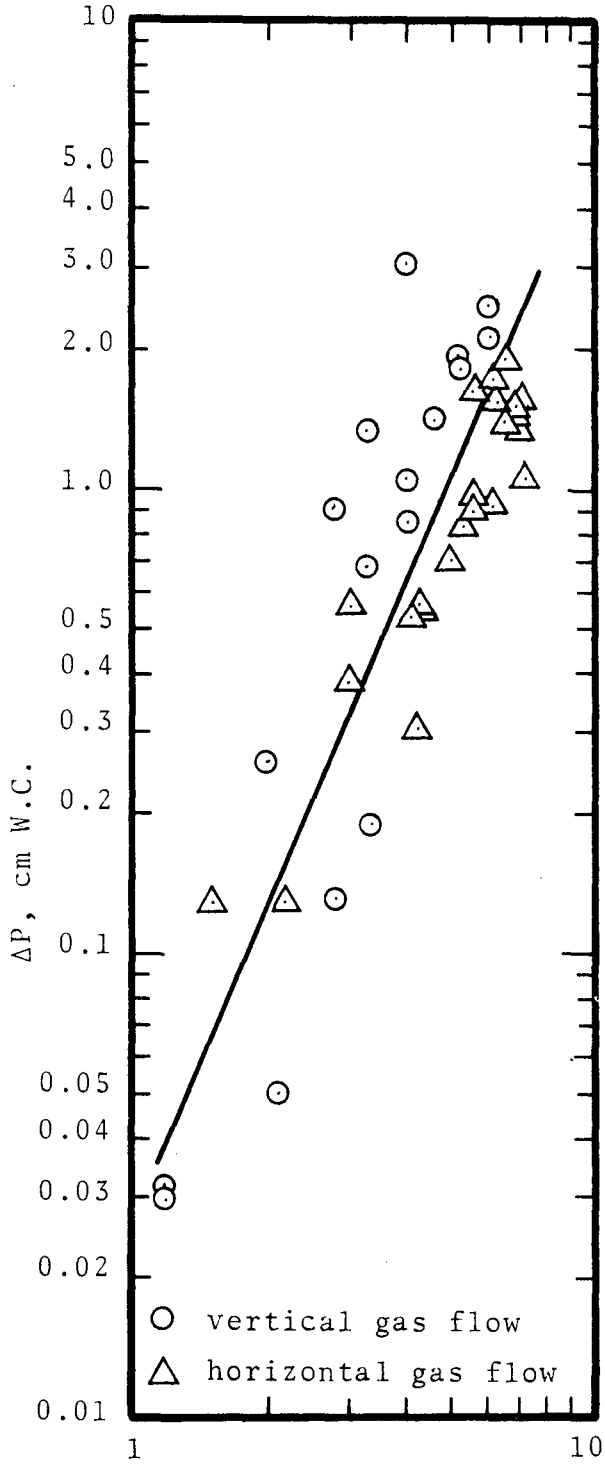

Figure 7-8. Wet pressure drop in tube bank.

equation). This is probably due to the difference in shades of the tube used.

Figure 7-10 is a similar plot for vertical gas flow. This graph gives, at a given liquid load, the gas velocity at which reentrainment increased sharply.

Figures 7-9 and 7-10 indicate that at a given gas velocity, due to its better drainage characteristic, vertical tube with horizontal gas flow can handle a higher liquid load.

CONCLUSIONS

1. Experimental primary efficiency agrees with the theory.
2. Heavy reentrainment in vertical tube banks using horizontal gas flow starts around 7 m/sec. Liquid load does not have a significant effect on this velocity. However, the onset of reentrainment velocity of tube banks with vertical air flow is highly dependent upon the liquid load. Reentrainment starts at a gas velocity of as low as 3 m/sec.
3. Pressure drop is predictable by means of correlations available from the published literature relating to heat exchanger tube bundles.

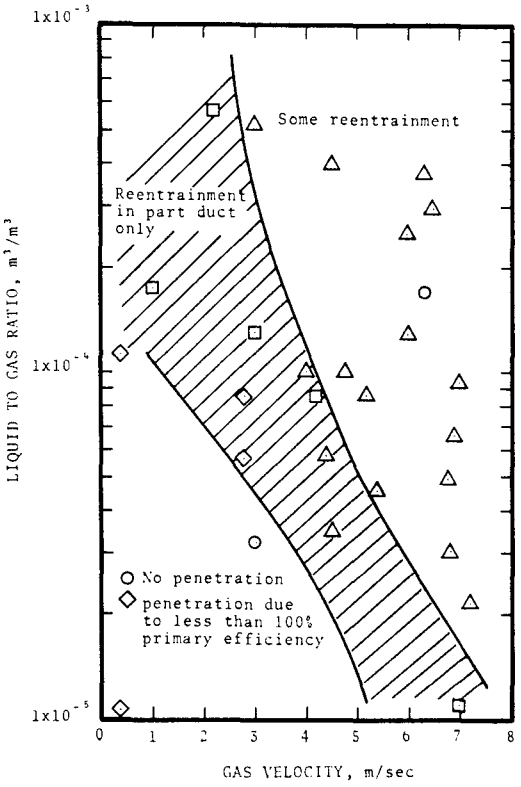

Figure 7-9. Experimental results showing the effect of gas velocity and liquid load on performance of tube bank in cross-flow pattern.

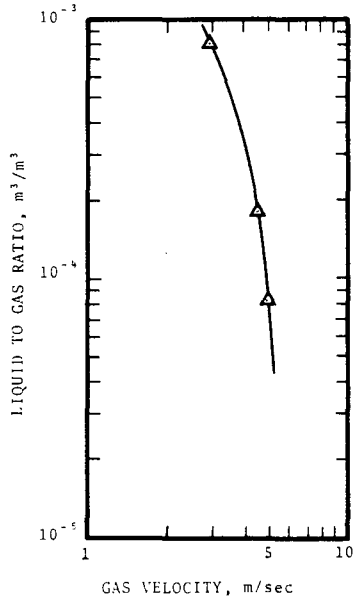

Figure 7-10. Experimental results showing the effect of gas velocity and liquid load on reentrainment for tube banks with vertical gas flow.

CHAPTER 8

CYCLONE

Commercially available cyclones in standard designs for entrainment separators have a maximum capacity of up to 141 m^3/sec (300,000 CFM) of gas. Efficiencies of about 95% are claimed for 5 μm diameter drops in a well-designed cyclone. Some manufacturers use a bundle of small cyclones (multicyclones), which can efficiently collect drops as small as 2 μm in diameter. However, this arrangement reduces the capacity of the device.

MATHEMATICAL MODEL

Primary Efficiency

Leith and Licht (1971) derived an equation to predict primary collection efficiency in conical bottom cyclones as pictured in Figure 8-1. With slight modification it can be applied to cylindrical cyclones. The following assumptions were made:

1. The drag force in the radial direction on the drop is given by Stokes law.
2. The tangential velocity component of the drop is related to the radial position by a modified form of the equation for a free vortex in an ideal fluid:

$$u_{tg}\, r^n = \text{constant} \qquad (8\text{-}1)$$

where "r" is the distance from the vertical axis of the cyclone and "n" is the vortex component and is defined below in equation (8-3).

3. Backmixing of the drops takes place in the gas phase.

The final equation for predicting primary collection efficiency is:

$$\ln Pt = -2\left[\frac{\rho_d}{9\mu_G}\left(\frac{2d_d\, u_{tg}}{dc}\right)^2 (n+1)t\right]^{\frac{1}{2n+2}} \qquad (8\text{-}2)$$

where $$n = 1 - \left[\frac{T}{283}\right]^{0.3}\left[1 - \frac{(0.393\, d_c)^{0.14}}{2.5}\right] \qquad (8\text{-}3)$$

Pt = penetration, fraction

ρ_d = drop density, g/cm^3

μ_G = gas viscosity, poise

d_d = drop diameter, cm

u_{tg} = tangential velocity, cm/sec

t = mean residence time of the gas in the cyclone, sec

T = gas temperature, °K

The mean residence time of the gas stream in the cyclone is:

$$t = \frac{V_e}{Q_G} \qquad (8\text{-}4)$$

where V_e = effective volume of the cyclone, m^3

Q_G = volumetric gas flow rate, m^3/sec

$= u_G A$

A = inlet area, cm^2

u_G = inlet gas velocity, cm/sec

The effective volume of the cyclone, "V_e" is defined as the volume of the cyclone minus the volume occupied by the exit duct and exit gas core. The diameter of the exit gas core can be assumed equal to the diameter of the exit duct. Leith and Licht (1971) gave the following equations for the

determination of effective volume of a conical bottom cyclone:

$$V_e = V_1 + V_2 \tag{8-5}$$

where V_1 = annular shaped volume above exit duct inlet to mid-level of entrance duct

$$= \frac{\pi}{4}\left(S - \frac{a}{2}\right)\left(d_c^2 - d_e^2\right) \tag{8-6}$$

V_2 = volume of cyclone below exit duct inlet to the natural length of the cyclone

$$V_2 = \frac{\pi d_c^2}{4}(h_s - S) + \frac{\pi(L+S-h_s)d_c^2}{12}\left(1+\frac{d}{d_c}+\frac{d^2}{d_c^2}\right) - \frac{\pi d_e^2 L}{4} \tag{8-7}$$

where $d = d_c - (d_c - b_e)\left(\frac{S+L-h_s}{h-h_s}\right)$ (8-8)

and L = natural length of the cyclone

$$= 2.3 d_e \left(\frac{d_c^2}{ab}\right)^{1/3} \tag{8-9}$$

a, b, d_c, d_e, S, h, h_s are cyclone dimensions defined in Figure 8-1. Figure 8-2 shows the theoretical grade efficiency curve for the cyclone used in the present study with inlet gas velocity as parameter.

Pressure Drop

Shepherd and Lapple (1940) derived an equation for a cyclone with inlet vanes for pressure drop as a function of inlet gas velocity and the cyclone inlet and outlet dimensions:

$$\Delta P = 0.00513\ \rho_G \left(\frac{Q_G}{ab}\right)^2 \left(\frac{7.5\ ab}{d_e^2}\right) \tag{8-10}$$

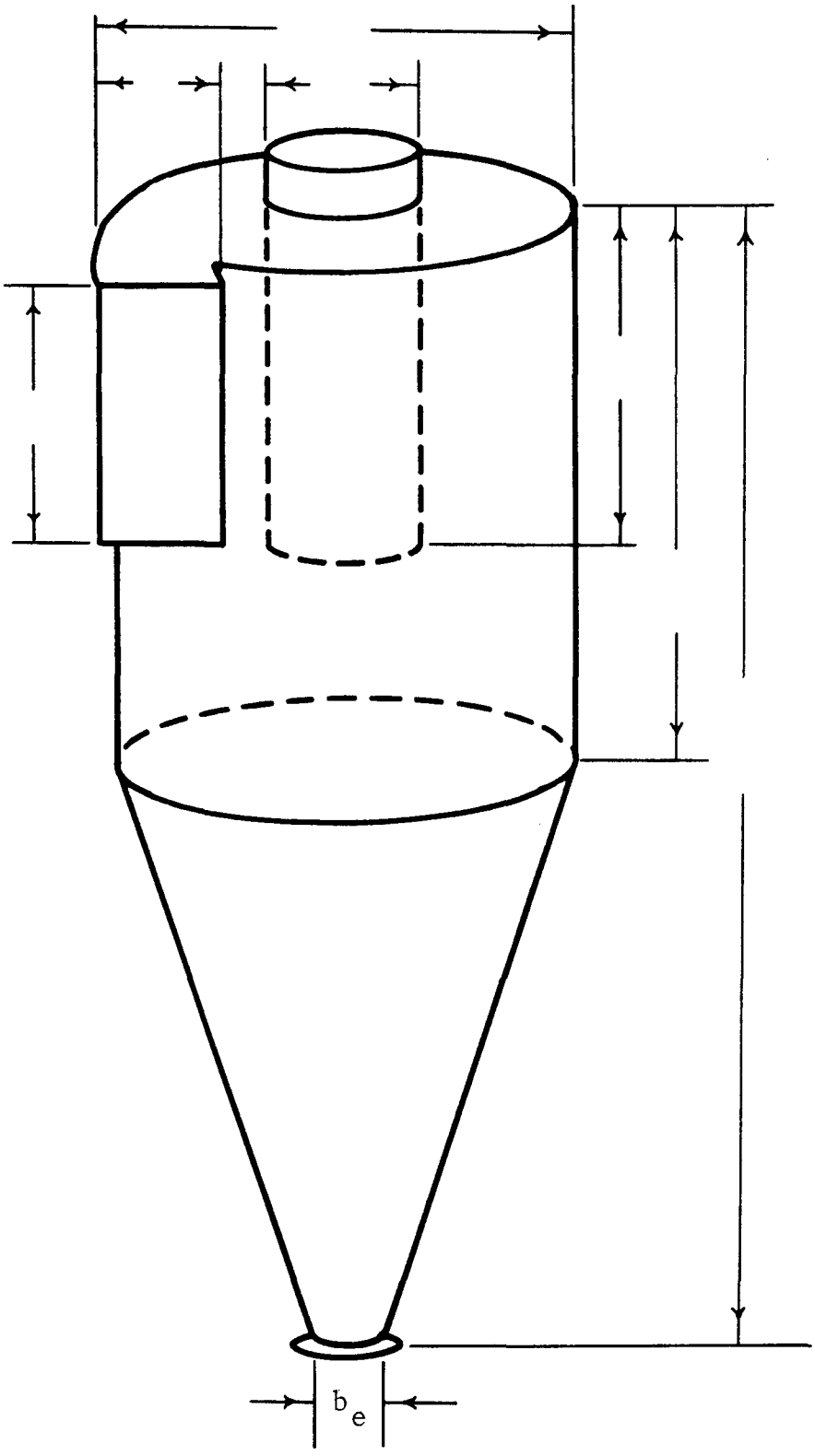

Figure 8-1. Cyclone with tangential gas inlet.

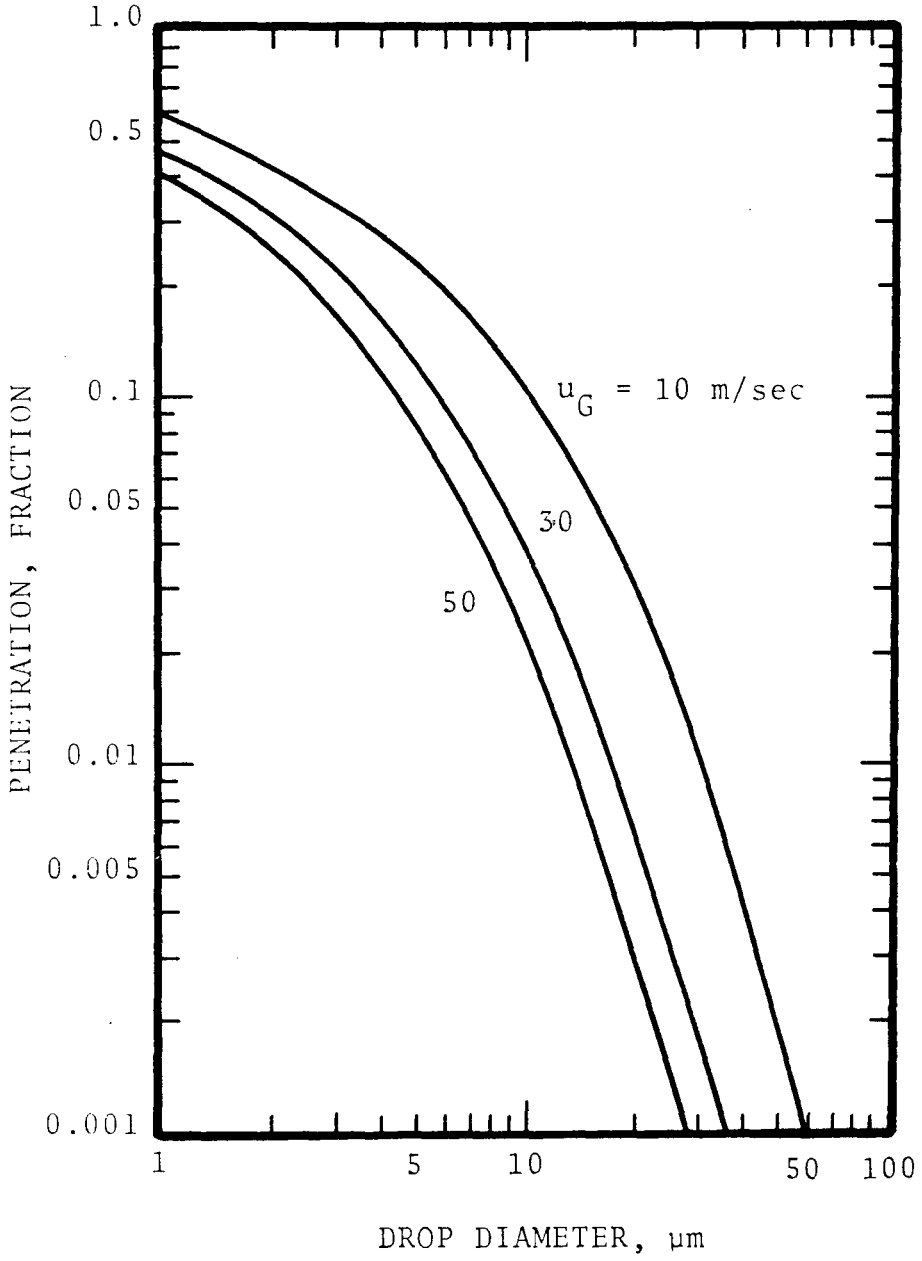

Figure 8-2. Theoretical grade efficiency curve of the cyclone used in the present study with inlet gas velocity as parameter.

where ρ_G = gas density, g/cm^3
Q_G = gas volumetric flow rate, cm^3/sec
a = cyclone inlet height, cm
b = cyclone inlet width, cm
d_e = cyclone exit pipe diameter, cm

Equation (8-3) can be modified by writing it as a function of the geometric average of the gas velocity at the cyclone inlet and outlet:

$$\Delta P = 0.00513\ \rho_G v_{Ave}^2 \tag{8-11}$$

Shepherd and Lapple also developed an equation for a cyclone without inlet vanes:

$$\Delta P = 0.00513\ \rho_G \left(\frac{Q_G}{ab}\right)^2 \left(\frac{16ab}{d_e^2}\right) \tag{8-12}$$

Reentrainment

Onset of Reentrainment - There is a great disagreement among results for the onset of reentrainment obtained by different investigators. This is indicative of the problem of defining the onset of reentrainment. Zhivaikin (1962) defined the onset of entrainment as occurring when it is first detectable. Steen and Wallis (1964) defined the onset of entrainment as that air velocity which represents the extrapolation of the straight line portion of a graph of entrainment percentage versus air velocity. Since the increase in entrainment with air velocity is similar to the exponential function, their results lie considerably above those of Zhivaikin. Chien and Ibele (1962) defined the transition on the basis of pressure drop versus gas flow rate curves. A change in the slope of the curve was

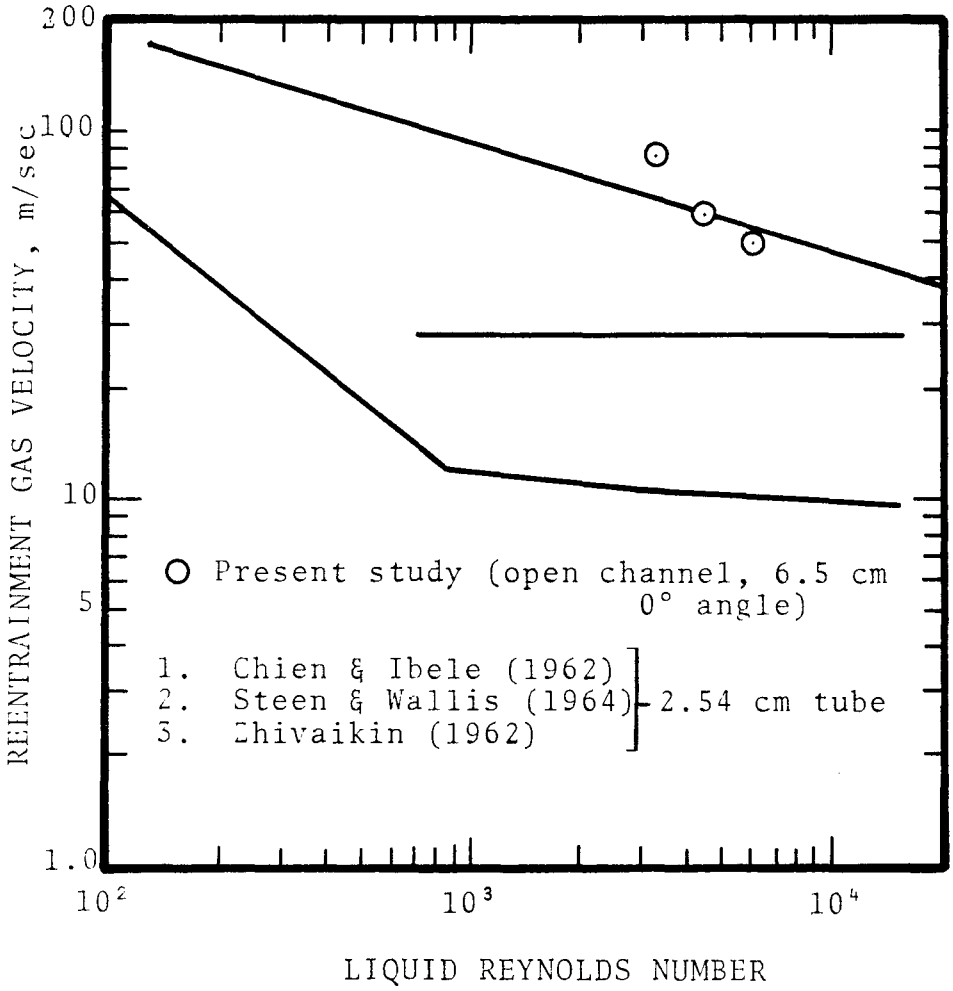

Figure 8-5. Comparison of entrainment onset velocity by different investigators.

taken to indicate the onset of gross entrainment. Their results apply to conditions where a large fraction of the total liquid flow is entrained.

In view of our need for a correlation for onset of entrainment, a small scale open channel experiment was carried out to make observations of the transition from separated flow to separated-entrained flow. Details of the experimental set-up and sampling method were presented in the "Initial Report". It was found that entrainment velocity depends upon liquid Reynolds number. Experimental data are shown in Figure 8-3 along with other investigators' results. As can be seen, the present results are comparable with those of Chien and Ibele's data for two phase flow in a 2.5 cm diameter tube. Since the liquid flow in a cyclone can be approximated by open channel flow with channel width equal to inlet height. Therefore, Chien and Ibele's line in Figure 8-3 could be used to predict the reentrainment velocity for a cyclone with liquid Reynolds number defined as

$$N_{Re,L} = \frac{4Q_L}{d_o \upsilon_L} \qquad (8\text{-}13)$$

where Q_L = volumetric liquid flow rate, cm^3/sec
υ_L = kinematic viscosity of the liquid, cm^2/sec
d_o = channel width, cm
= cyclone inlet height

Drop Diameter of Reentrainment - The drop diameter of the reentrained liquid has a size distribution which varies with gas flow rate, liquid flow rate, fluid properties and perhaps pipe diameter. The average drop diameter decreases with increase in gas flow rate. On the other hand, the liquid flow rate has only a weak and ambiguous effect. When the gas velocity exceeds 6,000 cm/sec, high liquid flow rate has no effect on the drop size distribution.

Rate of Reentrainment - It is believed that reentrainment takes place due to penetration of liquid waves into the turbulent zone of the gas. The amplitude of the waves increases exponentially with liquid flow rate. Therefore, reentrainment is assumed to take place in proportion to $\exp(K_1 N_{Re,L})$ where "K_1" is a constant.

The rate of reentrainment depends upon gas flow rate, liquid flow rate and fluid properties. According to Anderson et.al.(1964), the rate of reentrainment is approximately 4% of inlet entrainment for $N_{Re,L} > 2,750$ and is seen to increase slightly with $N_{Re,G}$ (3.5% for $N_{Re,G} = 3 \times 10^4$, 4% for $N_{Re,G} = 1.6 \times 10^5$). Below $N_{Re,L} = 2,750$, the only data available are for $N_{Re,L} = 1,150$, at which point reentrainment is 0.5%.

RESULTS AND DISCUSSION

Overall Collection Efficiency

Figure 8-4 shows the experimental penetration versus inlet gas velocity. Data were collected with and without the use of inlet vane in the cyclone. For the case without the inlet vane, the inlet area was 30.5 cm x 15.0 cm and the maximum inlet gas velocity was 22 m/sec. M-26 nozzles were used to generate the drops. When the cyclone was operated with the inlet vane, the inlet area was 30.5 cm x 7.5 cm and the maximum inlet gas velocity was 61 m/sec. Small garden hose was used to produce the entrainment and the maximum liquid flow rate was 1.5×10^{-3} m^3/m^3 of gas (11.5 gal/MCF).

In all experiments for gas velocity below 40 m/sec, collection efficiency was 100%. For gas velocities between 40 m/sec and 60 m/sec, reentrainment was negligible (<0.5%). Theoretical predictions based on equation (8-2) predicted 100% collection efficiency for all conditions.

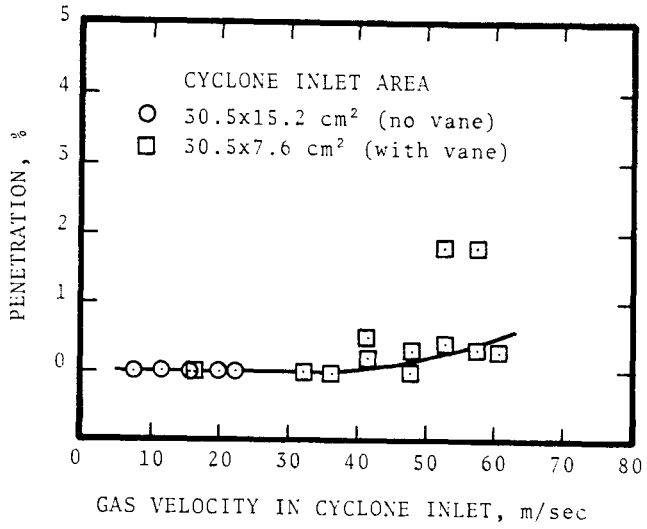

Figure 8-4. Experimental penetration versus gas velocity in cyclone inlet with and without vane.

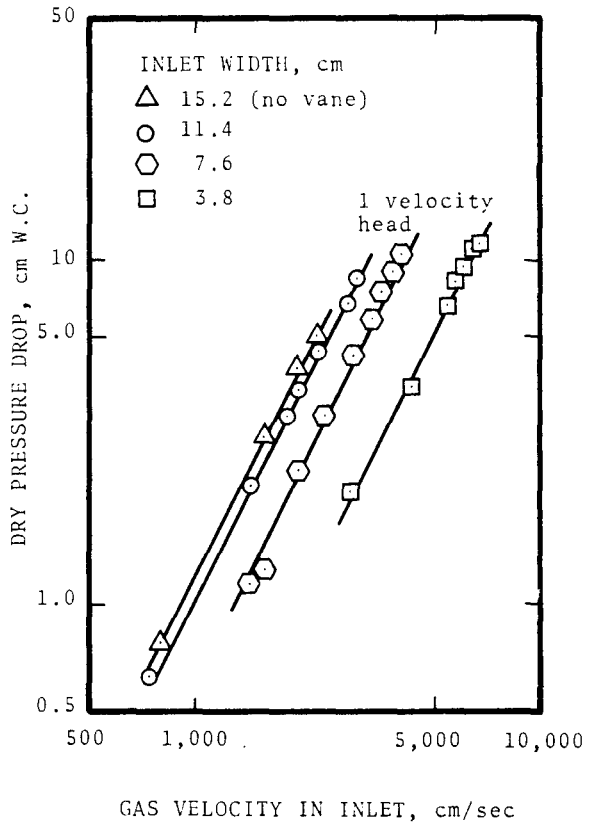

Figure 8-5. Experimental dry pressure drop versus gas velocity in cyclone inlet.

Pressure Drop

The experimental pressure drop data in the cyclone are plotted in Figures 8-5 through 8-7. The effect of gas velocity on pressure drop is shown in Figure 8-5. Cyclone inlet width is used as a parameter. The slope of the experimental pressure drop curves, on log-log graph paper is 2. The effect of reducing the inlet width of the cyclone is a proportionate reduction in the pressure drop, i.e., if the cyclone inlet width is reduced to half, the pressure drop will be reduced to half provided the gas velocity through the cyclone inlet is kept constant. For comparison, a straight line for 1 velocity head was also plotted in Figure 8-5.

The effect of volumetric flow rate through cyclone on pressure drop is shown in Figure 8-6. At a given volumetric flow rate, pressure drop through the cyclone inlet increases with reduction in the inlet area.

The effect of geometric average gas velocity in the cyclone inlet and outlet on pressure drop is shown in Figure 8-7. All the experimental data falls on a straight line represented by

$$\Delta P = 0.000513 \quad \rho_G \left(\frac{Q_G}{a\ b}\right)^2 \left(2.8\ \frac{a\ b}{d_e^2}\right) \qquad (8\text{-}14)$$

where ΔP = pressure drop, cm H_2O

ρ_G = gas density, g/cm^3

Q_G = volumetric flow rate, cm^3/sec

a = cyclone inlet height, cm

b = cyclone inlet width, cm

d_e = cyclone exit diameter, cm

The above equation agrees in form with the pressure drop equation for cyclone with inlet vane, given by Shepherd & Lapple (1940), i.e. equation (8-10). However,

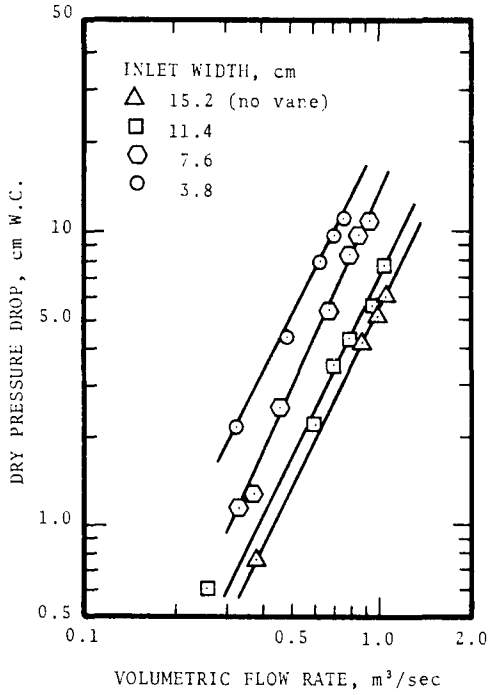

Figure 8-6. Experimental dry pressure drop versus volumetric flow rate in cyclone.

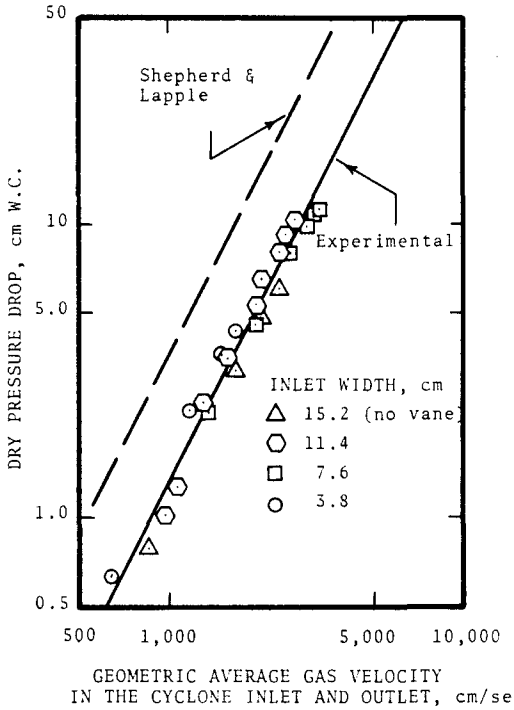

Figure 8-7. Comparison of experimental pressure drop data and predicted pressure drop for cyclone with inlet vane by Shepherd & Lapple (1940).

predictions by Shepherd & Lappe give 2.7 times higher pressure drop than predicted from equation (8-15).

Reentrainment

From Figure 8-4, it is observed that the onset of reentrainment gas velocity is between 40-50 m/sec. For the cyclone, the air inlet duct has a height of 30.5 cm. It was assumed that all the liquid collected inside the cyclone flows along the inside surface as a film having a width of 30.5 cm. During the experiments, the liquid flow rate was about 810 cm^3/sec. Accordingly, liquid Reynolds number was

$$N_{Re,L} = \frac{(4)(810)}{(30.5)(0.01)} = 10,600$$

From Figure 8-3, using Chien and Ibele's correlation for a liquid Reynolds number of 10,600, the reentrainment gas velocity is 40 m/sec which agrees with observation.

Some Observations of Gas-Liquid Flow In Cyclone

It was observed that most of the entrainment was collected on the cyclone surface near the inlet. The liquid drained on the cyclone surface as a spiral. It drained from the top of the cyclone to the bottom during the angular rotations equal to 2/3 of a circle. The width of the bend increased with increase in the liquid flow rate. The width was 50 cm when the liquid flow rate was 8,000 cm^3/min (2.1 gpm) and air inlet velocity was 3,680 cm/sec. Waves, as shown in Figure 5,were present in the liquid. At the above flow rate, the wave amplitude was almost equal to the film thickness (1 - 1.5 mm). A few drops were torn away from the liquid film at the top and drained down on the serrated cap on the exit.

At higher liquid flow rates, $6x10^4$ cm^3/min (15 gpm) and the same gas velocity all the inside surface (including

top) was covered with water. Liquid drained as jets of liquid from the corners of the serrated cap on the exit.

CONCLUSIONS

1. The experimental results show that the primary collection efficiency in a cyclone is approximately 100%.
2. Pressure drop data can be correlated by the equation:

$$\Delta P = 0.000513\ \rho_G \left(\frac{Q_G}{a\ b}\right)^2 \left(2.8\ \frac{a\ b}{d_e^2}\right) \qquad (8\text{-}10)$$

3. The Chien and Ibele correlation gives a better prediction of the onset of reentrainment gas velocity. Thus, the Chien and Ibele curve is recommended for determining the onset of reentrainment in a cyclone.

CHAPTER 9

ZIGZAG BAFFLES

Baffles can efficiently separate drops greater than 10 μm in diameter, while some of the better designed devices can separate drop diameters of 5-8 μm. Common gas velocities are 2.0 - 3.5 m/sec, and the pressure drop for a 6-pass separator is about 2 - 2.5 cm W.C.

The most common baffle shape is zigzag with 3 to 6 passes. These can be fabricated from a continuous wavy plate or each pass is separated, in which case the separation distance is normally smaller than the width of the baffles. Cross-flow baffles are claimed to have higher drainage capacity than countercurrent flow baffles.

MATHEMATICAL MODELS

Primary Collection Efficiency

A model to predict primary efficiency was developed in this study and was presented in the initial report. Based on turbulent mixing, the primary collection efficiency of a continuous zigzag baffle section is

$$\eta = 1 - \exp\left[-\frac{u_{tc}\, nw\theta}{57.3\, u_G\, b \tan\theta}\right] \qquad (9\text{-}1)$$

where η = primary collection efficiency, fraction
u_{tc} = drop terminal centrifugal velocity, in the normal direction, cm/sec
u_G = superficial gas velocity, cm/sec
n = number of bends or rows
θ = angle of inclination of the baffle to the flow path, degrees
w = width of baffle, cm
b = spacing between two consecutive baffles in same row, cm

The drop terminal centrifugal velocity can be determined by performing a force balance on the drop. The result is

$$u_{tc} = \left[\frac{4}{3} \frac{d_d \rho_d a}{C_D \rho_G} \right]^{0.5} \qquad (9\text{-}2)$$

where d_d = drop diameter, cm
ρ_d = drop density, g/cm^3
a = acceleration due to centrifugal force, cm/sec^2
C_D = drag coefficient
ρ_G = gas density, g/cm^3

If the drop Reynolds number is low ($N_{Re,D} < 0.1$), Stokes' law applies. For this condition, the drag coefficient is given by

$$C_D = \frac{24}{N_{Re,D}} \qquad (9\text{-}3)$$

where $N_{Re,D}$ = drop Reynolds number

$$= \frac{d_d \, u_{tc} \, \rho_G}{\mu_G}$$

By combining equations 9-2 and 9-3, we obtain

$$u_{tc} = \frac{d_d^2 \, \rho_d \, a}{18 \, \mu_G} \qquad (9\text{-}4)$$

The acceleration due to centrifugal force is defined by the following equation

$$a = \frac{2 \, (u_G')^2}{w \cot \theta} = \frac{2 \, u_G^2 \sin \theta}{w \cos^3 \theta} \qquad (9\text{-}5)$$

where u_G' = actual velocity between baffles, cm/sec
u_G = superficial gas velocity, cm/sec

If $N_{Re,D}$ >0.1, another appropriate drag coefficient should be used in equation 9-2. Foust, et al. (1959) gave a plot of drag coefficient as a function of Reynolds number in Figure 9-1, which can be used to determine "u_{tc}". The effect of surrounding drops on the motion of any individual drop is neglected.

Pressure Drop

Determination of the pressure drop is based on the drag coefficient, "f_D", for a single plate held at an angle "θ" to the flow as presented in Figure 9-2 (Fage and Johanson, 1927). Neglecting the effect of neighboring plates, pressure drop may be expressed as:

$$\Delta P = \sum_{i=1}^{n} 1.02 \times 10^{-3} f_D \rho_G \frac{u'^2_G}{2} \frac{A_p}{A_t} \qquad (9\text{-}6)$$

where ΔP = pressure drop, cm W.C.

A_p = total projected area of baffles per row in the direction of inlet air flow, cm^2

A_t = duct cross-sectional area, cm^2

The summation is made over the number of rows of baffles.

The actual gas velocity, "u'_G", in the baffle section should be used in Equation (9-6). The actual gas velocity is related to superficial velocity by

$$u'_G = u_G/\cos\theta \qquad (9\text{-}7)$$

Note that the angle of incidence for the second and subsequent rows of baffles will be twice the angle of incidence for the baffles in the first row.

Reentrainment

A mathematical model to predict reentrainment in the zigzag baffles was derived and presented in the "Initial Report". The models used to predict reentrainment were based

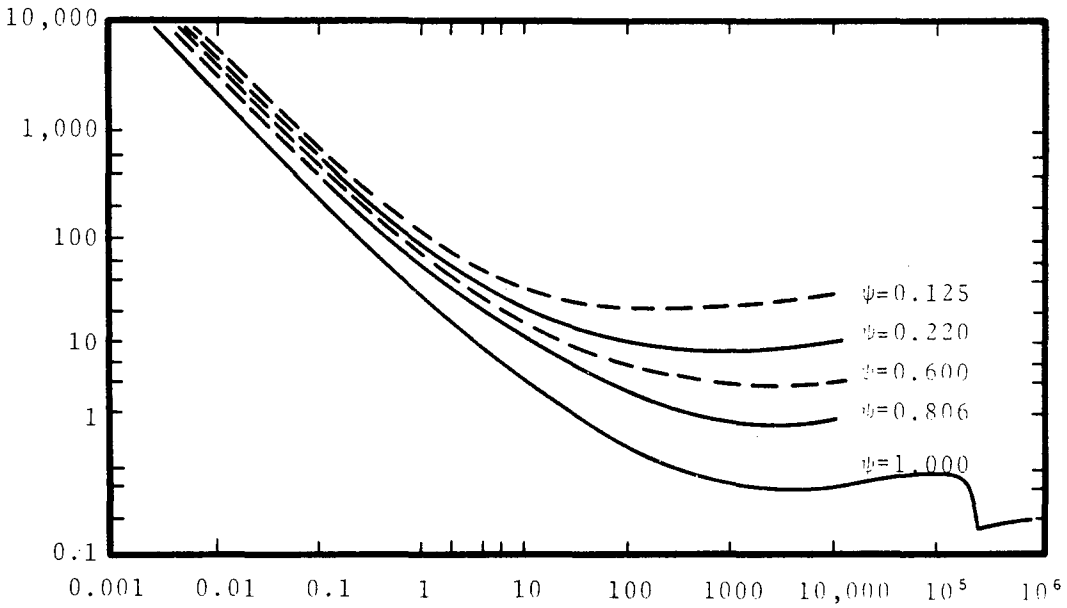

Reynolds number $N_{Re,p} = \frac{d_d \, u_{tc} \, \rho_G}{\mu_G}$

Figure 9-1. Drag coefficient versus Reynolds number after Foust et al (1959), with sphericity ψ as the parameter.

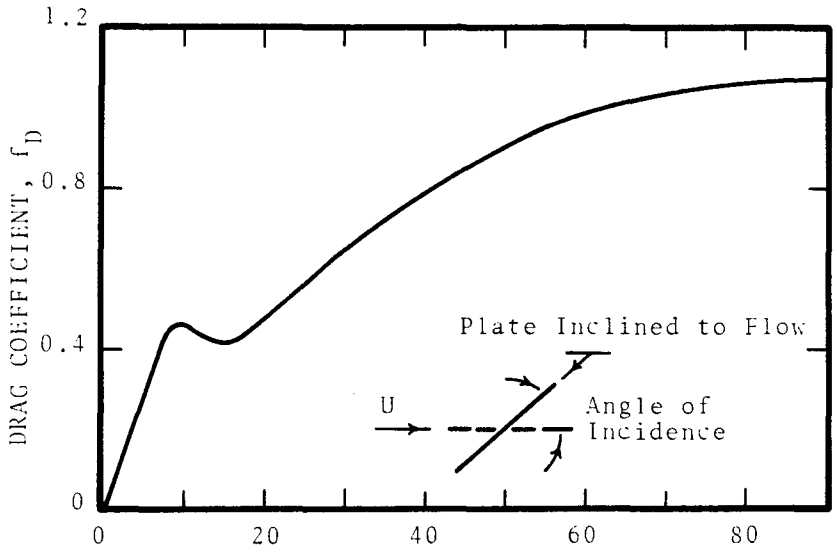

Figure 9-2. Drag coefficients for flow past inclined flat plates (data from A. Fage & F.C. Johansen, (1927).

on the assumption of film flow and it predicted a lower reentrainment velocity than that observed in the experiments. In the experiment with zigzag baffles, it was observed that the liquid flow on the baffles was dropwise. Therefore, an attempt was made to predict reentrainment due to tearing off drops from the baffle edges.

An additional factor to consider is that not all of the reentrained drops appear in the outlet. This is due to their settling out in the distance between entrainment separator elements and the outlet where sampling is done. The effect of gravity therefore reduces the amount of reentrainment measured at the sampling point.

Consider a drop hanging on the baffle edge prior to reentrainment. The necessary condition for the drop to be torn off from the baffle with vertical gas flow is when the drag force due to gas flow is balanced by gravitational force and surface tension effect, i.e. when

$$\left(\frac{C_D\ \rho G\ (u'_G)^2}{2}\right)\left(\frac{\pi\ d_d^2}{4}\right) = 2\sigma\ d_\ell + \frac{\pi}{6}\ d_d^3\ \rho_L g \qquad (9\text{-}6)$$

where C_d = drag coefficient
ρ_G = gas density, g/cm^3
u'_G = gas velocity for onset of reentrainment, cm/sec
d_d = drop diameter, cm
d_ℓ = drop attachment length, cm
σ = surface tension of liquid, dyne/cm
ρ_L = drop density, g/cm^3
g = gravitational acceleration, 980 cm/sec^2

Solve equation 9-6 for "u'_G", to obtain

$$u'_G = \left[\frac{16\ \sigma\ d_\ell}{\pi\ C_D\ \rho_G d_d^2} + \frac{4}{3}\ \frac{d_d\ \rho_L\ g}{\rho_G\ C_D}\right]^{0.5} \qquad (9\text{-}7)$$

If the drop attachment length is assumed equal to drop diameter, i.e. $d_\ell = d_d$, then the expression for reentrainment velocity becomes

$$u_G' = \left[\frac{16\ \sigma}{\pi\ C_D \rho_G\ d_d} + \frac{4}{3} \frac{d_d\ \rho_L g}{\rho_G\ C_D} \right]^{0.5} \qquad (9\text{-}8)$$

In reality, the drop oscillates due to drag forces exerted by gas flow and the drop attachment length may not be equal to one drop diameter. Another consequence of drop oscillation is that the drop shape is not spherical and may be quite "flat", such that the form drag area is increased.

For the case of horizontal gas flow, the reentrainment condition is that the drag force has to overcome the surface tension effect

$$\frac{C_D\ \rho_G\ (u_G')^2}{2}\ \frac{\pi d_d^2}{4} = 2\sigma\ d_\ell \qquad (9\text{-}9)$$

Rearranging equation 9-9, we obtain for reentrainment velocity

$$u_G' = \left[\frac{16\ \sigma\ d_\ell}{\pi\ \rho_G\ C_D\ d_d^2} \right]^{0.5} \qquad (9\text{-}10)$$

The reentrainment velocity predicted either by equation 9-7 or equation 9-10 is the actual gas velocity in the zigzag baffles. Depending upon the angle of baffles, the superficial reentrainment velocity is lower than the actual velocity. Superficial reentrainment velocity is related to actual reentrainment velocity by

$$u_G = u_G' \cos \Theta \qquad (9\text{-}11)$$

The value of the drag coefficient, "C_D", depends upon the drop Reynolds number and the sphericity of the drop.

The drop Reynolds number depends upon the gas velocity relative to the drop. Thus, equations 9-7 and 9-10 should be solved by trial and error method.

The predicted superficial reentrainment velocity due to tearing of drops is shown in Figures 9-3 and 9-4 for vertical gas flow and horizontal gas flow respectively with drop attachment length and baffle angle as parameters. The drop sphericity factor, "ψ", is assumed equal to 0.6. Drop sphericity is defined as the ratio of the surface area of a sphere of same volume as the drop to the surface area of the drop. As mentioned earlier, not all drops that are torn off the baffle are reentrained. For the case of vertical gas flow, only those drops with settling velocities smaller than the upward gas flow will be carried away by the gas as reentrainment. Curve 3 in Figure 9-3 shows the drop terminal settling velocity. If the reentrainment velocity lies above curve 3, the drops will be carried away. Thus. the lowest reentrainment velocity detectable will be at the point where the reentrainment and curves intersect. For the baffle test section used in the present study, the lowest detectable reentrainment velocity will be 5 m/sec if the drop attachment length is equal to half the drop diameter and will be 6 m/sec if drop attachment length is one drop diameter.

When the gas velocity is horizontal, some of the drops that tear off will be settled out due to sedimentation between the entrainment separator element and the sampling point. Curve 4 in Figure 9-4 gives the maximum drop diameter that may be sampled in the pilot plant of the present study. The vertical height = 60 cm and horizontal distance = 90 cm, are used to obtain curve 4. If the reentrainment velocity lies above curve 4, the drop will be present at the sampling point. Figure 9-4a shows the predicted lowest detectable reentrainment velocity and maximum

drop diameter as a function of drop sphericity factor for baffle section with horizontal flow. Drop attachment length was assumed equal to half the drop diameter.

The agreement between the predicted reentrainment onset velocity and the experimental reentrainment velocity was not known since the drop attachment length and drop sphericity, which depend on gas velocity, were not measured in the present study.

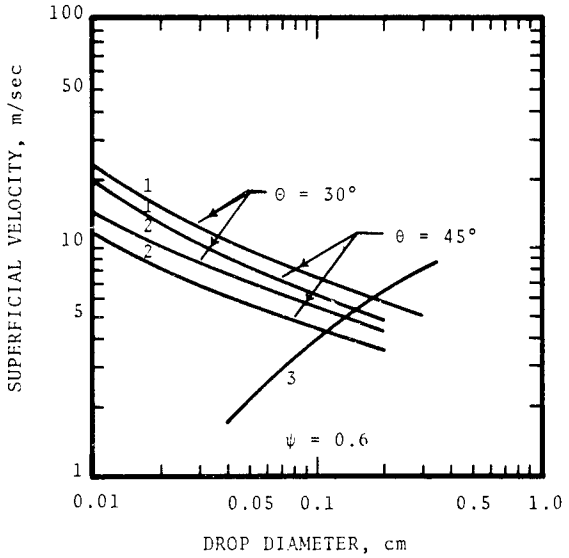

Figure 9-3. Predicted superficial reentrainment velocity due to tearing of drops with vertical flow.

Curve 1 - Reentrainment velocity for drop attachment length equal to drop diameter.
2 - Reentrainment velocity for drop attachment length euqal to half the drop diameter.
3 - Drop terminal velocity.

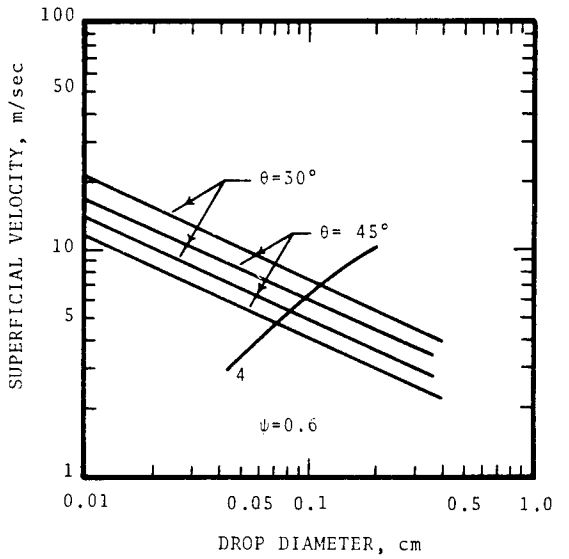

Figure 9-4. Predicted superficial reentrainment velocity due to tearing of drops with horizontal flow.

Curve 1 - Reentrainment velocity for drop attachment length equal to drop diameter.
2 - Reentrainment velocity for drop attachment length equal to half the drop diameter.
4 - Maximum drop diameter that can occur at sampling point.

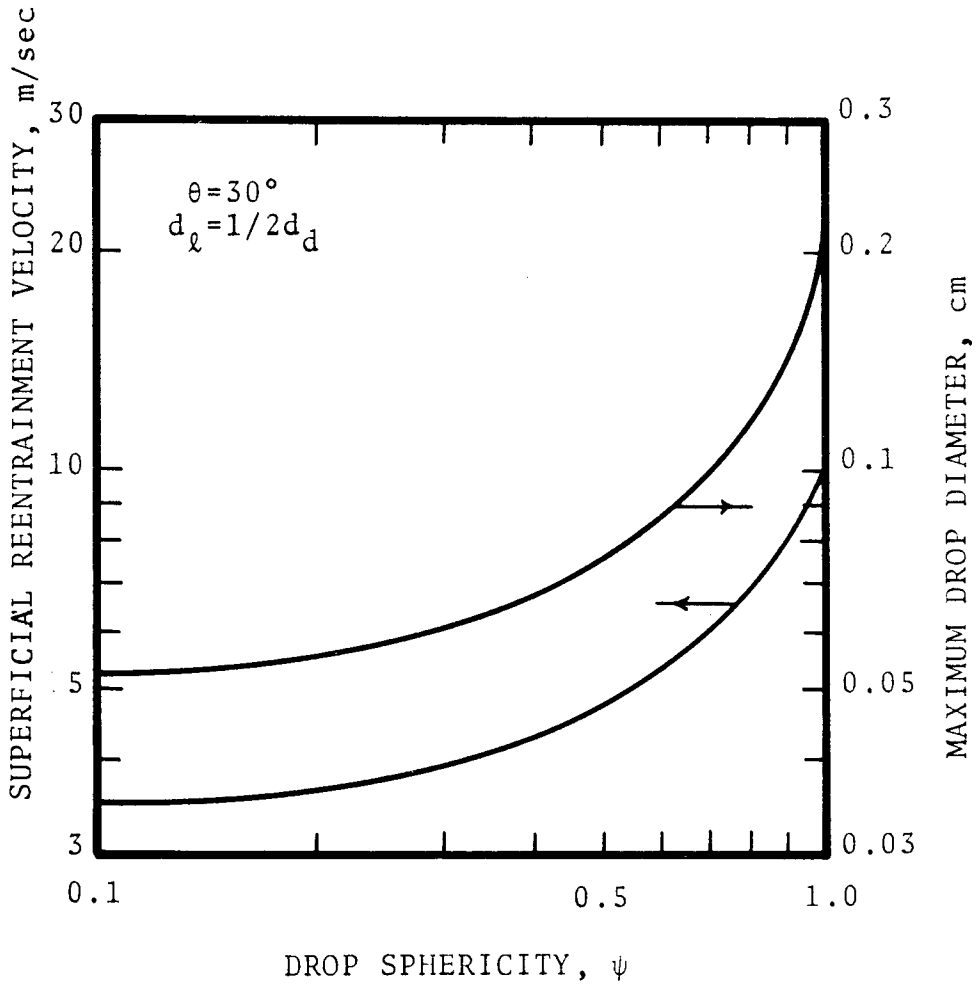

Figure 9-4a. Predicted superficial reentrainment velocity and maximum reentrained drop diameter for horizontal gas flow.

EXPERIMENTAL RESULTS AND DISCUSSION

Overall Efficiency

Vertical Baffle - The overall collection efficiency for horizontal gas flow through vertical zigzag baffles was determined as a function of gas velocity as shown in Figure 9-5. The separator attains 100% efficiency for gas velocities between 3.0 and 6.0 m/sec.

Figure 9-6 is collection efficiency for inlet entrainments with mass median drop diameter of 84 μm. The efficiency falls sharply for gas velocities below 3.0 m/sec. Reentrainment velocity was not reached even at the maximum flow rate achievable in the present pilot plant.

Experimental results reported by Bell and Strauss (1973) for zigzag baffles are plotted in Figure 9-7 along with points obtained in this study for d_{pg} = 380 μm and a line representing the data of Houghton and Radford (1938). The inlet entrainment of the Bell and Strauss experiments was comparable to this study, but their overall efficiency was much lower. This is probably due to the differences in separator design as reported in Table 9-1.

Houghton and Radford's experiments were conducted under two operating conditions: (1) Liquid flow rate = 38 cm^3/min and spray drop diameter ranging from about 1 to 60 μm, the predominant size being 40 μm, and (2) Liquid flow rate = 12.3 ℓ/min and spray drop diameter ranging from 2 to 800 μm, the predominant size being about 300 μm. The results obtained under both conditions were similar and were comparable with the present results due to similarities in the design, as summarized in Table 9-1.

Horizontal Baffles - Experimental penetration as a function of gas velocity in vertical direction for horizontal zigzag baffles is shown in Figure 9-8. Liquid flow rate is used

Table 9-1. COMPARISON OF BAFFLE TYPE ENTRAINMENT SEPARATORS

	Present Design	Bell & Strauss (1973)	Houghton & Radford (1938)
Number of rows	6	4	6
$\theta°$	30	45	30
Lip to prevent reentrainment	none	1.9 cm on 1st & 3rd row only	0.5 on 4th & 5th row only
Staggering of rows	2.5 cm	none	none
Distance between rows	2.5 cm	3.1 cm between 2nd & 3rd row only	0
Spacing between baffles in a row	6.9 cm	8.8 cm	2 cm
Width of baffles	7.5 cm	6.2 cm	5 cm

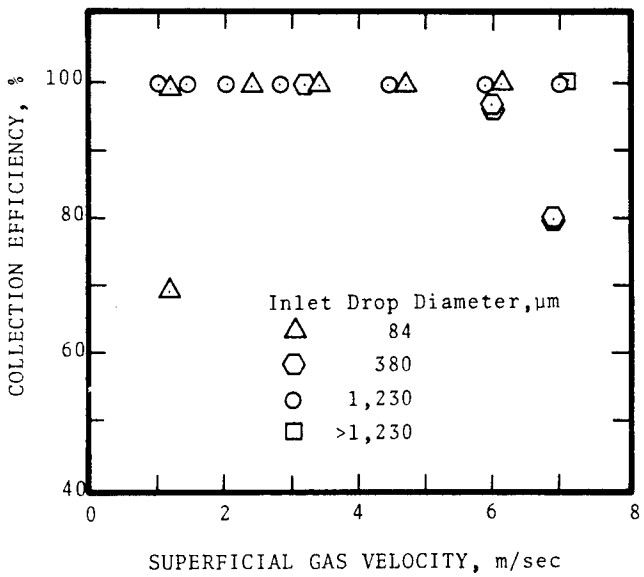

Figure 9-5. Experimental collection efficiency for zigzag baffle.

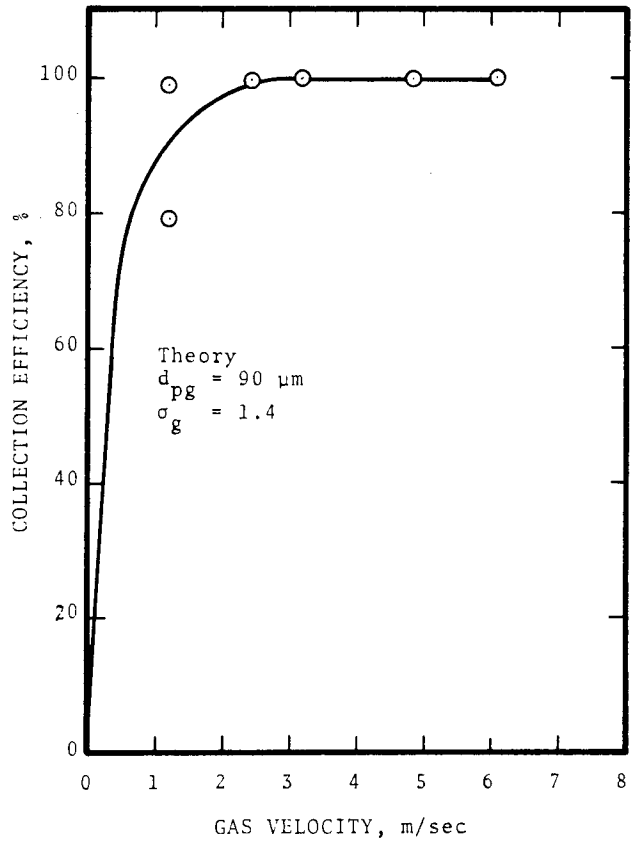

Figure 9-6. Collection efficiency for vertical zigzag baffle device.

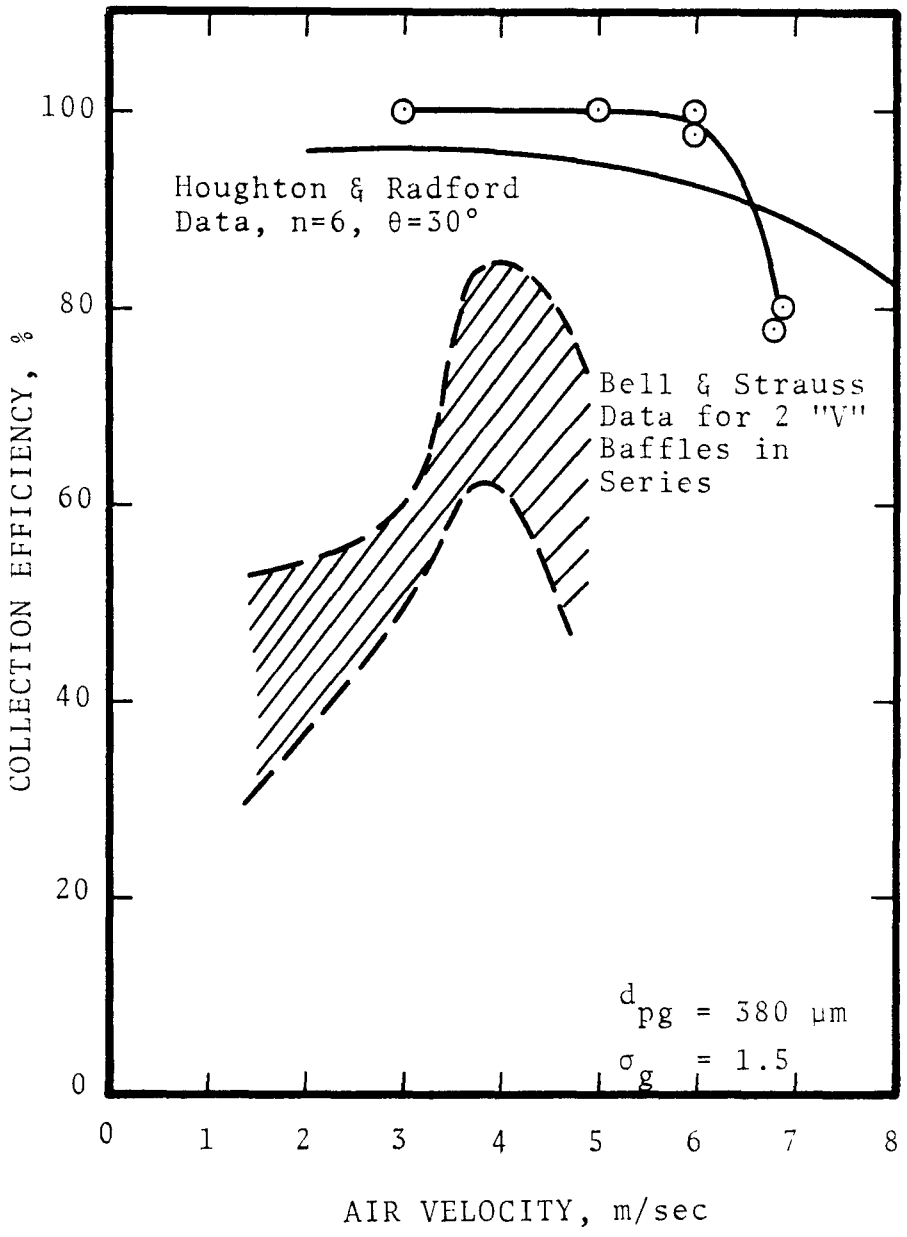

Figure 9-7. Collection efficiency for vertical zigzag baffle.

as a parameter. The inlet drops have a mass median drop diameter of 90 μm. As seen in the figure, reentrainment was not present for water flow rate = 13.5 ℓ/m^2-min and gas velocity up to 7.2 m/sec. At higher liquid flow rate (28 ℓ/m^2-min), reentrainment started at 5.2 m/sec. Penetration increased from 0 to 6.2% with the increase in gas velocity from 4.6 m/sec to 7.2 m/sec.

Inclined Baffles - Figures 9-9 and 9-10 are plots of overall penetration versus vertical gas velocity for baffles inclined at 45° to the horizontal. Liquid flow rate was used as a parameter. It was observed that the primary collection efficiency was close to 100%. Figure 9-9 also reveals that the reentrainment velocity depends on liquid loading. The higher the liquid loading the lower will be the reentrainment velocity.

Figure 9-11 is a plot of overall penetration versus vertical gas velocity for baffles inclined at 30° to the horizontal.

By comparing the primary collection efficiency curves for these different baffle orientations, it indicates that the baffle orientation has no effect on primary collection efficiency. However, the gas velocity for onset of reentrainment depends heavily on baffle installation method. Vertical baffle has highest drainage capability, therefore, its reentrainment velocity is highest. Comparison between reentrainment velocities for different baffle orientations will be discussed later.

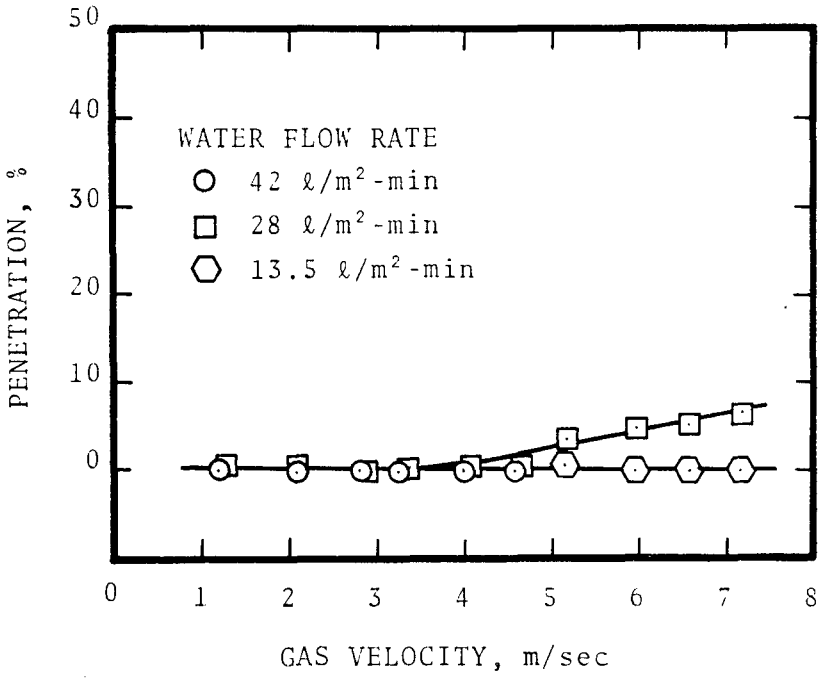

Figure 9-8. Experimental penetration versus gas velocity in vertical direction in zigzag baffles.

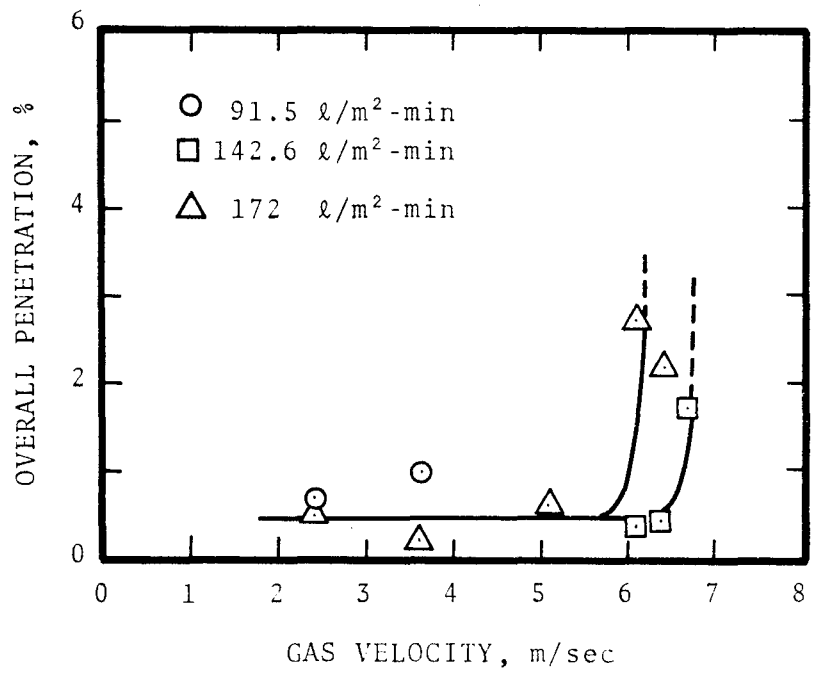

Figure 9-9. Overall penetration versus vertical gas velocity for drops having mass median diameter of 1230 μmA for 45° inclined baffles.

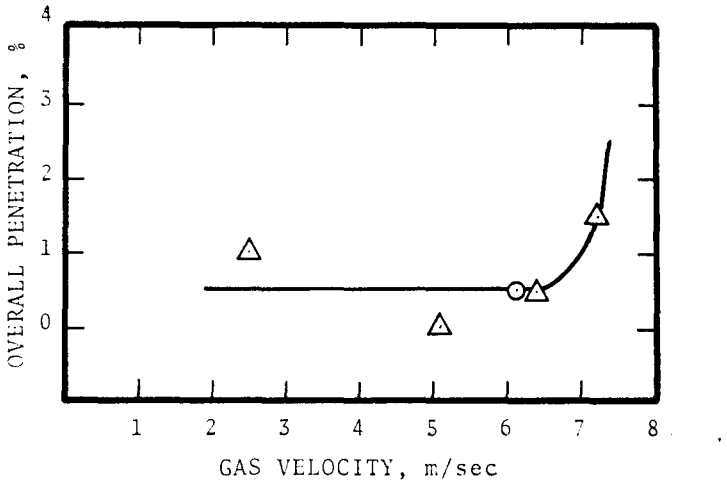

Figure 9-10. Overall penetration versus vertical gas velocity for drops having mass median drop diameter of 400 μm for 45° inclined baffles.

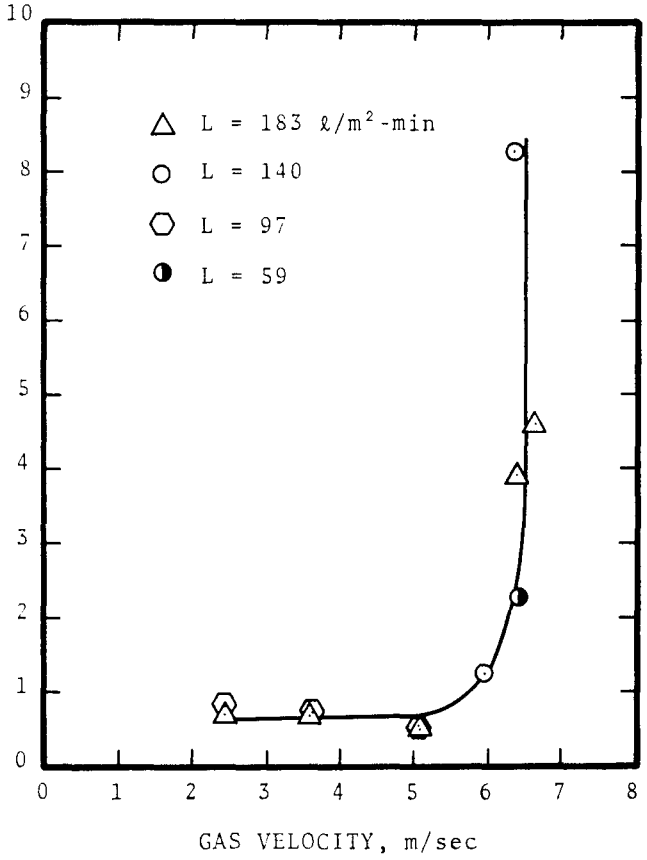

Figure 9-11. Overall penetration versus vertical gas velocity for baffles inclined at 30° to horizontal.

Pressure Drop

Experimental dry and wet pressure drop were plotted against superficial gas velocity for baffles in Figures 9-12 and 9-13 respectively. In both figures the solid lines represent the theoretical prediction of pressure drop as presented in Equation 9-6. As can be seen, theory agrees fairly well with experimental data. However, it predicts a slightly lower wet pressure drop than those observed in the experiments. By comparing these two figures, it reveals that the liquid load does not have a significant effect on pressure drop in the baffle section. This should be expected as liquid holdup in the baffles is small because of the high drainage rates.

An attempt was made to correlate the pressure drop data by using generalized pressure drop correlations for packed bed. The generalized pressure drop correlations are applicable to counter-current flow. In the present pilot plant, experimental pressure drop data were obtained using horizontal air flow and vertical air flow. The vertical air flow is more comparable to counter flow than to horizontal air flow.

In Figure 9-14, predicted pressure drop from generalized pressure drop correlations for packed bed is plotted against experimental pressure drop for baffles. As expected the data for vertical flow show better agreement. In the system with vertical air flow, reentrainment was observed to start at ΔP = 0.03 cm W.C./cm length of baffle section.

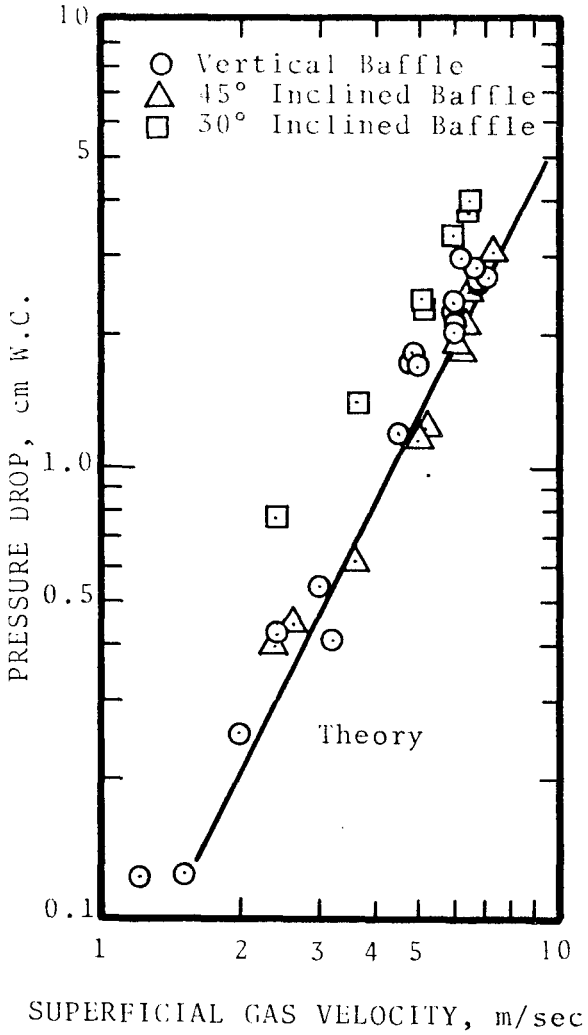

Figure 9-12. Dry pressure drop in zigzag baffles.

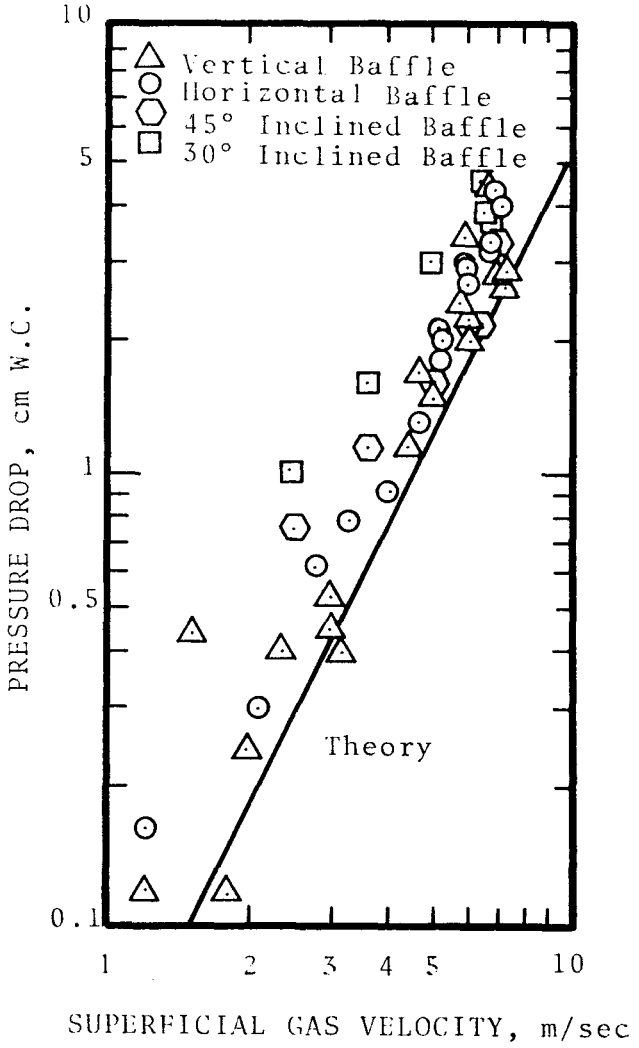

Figure 9-13. Wet pressure drop in zigzag baffles.

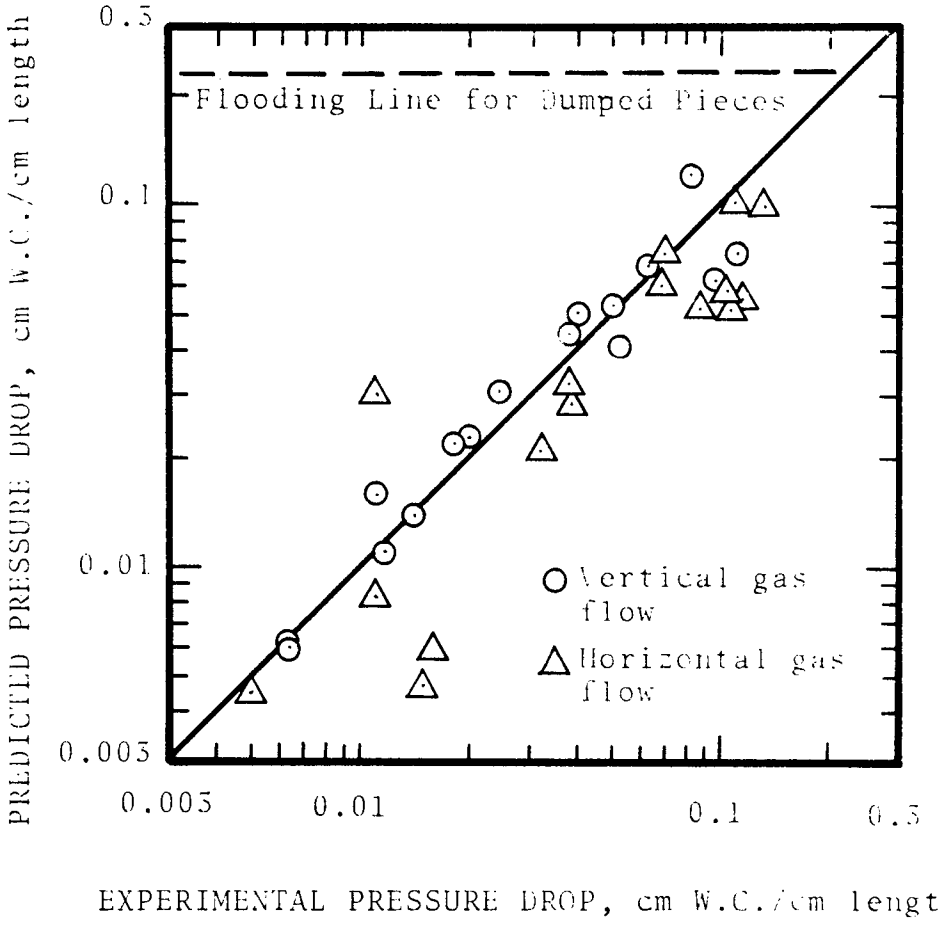

Figure 9-14. Predicted pressure drop from generalized pressure drop correlations for packed bed versus experimental pressure drop in zigzag baffles.

Reentrainment

Two very important parameters for determining reentrainment are gas velocity and the liquid to gas ratio. The combination of these two, which results in reentrainment as observed experimentally, is shown in Figures 9-15 through 9-18 for vertical baffles, horizontal baffles, 30° and 45° inclined baffles, respectively.

Drops were first observed to be torn off the baffle edge, i.e. onset of reentrainment, in the shaded area in Figure 9-15. Most of these drops were settled out in the observation section. The reentrainment rate was low (<0.1% of inlet loading) in this region. Sometimes, it was too low to be determined quantitatively. In the region above the shaded area, even though reentrainment is appreciable, it still did not have much effect on overall collection efficiency.

Figures 9-16 through 9-18 show the performance for vertical gas flow. The dash line in these three figures was the condition at which reentrainment sharply increased. In order to prevent heavy reentrainment, this line shows the maximum superficial gas velocity at a given liquid loading. The region below the dash line corresponds to the region above the shaded area in Figure 9-15.

By comparing these four figures, it is evident that reentrainment velocity depends strongly on liquid drainage capability. Vertical baffle has the highest drainage capability, heavy reentrainment was not observed to occur even at the maximum capacity of the present pilot plant.

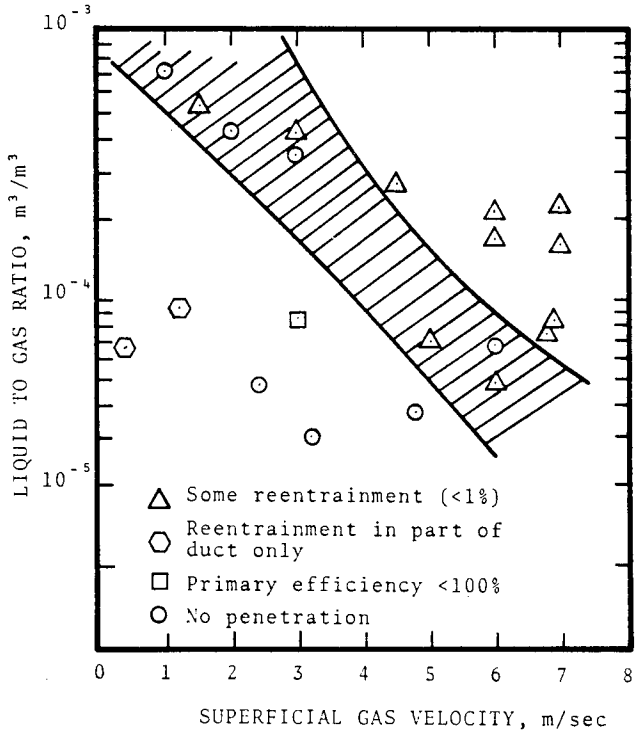

Figure 9-15. Effect of gas velocity and liquid load on performance of vertical baffles. (Horizontal gas flow)

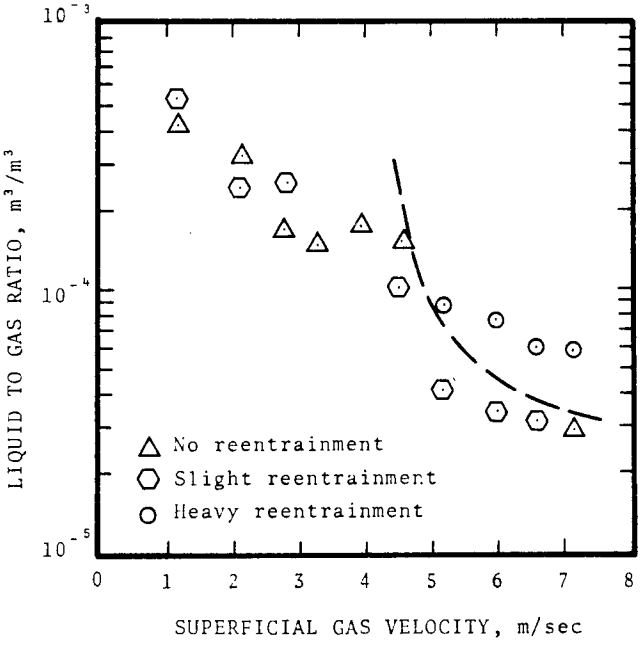

Figure 9-16. Effect of gas velocity and liquid load on performance of horizontal baffles. (Vertical gas flow)

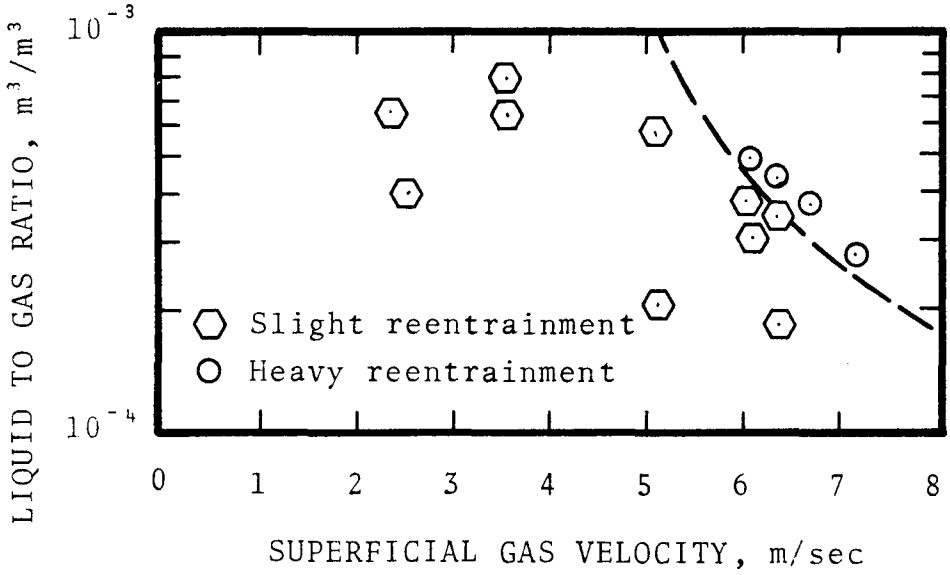

Figure 9-17. Effect of gas velocity and liquid load on performance of 45° inclined baffles (vertical gas flow).

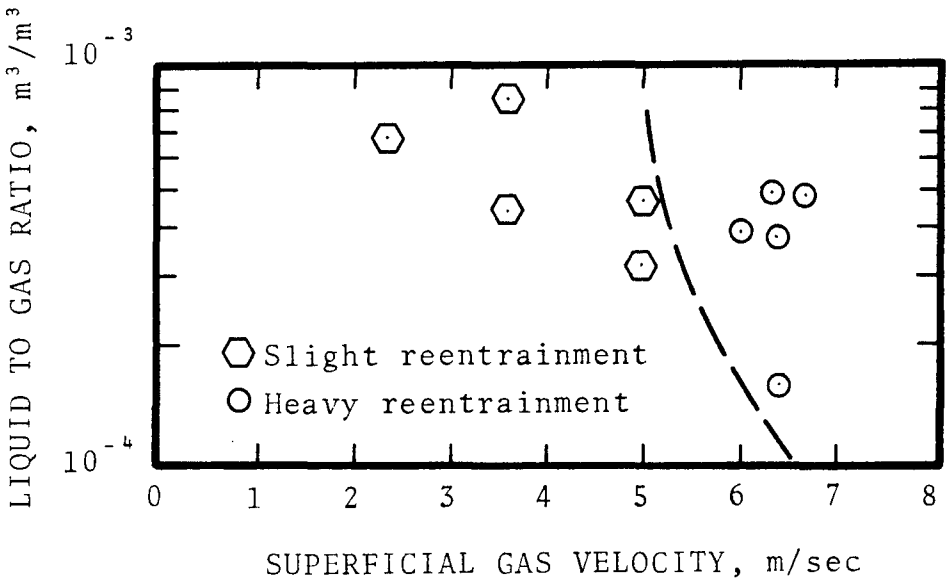

Figure 9-18. Effect of gas velocity and liquid load on performance of 30° inclined baffles (vertical gas flow).

Liquid Flow on the Baffles

Flow of liquid on the baffle surface was observed in some of the runs. As the flow increases, the film thickness of the liquid near the downstream edge increases. The gas stream forms a wake at the back side of the baffle, which tears away some of the liquid at the downstream edge. The approximate shape of the wake is shown in Figure 9-19. The wake formation becomes more pronounced with increasing gas velocity. The flow of liquid film on the back side of the baffle is shown in the same figure.

If the liquid flow on the baffle surface is small, only drop flow takes place on the back side of the baffle. Some of these drops reach the upstream edge of the baffle, where they are reentrained. The reentrained drops splash on the adjacent baffle in the same row and disintegrate. Some of these small drops are reentrained in the air. The drops normally splash on the third quarter width of the baffles as measured from the upstream. The drops flowing on the back side of the baffles are 3-4 mm in diameter.

Reentrainment from the downstream edge of the baffle was more significant compared to reentrainment from the upstream edge. If the liquid flow on the baffle surface was drop flow, some of these drops reached the downstream edge and (1) were reentrained, (2) were turned to the back side of the baffle, (3) fell down at the edge due to gravity, or (4) stayed at the edge of the baffle until they grew by coalescing with other drops. Most of the drops were collected by the third or fourth step. If the liquid was flowing as a film on the baffle, part of the film was torn and reentrained at the downstream end. The drops reentrained from the downstream edge of the baffle were 3-5 mm in diameter. These drops were normally collected on

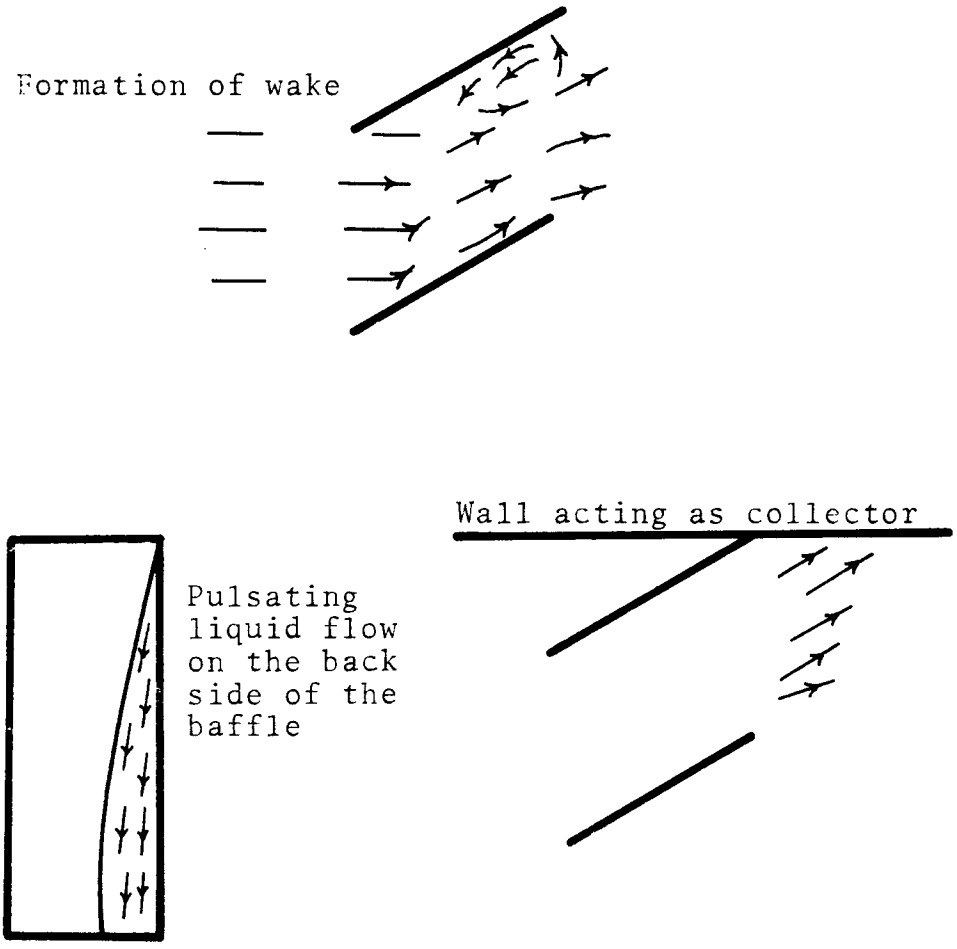

Figure 9-19. Some observed phenomena in entrainment separator (a) formation of wake (b) liquid flow on the back side of the baffle (c) wall effect.

the baffles of the second row, i.e., drops reentrained from the second row were collected on the baffles in the fourth row.

Some wall effect was observed in the baffle section. There were four baffles in a row and the side walls of the test section acted as collectors for the entrainment. This effect is shown in Figure 9-19.

The liquid flow pulsated whenever reentrainment took place and occurred in film flow and in drop flow. It was difficult to determine the amplitude of the pulsating film which may have been of the order of 0.05 cm. The frequency of the wave was not measured.

CONCLUSIONS

1. The theoretical model based on turbulent mixing agrees quite well with the experimental results.
2. The dry pressure drop in zigzag baffles can be determined from drag coefficients for inclined plates held in the flow. The effect of liquid load on pressure drop is small.
3. Wet pressure drop for vertical gas flow in zigzag baffles can be predicted from generalized pressure drop correlation for packed bed.
4. The onset of reentrainment velocity depends upon the drainage capability of the baffles. Vertical baffles with horizontal gas flow has the highest reentrainment velocity at a given liquid loading.

CHAPTER 10

AIR-WATER-SOLID EXPERIMENTS

The purpose of this study is to determine the effects of solids suspension on separator performance and plugging due to solids deposition. The type of entrainment separator studied includes the cyclone and the zigzag baffles.

Experimental Set-up

Necessary modifications were done in the pilot plant to study entrainment separation with suspended solids present.

Figure 10 shows the revised system for air, water, and solids. This system incorporates a wash water system which is used to cut off the tanks holding slurry so the rest of the system may be washed. The wash system may be operated after observing the test section for scaling and plugging. This wash system has two advantages, 1) it keeps all the lines clean and 2) the slurry can be re-used in the experiments.

Pure "Cal O" ($CaCO_3$) were used as solids. The particles have a mass median diameter of 1.9 μm and a geometric mean derivation of 1.3. The solids concentration varies between 10% and 20% by weight. These concentrations are in the range used in industrial scrubbers.

Experimental Data and Observations

The Cyclone - The first set of experiments were made with the cyclone separator. The experimental results are summarized in Table 10-1. The results indicated that the presence of the solid did not affect the collection efficiency of the cyclone. However, the solid caused solid deposition problem.

Table 10-1. EXPERIMENTAL RESULTS FOR CYCLONE (AIR-WATER-SOLID SYSTEM)

Exp. No.	Test Section	Air Velocity cm/sec	L/G	Hours Of Operation	Collection Efficiency %	Pressure Drop cm H_2O	Reentrainment
181	Cyclone	5,280	3.072×10^{-4}	2	100	15.57	-
182	Cyclone	2,920	3.084×10^{-4}	1	100	12.60	-
183	Cyclone	2,400	3.45×10^{-4}	2	100	9.29	-
184	Cyclone	880	4.37×10^{-4}	2	100	1.28	-
185	Cyclone	2,400	3.08×10^{-4}	16**	100	8.59	-
186	Cyclone	880	4.37×10^{-4}	16**	100	1.16	-
187	Cyclone*	4,800	2.83×10^{-4}	16**	100	13.4	-

* Inlet vane present, inlet area = 30.5 cm x 7.5 cm

** Cyclone washed prior to experiment

Table 10-2. EXPERIMENTAL RESULTS FOR BAFFLE (AIR-WATER-SOLID SYSTEM)

Exp. #	Test Section	Air Velocity m/sec	L/G volumetric	Hrs. of operation	Collection Efficiency %	Pressure drop cm W.C.	Reentrainment
188	Baffle	3.0	4.26×10^{-4}	16*	99	0.91	little
189	Baffle	4.4	2.95×10^{-4}	16*	99.13	1.53	little
190	Baffle	5.4	3.068×10^{-4}	16*	99.05	2.11	little
192	Baffle	6.0	3.4×10^{-4}	16*	99	3.47	little
193	Baffle	2.2	4.63×10^{-4}	16*	99	0.54	—
194	Baffle	1.2	1.58×10^{-4}	16*	97.04	0.21	—
195	Baffle	3.6	5.02×10^{-4}	32*	99.3	1.53	—

* separator was washed with water prior to experiment

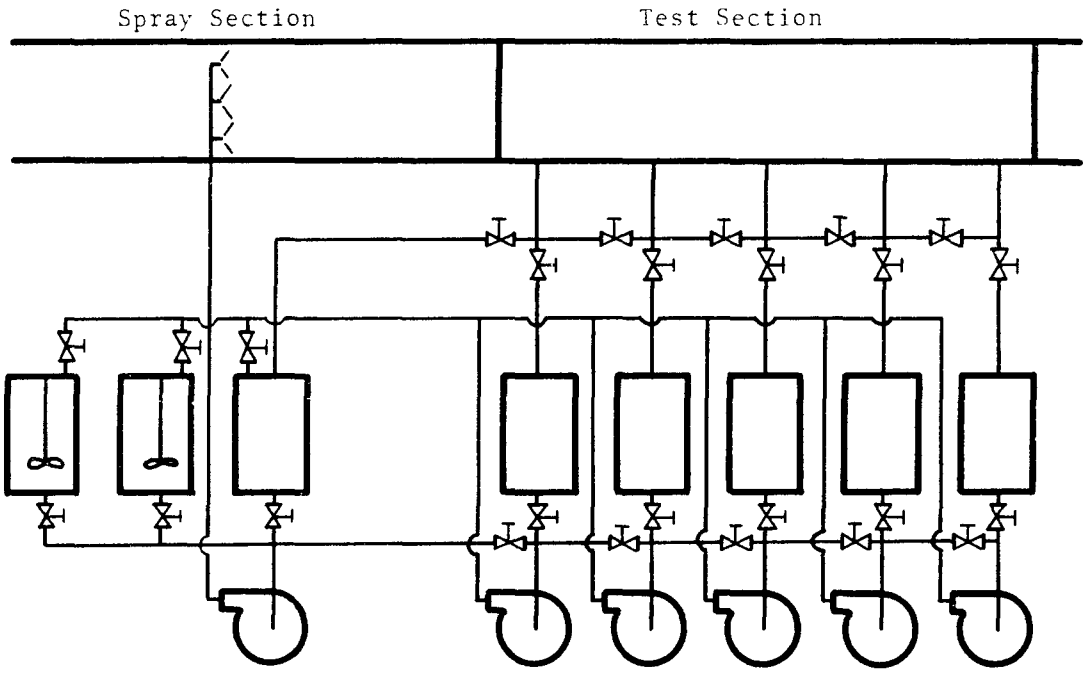

Figure 10. Air-water-solid system.

The cyclone was opened for visual observation of solid deposition pattern. It was discovered that most of the solid deposition occurred in the upper half of the cyclone. The thickness of the solid layer was 0.2 cm after 16 hours of operation. In the area close to cyclone inlet, solid deposition was not present. This is because most of the entrainment was collected near the cyclone inlet. The scouring action of the collected liquid prevented the deposition.

It was observed during experiment that some slurry drops were torn away from the liquid film on the cyclone surface and some drops did not form liquid film when they were collected. These drops were more susceptible to creep along the wall in the direction of gas flow. As these drops travel along the wall, solids were deposited at the wet-dry interface. The solids that deposited were not washed away by the slurry as the flow on this surface was not continuous.

An attempt was made to wash the cyclone with fresh water during the experiment. However, it was discovered that the fresh water was not flowing in the same area where solids were deposited. So at the end of one hour of washing, the cyclone inlet velocity was increased (from 24 m/sec to 30 m/sec). The cyclone was then found to be nearly clean after 30 minutes of washing. The total fresh water added during washing time was 9.4% by volume of slurry flow.

Zigzag Baffles

Vertical baffles were used in the experiment. The experimental data are presented in Table 10-2. Seven experiments were conducted at air velocities ranging from 1.2 m/sec to 6.0 m/sec. Each of the first six experiments was 16 hours long and was conducted in two 8-hour segments. Run #195 was conducted continuously for 32 hours. The collection efficiency was close to 99% in all the experiments except where it was 97% in experiment number 94,

and the air velocity was 1.2 m/sec.

The solids deposition was observed after each experiment. It was observed that the solids deposition increases as the air velocity is increased through the entrainment separator.

The solids deposition near the edges was more than on the center of the baffles. The last three rows had more deposition than the first three. The deposition on the back of the baffle was thicker than the frontal surface. The deposit was as thick as about 6 mm on leading edges and up to about 1 mm on the flat surfaces. There were heavy solid depositions on the side wall and ceiling of the test section after the baffle. The cake deposit pattern was very irregular and showed a strong influence of eddies and wake flow patterns, which caused deposition on downstream surfaces.

The overall performance was comparable with the air-water system, i.e., the presence of solids did not affect the collection efficiency or pressure drop.

CONCLUSIONS

1. The presence of solid in the entrainment does not affect the collection efficiency of the cyclone and baffle as long as the deposited solids do not change the geometry of separator considerably.
2. Solids will deposit on the wet-dry interface.
3. There appears to be a minimum slurry flow rate when scoring can occur. Below this minimum, solid deposition can occur even though the surface is wet.
4. The washing method is important. For the cyclone washing, the gas velocity should be different than in normal operation.

Page Intentionally Blank

CHAPTER 11

SOLIDS DEPOSITION

Solids deposition is a big problem in entrainment separators. Either suspended or dissolved solids in entrained drops can deposit in an entrainment separator and cause plugging, a deterioration in performance, and eventual inoperability of the scrubber system. The precipitation of dissolved solids depends on temperature, concentration, and nucleation conditions which are unique to any specific system and it is, therefore, to be controlled by the appropriate physical chemical conditions rather than a general design approach. Suspended solids deposition, on the other hand, appears to be amenable to a general treatment and it has been selected for study in this program.

MECHANISM OF SOLIDS DEPOSITION

There has been ample demonstration that suspended solids will deposit in any type of entrainment separator so our attention can be given to how it happens, how to predict its behavior, and how to prevent or minimize it. The mechanisms of suspended solids deposition can include the following:

1. Settling to non-vertical surfaces
2. Impaction due to:
   A. Surface curvature
   B. Liquid flow direction changes, including turbulence
3. Diffusion

4. Electrophoresis
5. Liquid loss from slurry drops due to:
    A. Drop running down a surface
    B. Evaporation
    C. "Blotting" by a partially dry surface, such as previously deposited material.

Once solids have deposited on a surface, the question is why they adhere to it. Adhesion of particles may be caused by:

1. Gravitational force on non-vertical surfaces
2. Trapping in surface roughness due to:
    A. The original surface
    B. Previously deposited solids
3. Electrostatic forces
4. Surface tension forces due to moisture in the spaces between particles.
5. Cementing due to the precipitation of slightly soluble materials.
6. Bridging of deposit between elements of the separator.

There have been a few adhesion studies dealing with the adhesion of solid particles in pure gases or liquids, but no studies have been known so far about the rate of deposition of suspended solids on an entrainment separator. H. Uno and S. Tanaka (1970) conducted a study on the adhesion of the suspension of particles on the wall, and they considered that wetting of the wall is the most important factor relating with the adhesion of particles on a surface.

There are three types of wetting, namely, adhesional wetting, immersional wetting, and spreading wetting.

Adhesional wetting is a state of water drop remaining on the water repellent surface. Immersional wetting is the state of particles trapped on the wall when the wall is immersed in a liquid medium, and spreading wetting is the state of water spreading freely on a clean surface. Among these three types of wetting, the spreading wetting has a predominantly strong trapping effect.

When a liquid film containing a suspension of particles flows down a surface, some of the suspended particles are trapped on the surface. The driving force for particle trapping is the surface tension of the liquid film acting upon the water line of the particle surface.

When the thickness of the liquid film becomes less than the diameter of the particles as in Figure 11-1 but not too thin like Figure 11-2, the pressure "P" on the particle due to surface tension can be expressed as:

$$P = 2\pi \sigma \sin \alpha \, (2r\delta - \delta^2)^{1/2} \qquad (11\text{-}1)$$

where r = radius of the particle, σ = surface tension, α = angle made between suspension surface and contact angle of the medium against the particle, δ = liquid film thickness. If "δ" is smaller than "2r", the particle is pressed against the wall and trapped. When the liquid film becomes very thin, as in Figure 11-2, the pressure at this stage is expressed as:

$$P = \sigma \left| \frac{1}{r'} - \frac{1}{R} \right| \qquad (11\text{-}2)$$

where "R" is the radius at the water line along the particle surface made by the remaining water and "r'" is the radius of curvature between the particle surface and the wall.

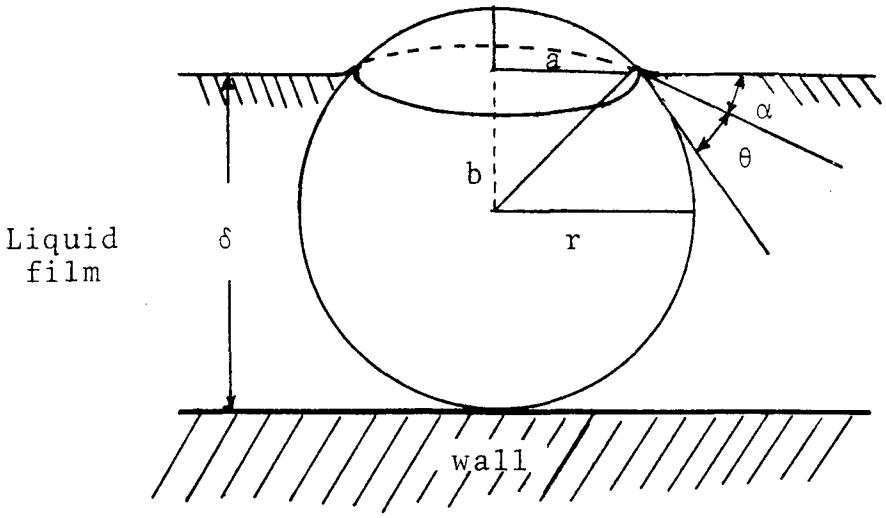

Figure 11-1 - Trapping of particle by thick liquid film.

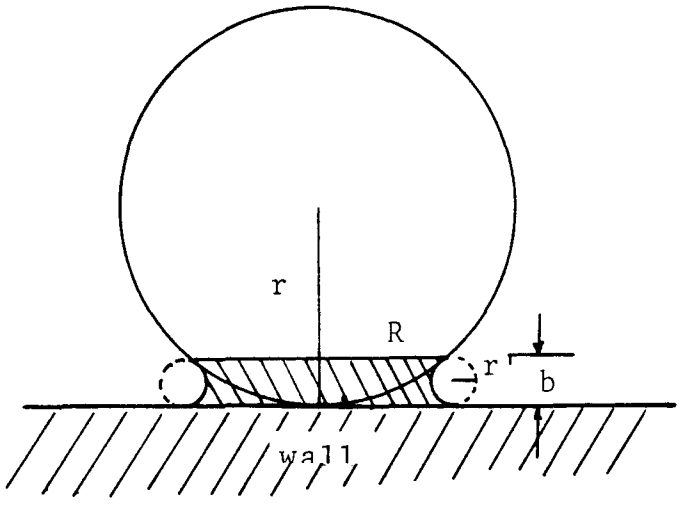

Figure 11-2 Trapping of particle by thin liquid film.

Removal of deposits can be accompanied by the elimination of attractive forces. Washing is the most common way of overcoming the attractive forces. From equation (11-1) it can be deduced that if the liquid film thickness is larger than the diameter of the particle, the particle is free from the attractive forces. The degree of freedom of the particle increases as the thickness of the liquid film is increased.

Based on this, it appears that the factors which affect the deposition of solids on a surface will be:

1. Particle properties, such as size, density, and shape
2. Slurry flow per unit area of collection surface
3. Liquid film thickness
4. Slurry drop size
5. Slurry concentration
6. Collection surface orientation.

EXPLORATORY EXPERIMENTS

Observations of air-water-solid experimental systems show that suspended solids will deposit and adhere to smooth vertical surfaces, and even on the underside of horizontal surfaces, under conditions where there is little or no evaporation of water and no cementation. Thus, one can conclude that there is less chance of finding a general means of stopping deposition and adhesion than of learning how to scour deposits away. The apparatus used to determine the minimum flow rate that scouring occurs is shown in figure 11-3. It consists of a constant head reservoir, through which an overflowing device gives a constant slurry flow. The air jet sprays the slurry onto the baffle. Three layers of hardware screen were used to

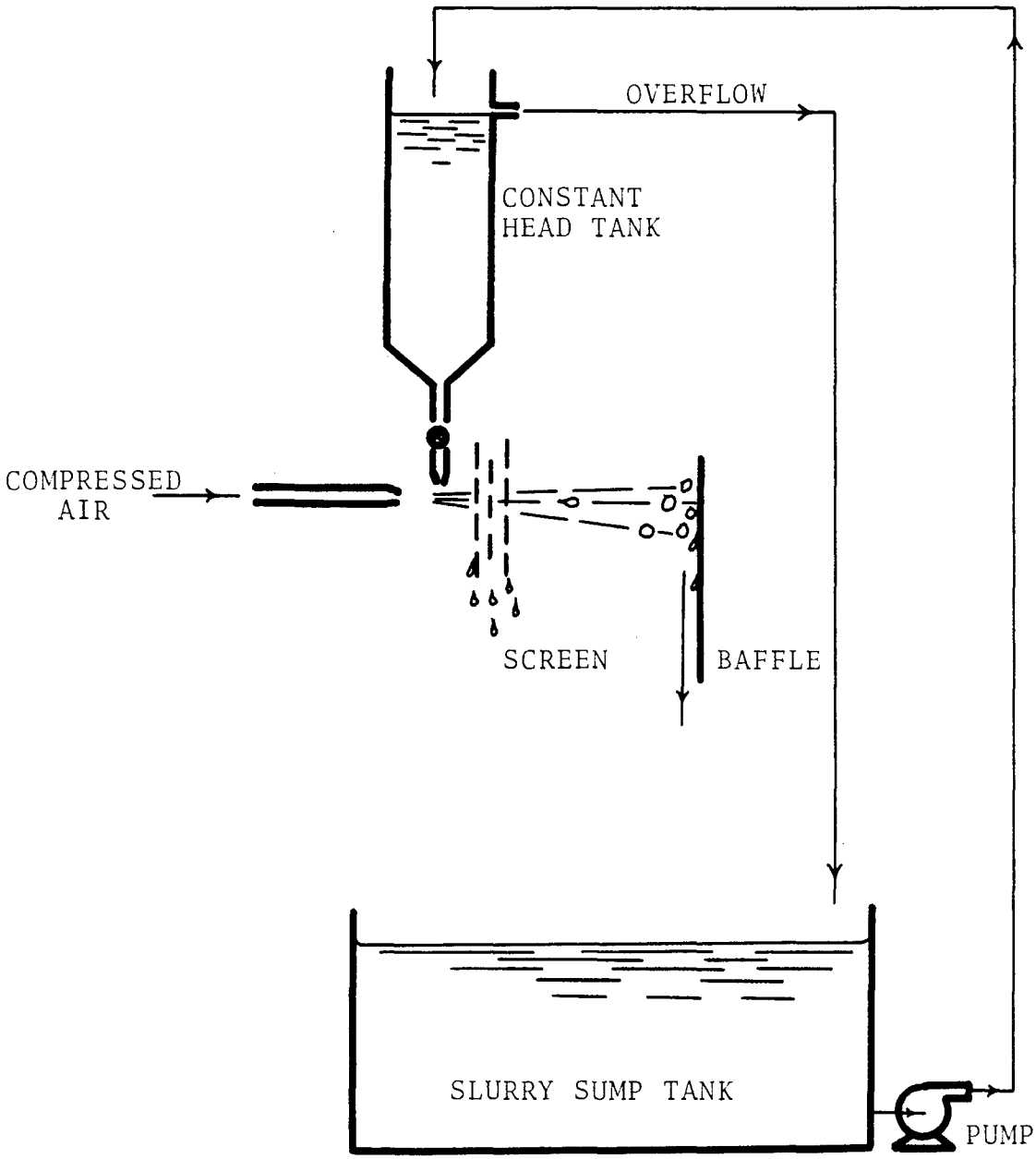

Figure 11-3. Experimental set-up for solid deposition test.

knock out large droplets and to control the amount of slurry reaching the baffle. The pump recirculates the slurry back to the head tank and thus the experiment can be run continuously.

The baffle is divided into eight sections - four on each side of the baffle. Each section is bounded by silicone rubber to prevent the slurry flowing from the above sections (See Figure 11-4). An aluminum foil of 7 cm diameter is clipped to each section. The slurry is then sprayed onto the baffle by the air jet. The flow rate at each section is determined by placing a 7 cm diameter filter paper in front of that section for about 60 seconds and measuring the increase in weight of the filter paper. The concentration of $CaCO_3$ in the slurry was calculated from the residual weight after evaporating the water away from a known quantity of slurry. The deposition rate was calculated from the dry weight gain of the aluminum foil after each run.

During this study, the effects of particle properties, slurry drop size, and collection surface orientation on slurry deposition were investigated.

Particle Properties

Calcium carbonate particles were examined under the microscope. They appeared to be irregular in shape. However, their size distribution is quite uniform.

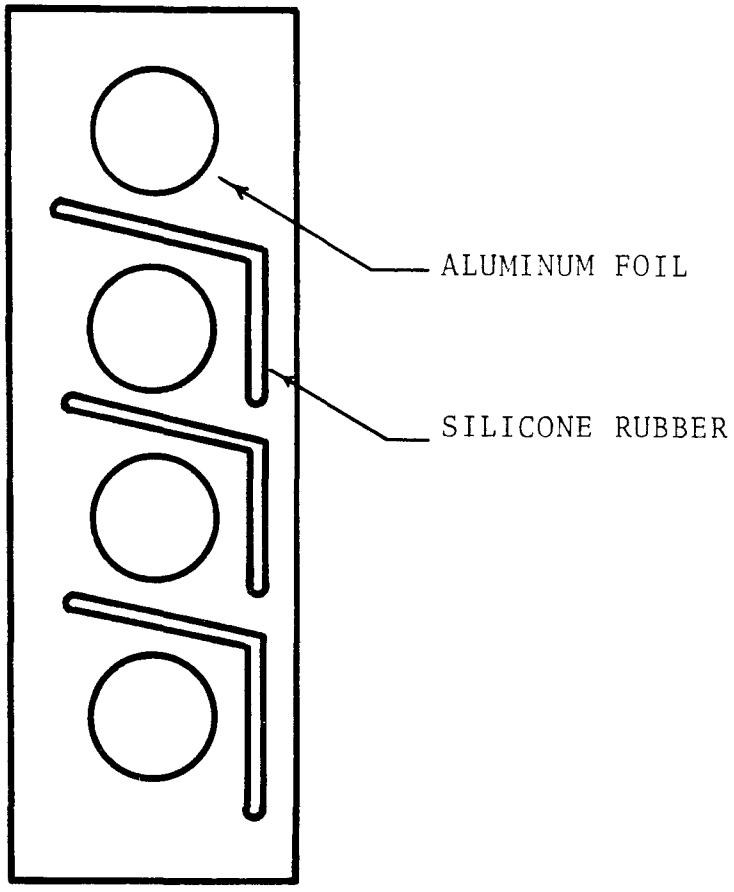

Figure 11-4. Baffle structure.

Figure 11-5 shows the particle size distribution of calcium carbonate particles. They have a number median diameter of 1.5 μm and a geometric standard deviation of 1.3. This corresponds to a mass median diameter of 1.9 μm with the same geometric standard deviation.

Collection Surface Orientation

Ten runs were conducted to investigate the effects of collection surface orientation on deposition rate. The first five runs were conducted with the baffle kept in a vertical position. Runs 6 through 8 were conducted with the baffle inclined and the slurry sprayed on the upper surface, and runs 9 and 10 were conducted with the baffle inclined and slurry sprayed at the lower surface. The weight percent of $CaCO_3$ in the slurry and the duration of each run are listed in the tabulation below:

Run No.	$CaCO_3$ concentration % by weight	Duration of run, min.
1	6.0	435
2	8.5	420
3	12.3	465
4	9.6	285
5	7.7	385
6	9.5	275
7	6.3	370
8	9.1	438
9	6.7	795
10	6.0	345

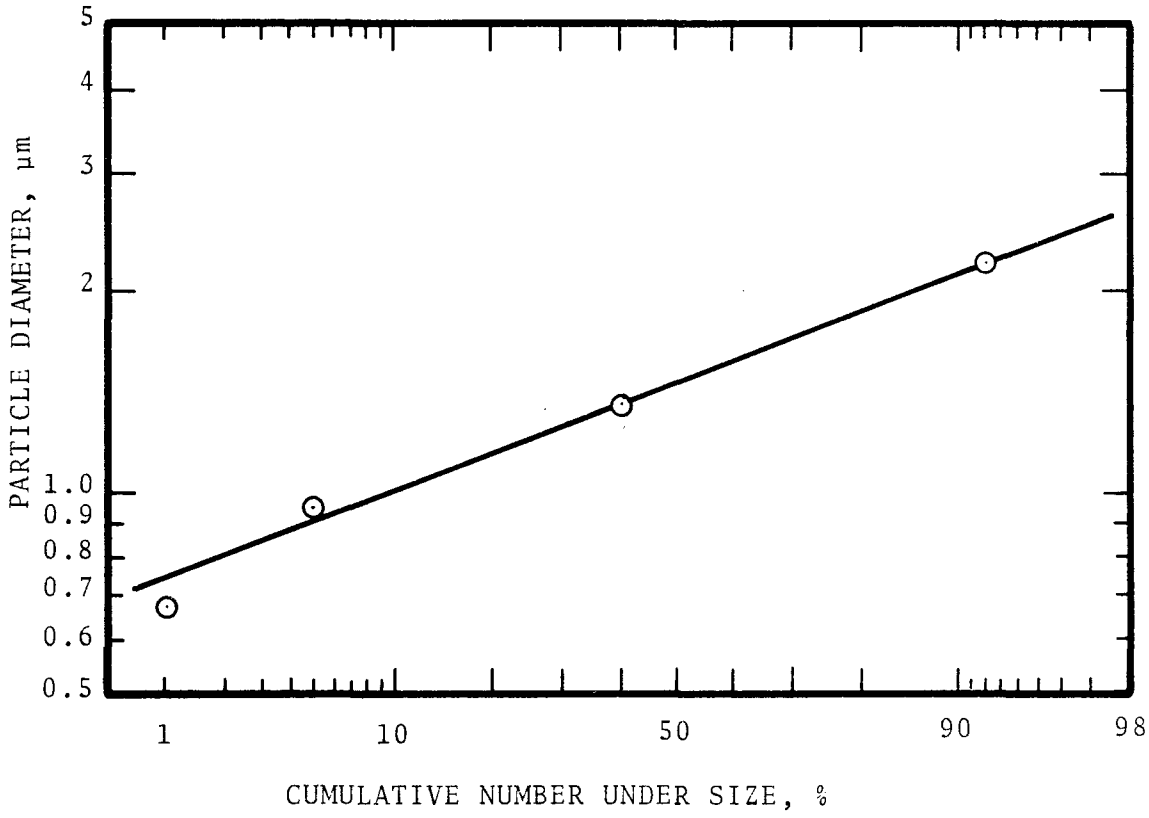

Figure 11-5. Particle size distribution for $CaCO_3$ particles.

Figures 11-6, 11-7, and 11-8 are plots of experimental data in the form of percent of solids in slurry deposited versus the total mass of slurry (liquid plus solid) flowing to a unit area in a unit time. Both figures show that solid deposition rate is small at high slurry flow rate.

Figures 11-6, 11-7, and 11-8 are plotted in Figure 11-9 for comparison. It can be seen that slurry sprayed on the upper surface of an inclined surface has the highest deposition rate. This phenomenon might be due to the higher settling rate of solids on inclined surfaces, as is reported by Eli Zahavi and Eliezer Rubin (1975).

The solids deposition data can also be plotted in the form of Figure 11-10, which shows deposition rate as a function of slurry flux. It is striking to see the sharp maximum at slurry flux less than a few tenths mg/cm^2-sec. For comparison with traditional engineering units, 0.1 mg/cm^2-sec corresponds to about 1.5×10^{-3} gal/ft^2-min and an entrainment rate of 1 gal/MCF would correspond to about 0.1 gal/ft^2-min for a zigzag baffle of the design we used. Thus, if the inlet entrainment rate were 1 gal/MCF the most rapid deposition rate, and the place where plugging would first occur, would be where the entrainment has been reduced to roughly 1% of the inlet loading. This is based on the assumption that the separation efficiency per baffle has dropped to 50% or less because the larger drops have been removed.

Drop Size Effect

It has been observed that cake formation at the back surface of the baffle is sometimes thicker than on the frontal surface. When the baffle is vertical and

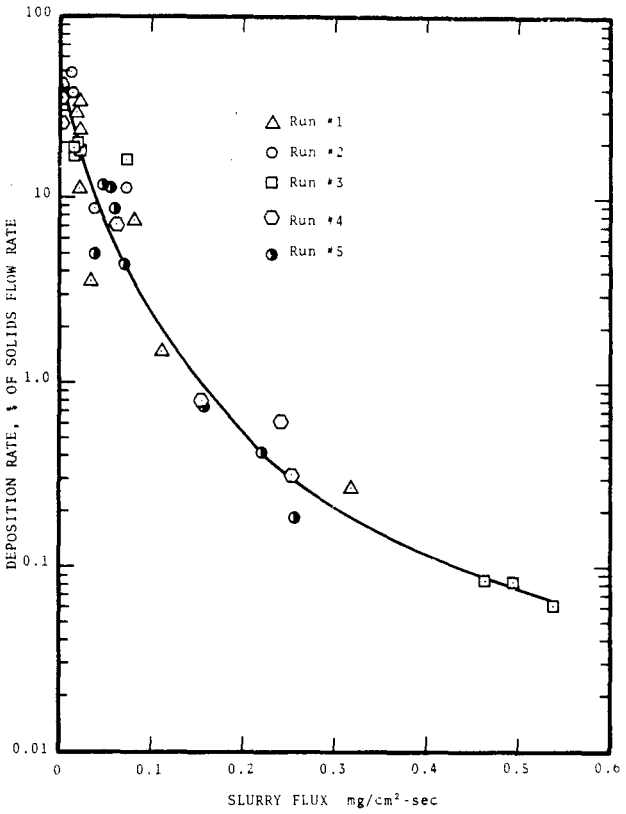

Figure 11-6. Solid deposition rate versus slurry flow rate for vertical baffle at an angle of 30° with the direction of gas flow.

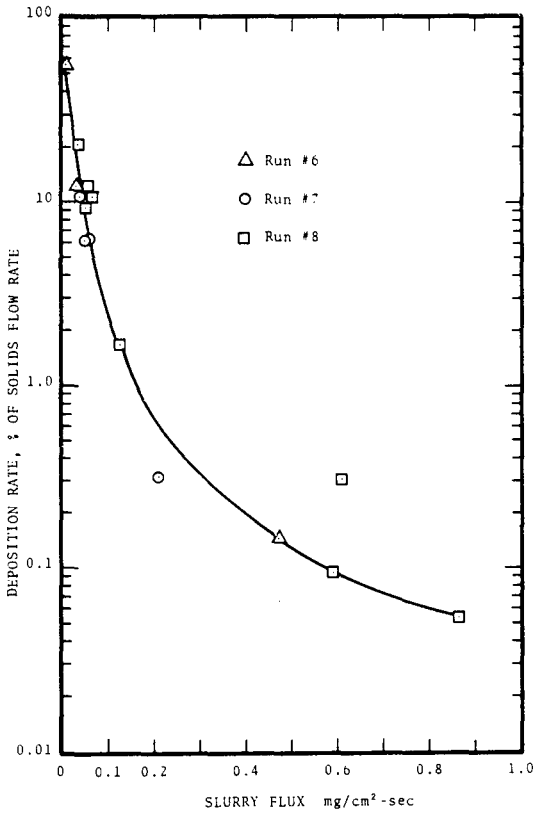

Figure 11-7. Solid deposition rate versus slurry flow rate for inclined baffle with slurry sprayed at the upper surface.

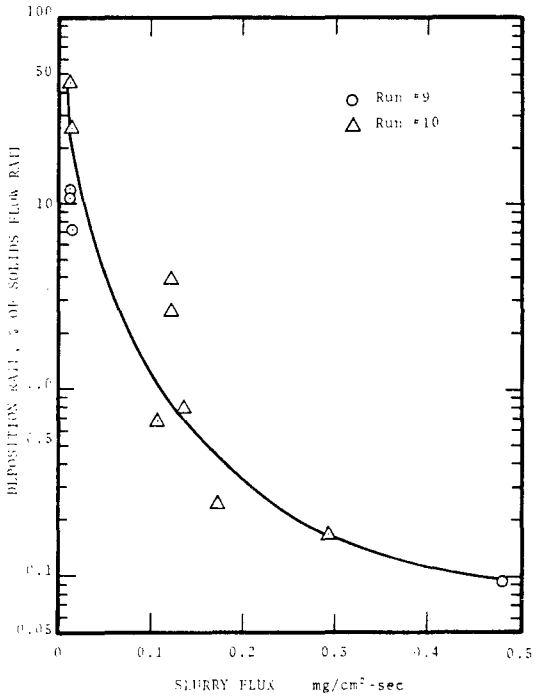

Figure 11-8. Slurry deposition rate versus slurry flux for inclined baffle and with the slurry sprayed at the under surface.

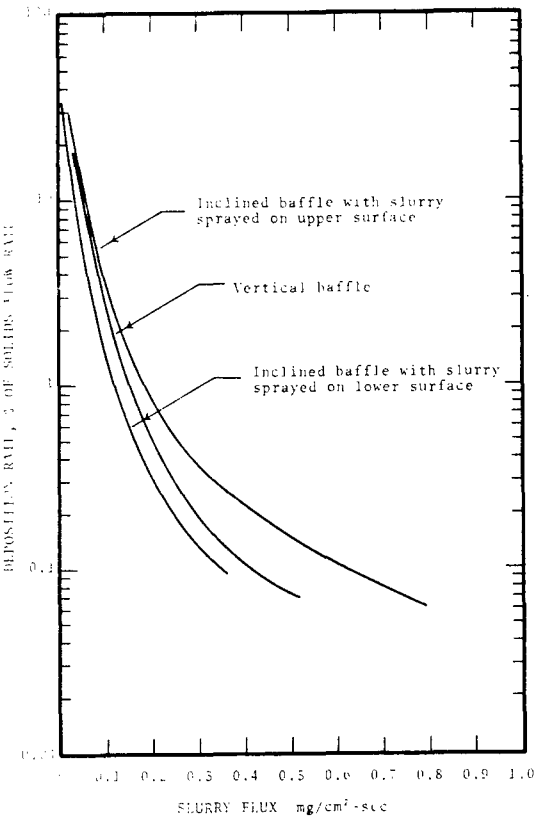

Figure 11-9. Comparison of Figures 11-6, 11-7, and 11-8.

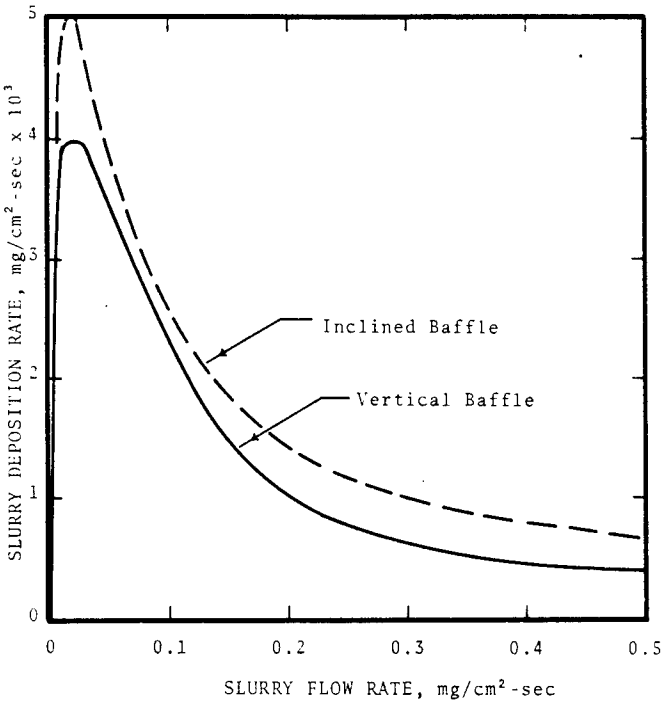

NOTE: Slurry deposition rate must be multiplied by fraction solids to get cake deposition rate.

Figure 11-10. Slurry deposition rates for inclined and vertical baffles.

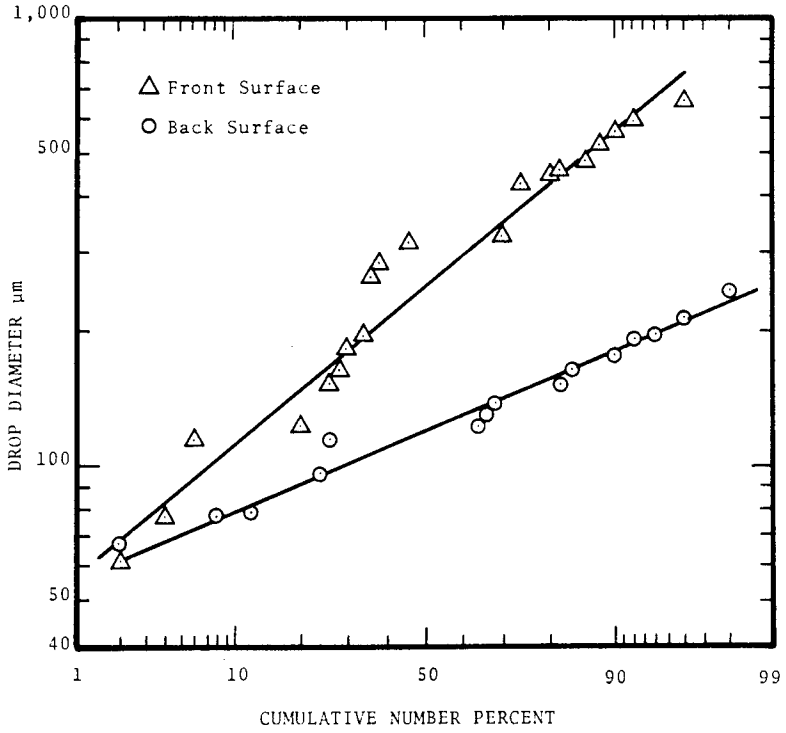

Figure 11-11. Drop size distribution plot for Run #10.

the slurry is sprayed normal to the baffle surface, deposits at the back surface are scarce. However, when the baffle is inclined at an angle to the vertical or if the slurry is directed at an angle to the baffle surface, as it will be in a zigzag arrangement, heavy deposits are obtained on the back surface. Sometimes deposition on the back surface is thicker than that on the frontal surface.

During run number 10, drop size measurement was taken from both surfaces and compared and the observations are summarized below. Figure 11-11 shows the drop size distribution from both surfaces.

	Front Surface	Back Surface
Slurry mass median drop diameter hitting the surface	830 μm	170 μm
Drop geometric standard deviation	1.9	1.4
Amount of deposition	Varies along the surface	Heavier than the front, no sign of washing is observed

Thus, it was suspected that the slurry drop size might have an effect on cake formation on baffle surfaces. Five experiments were then conducted to investigate the effect of drop size on the deposition rate on a baffle surface. Different drop sizes were generated by varying the orifice size of the air nozzle. Listed below is a summary showing the weight percent of $CaCO_3$ in the slurry, duration of each run, and drop sizes. The slurry sprays for runs 11 and 12 were generated by a 0.22 cm air

nozzle, while those of runs 13, 14, and 15 were generated by an air nozzle of 0.46 cm diameter.

Run No.	$CaCO_3$ Concentration (% by weight)	Duration of Run (min.)	Drop Size: Mass Median Drop Diameter (μm)	Drop Size: Geometric Standard Deviation
11	3.8	211	190	1.6
12	10.5	360	160	1.6
13	9.5	294	390	1.7
14	7.5	310	440	1.7
15	7.7	420	420	1.7

Figure 11-12 is a plot of experimental data in the form of slurry deposition rate versus slurry flux for small drops while Figure 11-13 shows the same relationship for large drops.

The two graphs are plotted in Figure 11-14 for comparison. It can be concluded that small drops have a slightly higher deposition rate than large drops at high flow rates.

Some Observations on Solids Deposition Experiments

During the exploratory experiments, the mechanisms of drop deposition on the baffle, particle adhesion, and washing were carefully observed. This was in order to develop a means of incorporating the data obtained during the experiments into a prediction of where deposition occurs most in the pilot plant. The following phenomena were observed:

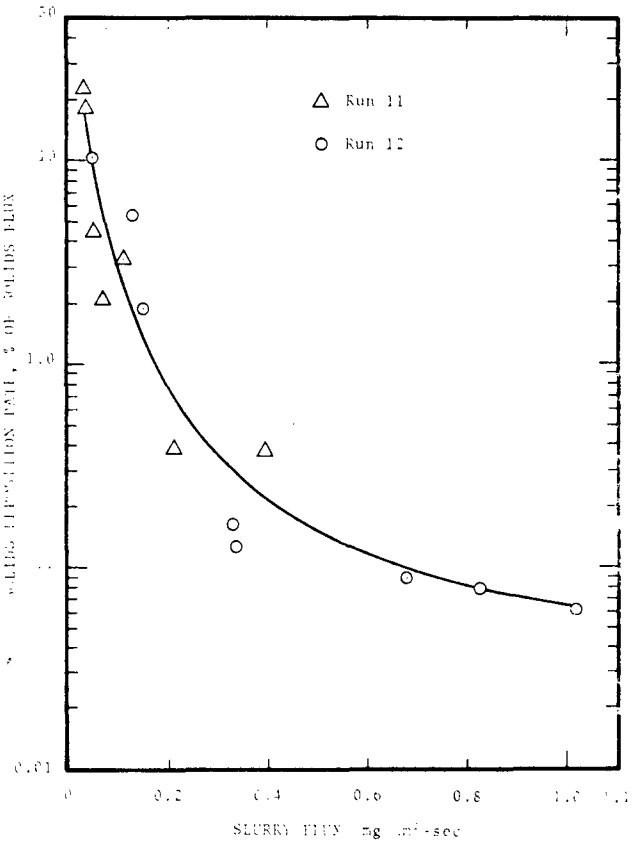

Figure 11-12. Solids deposition rate vs. slurry flux for big drops.

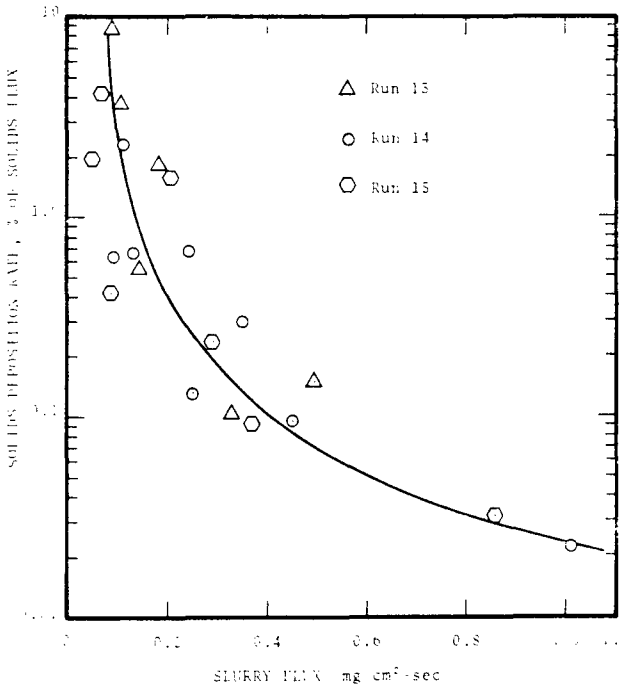

Figure 11-13. Solids deposition rate vs. slurry flux for big drops.

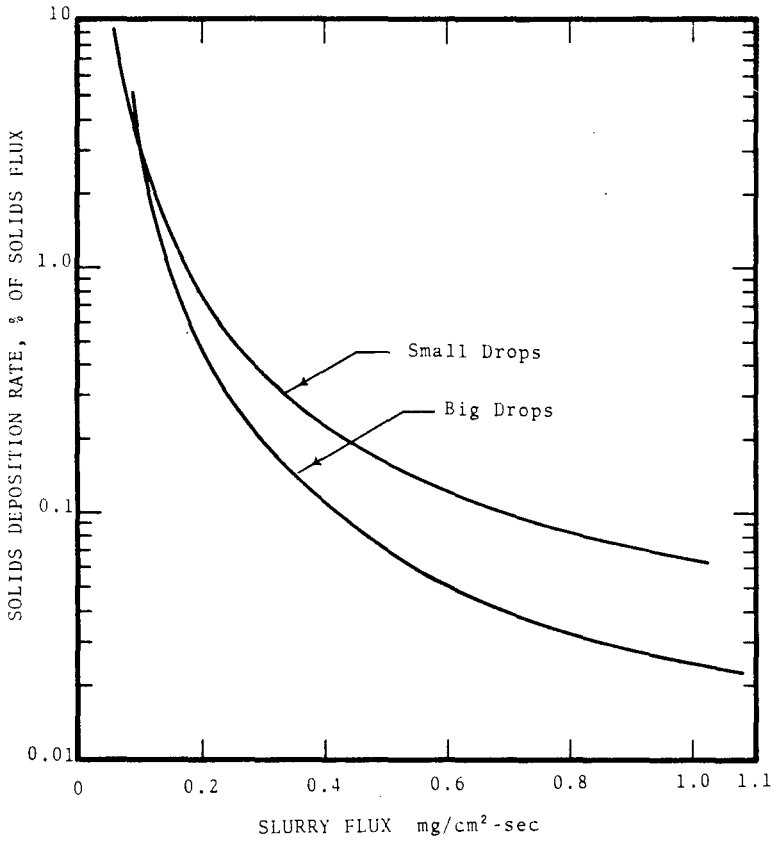

Figure 11-14. Deposition rate versus slurry flux for big and small drops.

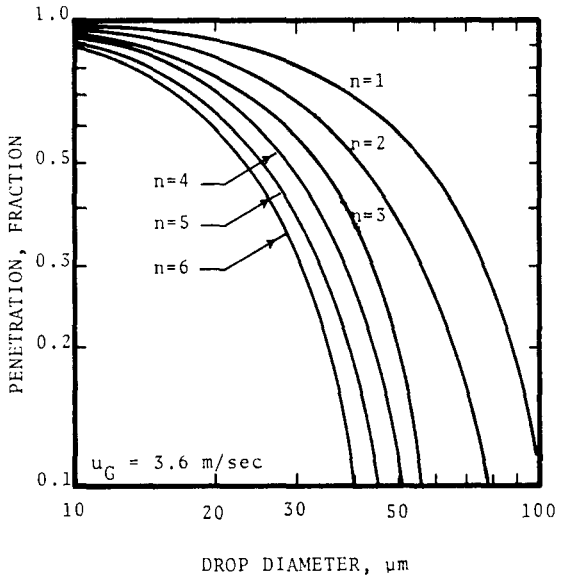

Figure 11-15. Predicted penetration versus drop diameter for zigzag baffles.

1. Fine drops depositing on the surface will first stick there. As more drops accumulate, they aggregate to a bigger drop.
2. As the aggregate of drops gets heavy, it slides down the surface, sweeping the other drops as it goes, forming a thin film.
3. As the film slides down, some of the particles are washed away, while some are left behind on the surface.
4. The top part of the collection surface always has the heaviest deposition. The deposition thickness gradually decreases at the lower end.

Conclusions on Solids Deposition Experiments

Based on the solids deposition experiments, the following conclusions can be drawn:

1. The solids deposition rate depends largely on particle properties, such as size, density, and shape, etc.
2. Deposition rate decreases as the slurry flux is increased.
3. Deposition rate decreases as the liquid film thickness is increased.
4. Deposition rate is higher on an inclined baffle than on a vertical baffle due to the increase in settling rate of solids suspensions.
5. Small drops are more susceptible to being caught in eddies which would bring them to the back surfaces of the baffles.
6. Small drops have a higher deposition rate than large drops.

SOLID DEPOSITION PREDICTION

The deposition experimental data can be correlated by the following empirical equation:

$$R_s = W\Phi \exp[-(0.13 + 0.53\Phi)\delta] \qquad (11\text{-}5)$$

where R_s = deposition rate of $CaCO_3$ on a vertical flat surface, mg/cm^2-sec

W = weight fraction of solid in slurry

ϕ = slurry flux, mg/cm^2-sec

δ = liquid film thickness, μm

To gauge the realism of the deposition experiment, the correlation was used to predict the behavior of our pilot plant zigzag baffle separator. Based on Equations (9-1), (9-2) and (9-3), the grade efficiency curve can be constructed. Figure 11-15 shows the grade efficiency curves for zigzag baffles with number of rows, n, as parameter. The following values of parameters were used in the calculations.

$W = 7.5$ cm

$b = 7.25$ cm

$\theta = 0.524$ rad (30°)

$\mu_G = 1.8 \times 10^{-4}$ poise

$u_G = 3.6$ m/sec (same as Run #195)

The overall collection efficiency for the zig-zag baffle can be obtained by the cut diameter method reported by Calvert (1974). Equations (9-1) through (9-3) can be combined to obtain the following equation in the appropriate form for using Figure 12-4.

$$Pt = \exp\left[-A\, d_p^2\right] \qquad (11\text{-}6)$$

$$\text{where } A = \frac{\rho_d\, a\, n\, W\, \theta}{\mu_G\, u_G\, b \tan \theta}$$

Based on this method, the following results were obtained. The cut diameters can be computed from equation (11-6) by setting Pt = 0.5.

n	d_{p50}, μm	Pt	E
1	57	0.0087	0.9913
2	40	0.00255	0.9975
3	33	0.0011	0.9989
4	28	0.00062	0.9994
5	25	0.0004	0.9996
6	23	0.0003	0.9997

A mass median of 400 μm and geometric standard deviation of 2 were assumed for the slurry drop size distribution in the above calculations. This is equivalent to the distribution generated by an M-26 spraying nozzle of Spray Systems Company.

The solid deposition rate in each row of the baffle can be calculated if the entrainment flow rate, gas velocity and weight percent of solid content are known. The following is an example of the calculation for the third row:

Assume entrainment flow rate = 190 cm^3/sec (3 GPM)

$CaCO_3$ concentration = 10% by wt.

$CaCO_3$ density = 2.7 g/cm^3

Then, the entrainment mass flow rate is 227 g/sec. The amount of slurry collected by 3rd row

$$= 227\ (E_{n=3} - E_{n=2})$$
$$= 0.318 \text{ g/sec}$$
$$= 318 \text{ mg/sec}$$

It is assumed that slurry is uniformly spread over the baffle surfaces (both front and back). Then slurry flux, ϕ, is:

$$\phi = \frac{318}{(7.5)(61)(8)} = 0.087 \text{ mg/cm}^2\text{- sec}$$

Slurry deposition rate can be calculated from equation (11-5) once the liquid film thickness "δ" is known. Calculation method for "δ" was presented in "Initial Report" for both horizontal and vertical baffles. As an illustration, at the leading edge or top edge of a vertical baffle, film thickness approaches zero. According to equation (11-5), the solid deposition rate will be

$$R_s = (0.1)(0.087)$$
$$= 0.0087 \text{ mg/cm}^2\text{- sec}$$

If the deposited cake has a porosity of 40%, then the cake density is $(2.7)(1-0.4) = 1.6$ g/cm^3. For a 32 hour experimental run, the cake thickness at the leading edge will be

$$= \frac{(0.0087)(3600)(32)}{(1000)(1.6)}$$
$$= 0.63 \text{ cm}$$

Following the same method, cake thickness at other location can be calculated. Figure 11-16 is a plot of cake thickness versus the horizontal distance from the leading edge along a surface 30 cm from the top and Figure 11-17 is a plot of deposit thickness versus the vertical distance from the top of the baffle. The deposit thickness is predicted to vary between 1 to 5 mm on the inside surfaces and 6 mm at the leading edge. This is what was observed in the pilot plant experiments.

These calculations indicated that equation (11-5) can be used to predict the most likely location for solid deposition to occur in the baffle and minimum amount of washing liquid required. Once the location and liquid requirement are known, one can design a washing system to wash clean this area.

For the baffle test section used in the present study, equation (11-5) predicts that solid deposition will start on the third row of the baffle. Thus spray nozzles for cleaning purpose could be installed between second and third row. Also fine spray should be used. This will allow the gas turbulence to carry some washing liquid to the back side of the baffle.

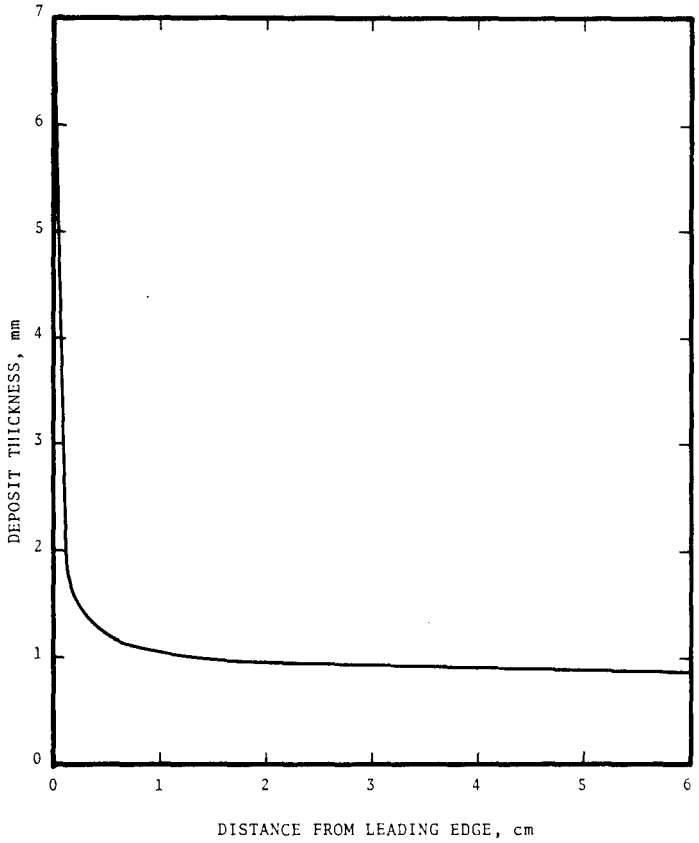

Figure 11-16. Predicted deposit thickness along a baffle surface 30 cm from top.

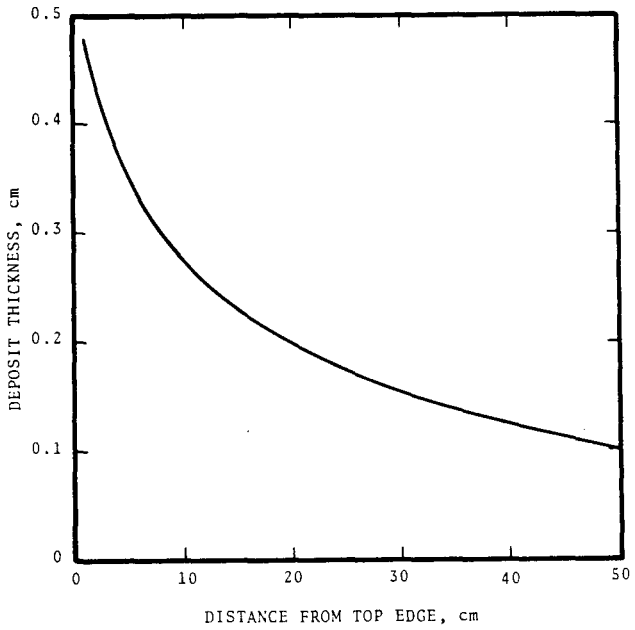

Figure 11-17. Predicted deposit thickness versus distance from top edge of baffle at 3 cm from leading edge.

CHAPTER 12

DESIGN APPROACH

Design equation for knitted mesh, packed bed, tube bank, cyclone and zigzag baffle are presented in Chapters 5 through 9. In this chapter, we will clarify and show the application of these equations in the design and selection of a proper entrainment separator. The following is a brief outline of topics that are covered in this chapter.

I. Requirement.
   - A. Performance requirement
   - B. Capacity requirement
   - C. Process and physical limitations

II. Entrainment information needed for design and selection.
   - A. Liquid phase
   - B. Gas phase

III. How to select the type of entrainment separator.
   - A. Choose possible type(s) for detailed study
   - B. Predict characteristics

REQUIREMENTS

Before one can design or choose an entrainment separator, he must first study the process and source of entrainments in order to specify the performance requirement, the capacity and the limitations. The following is an outline of the requirements needed to be considered in the design and selection of entrainment separator.

Performance requirement

The performance requirement of an entrainment separator could be defined in terms of:

1. collection efficiency
2. maximum outlet loading
3. behavior of the emitted entrainment

Collection efficiency is the overall efficiency of the separator or separators if several units are arranged in series. The overall collection efficiency is the difference between primary efficiency and reentrainment. The primary efficiency is the collection efficiency an entrainment separator would have if reentrainment were not present. Primary efficiency includes only the collection of drops present in the original entrainment. The reentrainment of these collected drops or the subsequent collection of these reentrained drops does not affect the primary collection efficiency. Reentrainment is the mass ratio of drops entering the gas from the liquid collected in the entrainment separator, to drops present in the original inlet entrainment. Due to reentrainment, the overall collection efficiency is always lower than the primary efficiency. In specifying the efficiency requirement, one should always define it in terms of overall efficiency.

In a wet scrubber, the scrubber liquor usually contains suspended and dissolved solids. These solids could be the separated particulates or the chemicals added to the scrubber liquid. Entrainment carryover will cause the solids in the drops to be re-suspended in the gas stream. Thus, the efficiency of the scrubber decreases and the emission loading increases. In order to set the maximum allowable outlet entrainment loading, one should determine the maximum allowable contribution of pollutants in the entrained droplets to the total emission. For example, one may specify that the acceptable contribution of entrainment to particulate emission is 5%. If the emission rate is 4.54 kg/hr (10 lb/hr), then 5% allowable contribution corresponds to 227 g/hr. If the solid concentration in the scrubber liquor is 10%, then the maximum allowable outlet loading of the entrainment will be 2.3 kg/hr or 2.3 l/hr if the liquid density is 1 g/cm^3. Of the two requirements just mentioned,

one should always choose the one that is more stringent as design basis.

Besides these two performance requirements,the behavior of the emitted entrainment droplets should also be specified. For example, there must be no "rain-out" of liquid drops in the vicinity of the emission point.

Capacity Requirements

Capacity requirements can either be defined in terms of gas flow rate or liquid flow rate, depending upon which one is the limiting factor. One should specify the maximum and minimum gas and liquid flow rate, in order to design an adequate entrainment separator that can cover the whole range of scrubber operating conditions, not only normal gas flow rate and liquid entrainment flow rate information.

Liquid flow rate has great effect on the onset of reentrainment. Data obtained in the present study showed that the higher the liquid flow, the lower will be the onset of reentrainment gas velocity and the higher will be the chance of flooding.

Process and physical limitations

Several physical and process limitations should be spelled out before the design of the separator. Some of the limitations are:

1. Pressure drop. What is the maximum pressure drop available for the operation of the entrainment separator? In the case of mechanically aided separator, the question is what is the maximum allowable power input.
2. Space. If the separator is to be installed inside the scrubber, then one should have the knowledge beforehand regarding the volume,

height, etc., inside the scrubber that is suitable for the installation of the separator. If the separator is to be installed as an independent unit of the pollution control system, then one should have information about the space available.

3. Materials
4. Maintenance
5. Susceptibility to plugging
6. Orientation

ENTRAINMENT INFORMATION

In order to design a proper entrainment separator, or to predict the collection efficiency of an entrainment separator, certain information on liquid phase and gas phase is needed. This includes

A. Liquid phase
   1. Entrainment drop size distribution. This is the most important single factor in the design and selection of an entrainment separator. Different entrainment separators are limited to certain drop diameters, below which their efficiency falls off sharply.
   2. Entrainment loading. If drop size distribution and entrainment loading are not known, they can be estimated based on method described in Chapter 3.
   3. Suspended and dissolved solids
   4. Densities
   5. Vapor pressure
   6. Nature of the entrainment, i.e. is it sticky, corrosive, oily, etc.

B. Gas phase
   1. Temperature
   2. Pressure

HOW TO SELECT THE TYPE OF ENTRAINMENT SEPARATOR

Preliminary selection

After analyzing the process and limitations, one should summarize all available information such as called for in the information sheet shown on Figure 12-1. Next, the possible type(s) for detailed study can be chosen after ranking by:

1. Efficiency capability
2. Maximum gas velocity for onset of reentrainment
3. Liquid capacity
4. Plug-ability
5. Installation and operating costs

Figure 12-2 shows the approximate application ranges for several common entrainment separators. From the drop size information, this figure can tell what types of entrainment separator are available that might be suitable. However, this figure does not give any information about the collection efficiency of these separators.

Table 12-1 lists other important limitations for these common separators.

For cases where drop collection efficiency requirements are stringent, the prediction of efficiency must be precise. The "cut diameter" method provides a convenient approach to the definition of separator efficiency.

The "cut diameter" method, first described in the "Scrubber Handbook" (Calvert et al. 1972) and further discussed by Calvert (1974), can be used as a convenient method for entrainment collection efficiency prediction. This method is based on the idea that the most significant single parameter to define both the difficulty of separating entrainments from gas, and the performance of entrainment separator, is the drop diameter for which collection efficiency is 0.5(50%).

Figure 12-1. ENTRAINMENT SEPARATOR DESIGN AND SELECTION INFORMATION SHEET

1. Application: (Describe service application of unit when possible) _____

2. Operating Conditions:

	Maximum	Minimum	Normal
Gas Flow Rate	_____	_____	_____
Entrainment Flow Rate	_____	_____	_____
Temperature	_____	_____	_____
Pressure	_____	_____	_____

3. Entrainment Phase

Source of Entrainment _____

Density _____ Viscosity _____ Surface tension _____

Composition or Nature of Entrainment (Corrosive,oily) __

Drop Size and distribution _____

Solids Content (Composition and Quantity) _____

Dissolved _____

Suspended _____

4. Performance

Allowable Total System Pressure Drop _____

Allowable Separator Pressure Drop _____

Allowable Entrainment _____

5. Special Conditions: _____

_____

_____

_____

_____

_____

_____

_____

_____

_____

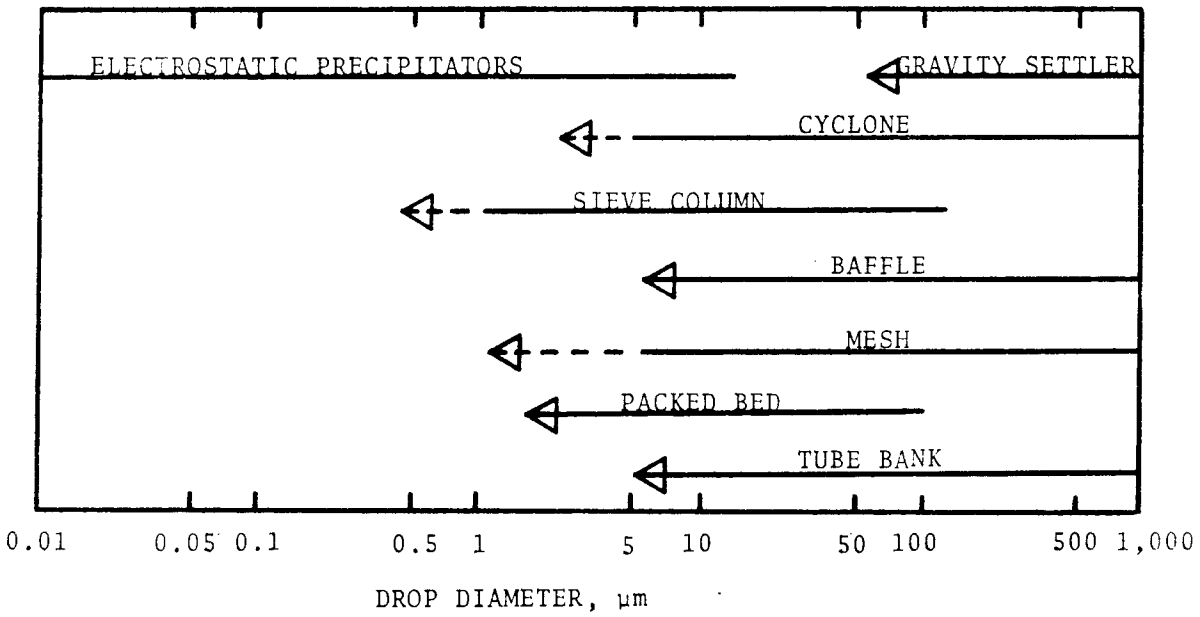

Figure 12-2. Entrainment separator approximate operating range

Table 12-1. Comparison of Various Types of Entrainment Separators

Separator Type	Construction Materials	Maximum Capacity	Minimum Drop Size	Separation Efficiency for Min. Drop Size	Liquid Load	Approximate Velocity for Reentrainment, m/sec	Limitations	Maintenance and Operating Costs	Comments
Cyclone	any	Up to 141 m^3/sec per cyclone	5μm(2μm for small cyclone)	95%	Can handle liquid to gas ratio as high as 40:1	∿40	Does not handle sticky materials	Very low	Useful when large liquid load and high gas velocities are encountered. Surface may erode easily. Life expectancy is very high
Gravity settler	any materials		50	Depends on residence time				Very low	Space requirement per unit gas handled is high
Wire mesh	Any material that can be drawn into wire	5m^3/sec-m^2 of mesh	5μm(1-5μm for series combination)	95%	2.5×10^{-3} g/sec-cm^2	3-5	Not for high solids content	Low	May be plugged easily. Useful for internal applications if conditions permit
Packed bed	Packing can be of any material	65 m^3/sec	3μm	85%	From generalized correlation	1-2.5	Not for high solids content	Fair	Better drainage in cross flow
Baffle	any material	7m^3/sec-m^2 of duct cross section	10μm	85-95%	Maximum liquid to gas ratio 1:1 by wt	2-7		Low	Vertical baffles give better drainage than horizontal. Can be used internally
Tube Bank	any material	10m^3/sec-m^2 of area	5μm		10% by wt. of gas flow rate	3-10	Not for sticky and high solids content	Low	Can be used internally

When a range of sizes is involved, the overall collection efficiency will depend on the amount of each size present and on the efficiency of collection for that size. We can take these into account if the difficulty of separation is defined as the diameter at which collection efficiency (or penetration) must be 50%, in order that the necessary overall efficiency for the entire size distribution be attained. This particle size is the required "separation cut diameter", "d_{RC}" and it is related to the required overall penetration, $\overline{Pt}$, and the size distribution parameters.

The number and weight size distribution data for most entrainment from scrubbers follow the log probability law. Hence, the two well established parameters of the log-normal law adequately describe the size distributions of the drops. They are the geometric mean weight diameter "d_{pg}" and the geometric standard deviation "σ_g".

Penetration for many types of inertial collection equipment can be expressed as a function of constants "A" and "B".

$$Pt = \exp\ (-A\ d^{B}_{d}) \qquad (12\text{-}1)$$

Packed bed, baffle, mesh, tube bank, cyclone and sieve plate columns follow the above relationship. For the packed bed, mesh, baffle, tube bank and sieve plate column "B" has a value of 2. For cyclone, "B" is about 0.67.

The overall (integrated) penetration, $\overline{Pt}$, of any device and size distribution will be

$$\overline{Pt} = \int_{o}^{W} (\frac{dw}{w}) Pt \qquad (12\text{-}2)$$

The right-hand side of the above equation is the integral of the product of each weight fraction of drop times the penetration on that fraction. If equation (12-2) is solved for a log-normal size distribution and collection as given by equation (12-1), the resulting equation can be solved to yield Figures 12-3 and 12-4.

Figure 12-3 is a plot of "$\overline{Pt}$" versus $(d_{p50}/d_{pg})^B$ with "B ln σ_g" as a parameter. For a required "$\overline{Pt}$" one can find the value of d_{RC} when "d_{pg}", "σ_g", and "B" are given. For convenience, Figure 12-4 is presented as a plot of "$\overline{Pt}$" versus (d_{p50}/d_{pg}) with σ_g as the parameter when B = 2.

To illustrate the use of the separation cut diameter, assume that 95% collection efficiency (5% penetration) is needed for drops with mass median diameter, d_{pg}, equal to 100 μm and geometric standard deviation, σ_g, = 3. If an entrainment separator such as baffle is to be used, Figure 12-4 shows that (d_{p50}/d_{pg}) = 0.15. Thus, the required cut diameter, d_{RC}, must be $(0.15)(d_{pg})$ = 15 μm. If the separator is capable of a smaller cut diameter, that is good; so "d_{RC}" is the maximum cut diameter acceptable.

Prediction of separator's cut diameter

Selecting an entrainment separator with the proper cut diameter requires some knowledge of its performance characteristics. The most important of these are primary efficiency, gas pressure drop, and capacity limitations.

The energy required for entrainment separation is generally a function of the gas pressure drop. Figure 12-5 is a plot of performance cut diameter, d_{pc}, versus gas pressure drop. Theoretical energy consumption is also plotted on the same figure. This figure was constructed based on

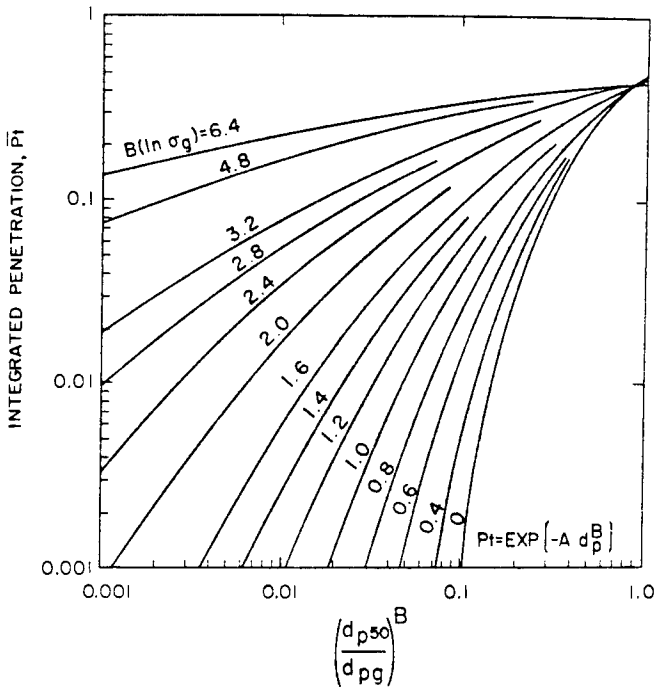

Figure 12-3. Integrated (overall) penetration as a function of cut diameter, particle parameters and collector characteristic.

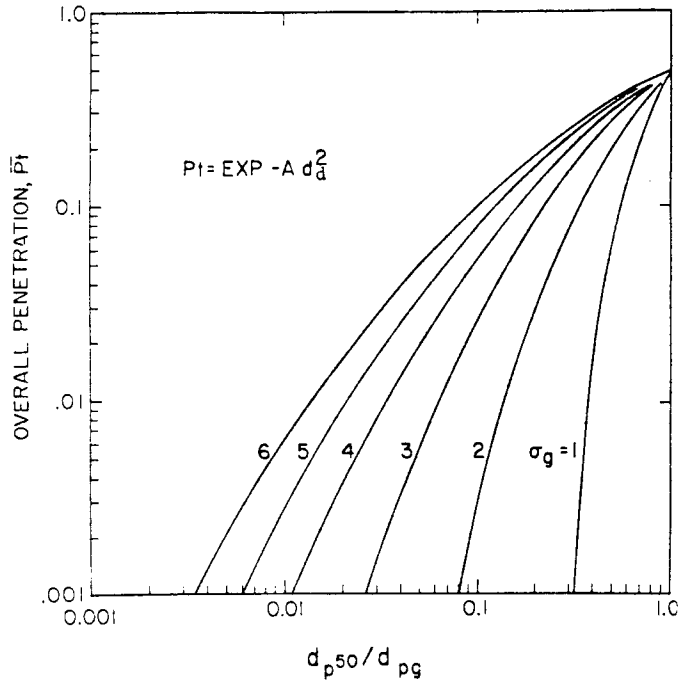

Figure 12-4. Overall penetration as a function of cut diameter and particle parameters for common scrubber characteristic, B = 2.

design equations and experimental correlation presented in Chapters 5 through 9.

For the example mentioned earlier, from Figure 12-5, for a required cut diameter, d_{RC}, of 15μm, the required pressure drop across the separator is 0.01 cm W.C. for knitted mesh and 2.5 cm W.C. for a six-row baffle. Suppose the maximum allowable pressure drop across the entrainment separator is less than 1 cm W.C., then this quick calculation indicates that baffle is not suitable for installation.

In some occasions, some entrainment separator manufacturers only give pressure drop versus gas velocity relations in their sale literature. In this case, Figure 12-5 can be used to predict the collection efficiency of the separator. For example, suppose a packing material manufacturer says that the pressure drop is 2.5 cm W.C. when the gas velocity is 3 m/sec (10 ft/sec), then from Figure 12-5, the expected performance cut diameter is 3.5 μm if this material is used as packing.

For the same drop size distribution as mentioned earlier, then

$$\frac{d_{p50}}{d_{pg}} = \frac{3.5}{100} = 0.035$$

From Figure 12-4, the expected collection efficiency of the packed bed is 99.8% (i.e. penetration = 0.002).

To estimate the penetration for drop diameters other than the cut size, under a given set of operating conditions, one can use the approximation of equation 12-1 with B = 2.0. Alternatively, one could use more precise data or design equations for a given separator. Figure 12-6 is a plot of the ratio of drop diameter to cut diameter versus penetration for that drop size on log-probability paper.

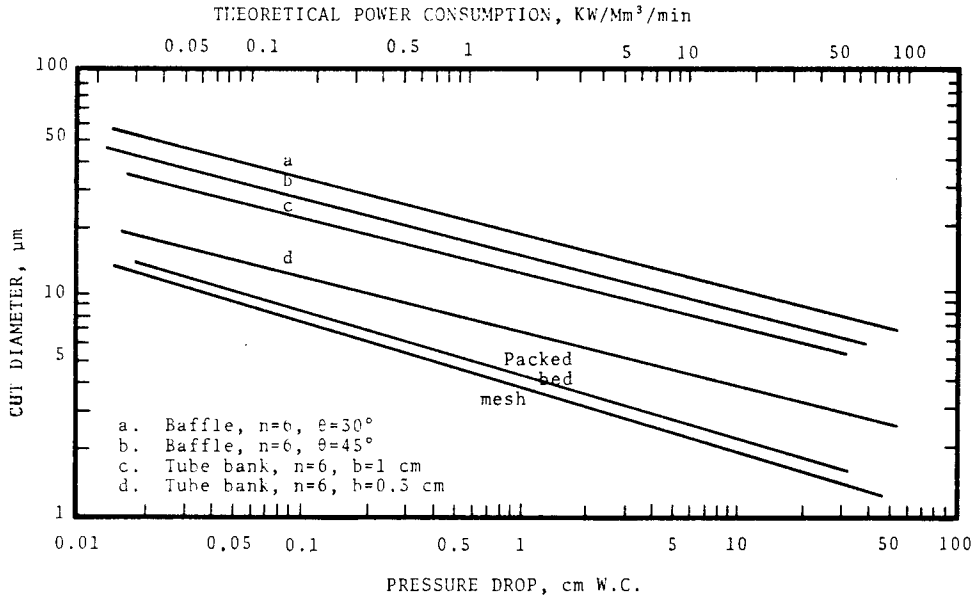

Figure 12-5. Performance cut diameter as a function of pressure drop for several entrainment separators.

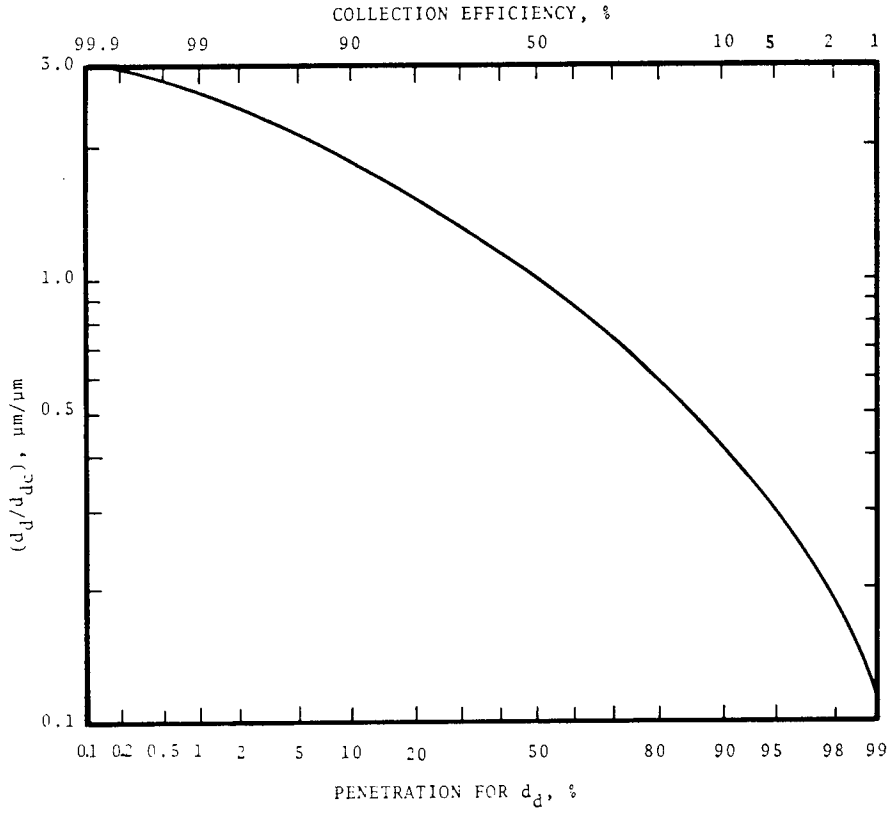

Figure 12-6. Ratio of drop diameter to cut diameter as a function of collection efficiency.

Note that the cut diameter method only gives an approximate collection efficiency, the exact characteristic of the entrainment separator could be predicted by the method described in next section.

Predict Characteristics

Table 12-2 is a summary of design equations and figures for common entrainment separators. The general steps in utilizing this table to predict the performance characteristics of an entrainment separator are as follows:

1. Based on process condition and separator configuration, construct the grade efficiency curve for the separation. Equations for primary efficiency can be used for this purpose. In case the gas velocity is higher than the reentrainment onset velocity, reentrainment should be subtracted from the primary efficiency.
2. Compute the collection efficiency for the whole population of the drops. This can be done either graphically or mathematically. For graphical solution, plot Pt_i versus fraction smaller than d_{di} (where Pt_i is penetration for drop size d_{di}). The area under the curve is the overall penetration. Outlet loading is equal to inlet loading times overall penetration.
3. Compute expected pressure drop.

In the process of designing an entrainment separator, the steps should be repeated for different proposed separator configuration. The final configuration can then be selected after optimization analysis.

Table 12-2. SUMMARY OF DESIGN INFORMATION

Type of Separator	Primary Efficiency	Pressure Drop	Reentrainment Velocity
Mesh	Eq. 5-1	Eq. 5-3	Eq.5-4, Fig. 5-13
Packed Bed	Eq. 6-1	Fig. 6-1	Figure 6-8
Tube Bank	Eq.7-2,7-3	Eq. 7-4	Figure 7-9,7-10
Cyclone	Eq. 8-2	Eq. 8-15	Fig. 8-3
Baffle	Eq. 9-1	Eq.9-6,Fig.6-1	Fig. 9-15
Gravity Settler	Eq. 3-7		
Sieve plates	Eq. 3-10	Eq. 3-12	

Page Intentionally Blank

CHAPTER 13

FUTURE RESEARCH AND DEVELOPMENT RECOMMENDATIONS

The primary objectives of the present research, i.e. to evaluate the technology on scrubber entrainment separators, advance theoretical development and solids deposition have been achieved in the present study. It is also important to define the areas where additional work is needed. The following paragraphs give an account of these areas.

REENTRAINMENT

One of the problems which present day entrainment separators suffer is their large size which is due to low operating velocities. The gas velocities are limited by reentrainment velocities and flooding conditions. Reentrainment may take place due to various mechanisms, depending on flow rates and geometry.

While the present program will provide information on the conditions under which reentrainment occurs in several separator configurations, it would be helpful to have more detailed knowledge of these phenomena. It is quite possible that a fundamental study of the mechanisms of reentrainment from different geometric arrangements would enable one to develop more efficient separator designs. At least the results of such a study would delineate the limits of possible performance and save effort which might otherwise be expended in unprofitable directions.

The study needed is onset of reentrainment conditions, rate of reentrainment, equilibrium constant between

entrainment and liquid in film, drop size distribution, smooth and shock type contact of gas and liquid, effect of duct dimensions, etc. The application to entrainment separator will include improving design methods to determine reentrainment under operating conditions, effect of higher gas velocities and improvements in design to reduce reentrainment.

SOLIDS DEPOSITION

Solids deposition and consequent plugging is a major operational problem in scrubber systems. While this study introduces the minimum flow rate required for washing, it would be helpful to have more research on the methods of washing.

As can be deduced from the results of the solids deposition studies, increasing the flux in the form of a fine spray will eliminate cake deposition on the backs of baffles as well as on sheltered regions of the duct walls. On the other hand, increasing the flux will lower the collection efficiency of the entrainment separator. Thus, research on finding the optimum flow rate required and the feasibility of intermittent washing would be required.

One other method of eliminating cake deposition would be increasing the liquid film thickness on the baffles. However, increasing the liquid film thickness will also increase the reentrainment rate. Thus, it would be helpful to have more knowledge of the degree of increase in reentrainment rate due to the increase in liquid film thickness.

FIELD TESTING OF INDUSTRIAL ENTRAINMENT SEPARATORS

Performance data on industrial entrainment separators are generally not available. The industrial data are collected to evaluate the overall performance of the scrubber and it is assumed that the entrainment separators have 100% efficiency. Also, all the liquid introduced in the wet scrubber is assumed to be removed by entrainment separator. The effects of sedimentation, bends in the duct carrying entrainment, etc. are neglected. The distance between sampling point and entrainment separator elements is important. Also, the effects of industrial operating conditions on performance of entrainment separators should be determined.

The aim of development of entrainment separators is to improve performance of separators under industrial conditions. Thus, it is necessary to collect data on industrial separators. The data, when compared with theoretical models, will represent possible problems resulting from industrial conditions and will help in designing future entrainment separators.

DEMONSTRATION PLANT

From the present contract work, it is felt that we can predict the performance of an entrainment separator with reasonable accuracy. It is possible to obtain improvement in the performance due to better design. We would like to move from the present research and development to a demonstration of an improved design in the field.

The capacity of the present pilot plant is 85 m^3/min. Therefore, the next size should be around 1,000 m^3/min (35,000 CFM).

The demonstration plant operation will involve selecting an organization which operates a suitable plant having entrainment separation problems and which is willing to participate in the demonstration plant program. The design effort will include obtaining the necessary data concerning the source of entrainment, preparing overall design and selecting a final design. The fabrication and start up will involve selection and negotiation with subcontractors, procurement of components and supervision of subcontractor efforts. The test program will be to determine performance, observe the effect of change in variables and compare the performance with theoretical developments.

STUDY OF COMBINATIONS OF ENTRAINMENT SEPARATORS

It is possible that if more than one entrainment separator is used in series, the combined unit will provide a synergistic effect. One can combine two different entrainment separators to include the best features of each. Some examples are as follows:

1. The maximum gas velocity in the entrainment separator is limited to the onset of reentrainment velocity. It is generally the case, however, that a separator which has high primary drop collection efficiency will have a low reentrainment velocity, while one with high reentrainment velocity will have low primary collection efficiency. If a combined unit is used with the first unit being used for

primary collection and coalescence of drops and the second one for collection of large drops while being below the onset of reentrainment velocity, increased capacity will result. The combination of efficiency and capacity will exceed what either unit can do alone.

Because the size of the entrainment separator will be smaller, the initial capital cost will be lower. The minimum drop size that can be separated in the entrainment separator is limited by the operating velocity. This problem can be solved by using a combination of entrainment separators.

2. Sometimes the entrainment load is high and constituted of particles in a wide size range. A single entrainment separator may be inefficient, flooded or may present reentrainment in this situation. A combined unit may be used in this case. The first separator is a precleaner with low pressure drop, which removes large particles constituting a significant fraction of the entrainment. The second separator will be an efficient device.

COLLECTION EFFICIENCY FOR SMALL DROPS

The drop size used in the present study was over 100 μm. Based on our sampling data on various scrubbers, it was discovered that there were substantial amount of entrainment droplets smaller than 10 μm in diameter. It would be helpful if more tests were performed to determine the collection efficiency for drops smaller than 10 μm.

Page Intentionally Blank

REFERENCES

Anderson, J.D., R.E. Bollinger, and D.E. Lamb. Gas Phase Controlled Mass Transfer in Two Phase Annular Horizontal Flow. AIChE Journal, 10: 640,1964.

Atteridge, et al. AIChE Journal 2: 3, 1956.

Bell, C.G.,and W. Strauss. Effectiveness of Vertical Mist Eliminators in a Cross Flow Scrubber. APCA Journal 23: 967-9, November 1973.

Bradie, J.K., and A.N. Dickson. Removal of Entrained Liquid Droplets by Wire Mesh Demisters. Paper 24 in Fluid Mechanics and Measurements in Two-Phase Flow Systems. (A joint symposium of the Inst. of Mech. Engr. and the Yorkshire Branch of the Inst. of Chem. Engr.) 24-25, London. September 1969.

Brooks, et al. Petroleum Engineering. C-32, August 1955.

Buerkholz, A. Drop Separation on Wire Filters. Chemie Ingenieur Tecknik. 42: 21, 1314-1321, 1970.

Calvert, S. Air Pollution. Stern, A.C. (ed.). 3, Academic Press, New York. 1968.

Calvert, S. Engineering Design of Fine Particle Scrubbers. APCA Journal, 24: 929-934, 1974.

Calvert, S., J. Goldshmid, D. Leith, and D. Mehta. Scrubber Handbook. Prepared for EPA Contract No. CPA-70-95. Vol. I and II, 1972.

Calvert, S., and D. Lundgren. Particle Collection in Closed Packed Arrays. Presented at AIHA. 1970.

Calvert, S., et al. Entrainment Separators for Scrubbers - Initial Report. NTIS Pub., PB-241-189.

Carpenter, C.L., and D.F. Othmer. Investigation of Wire Mesh as an Entrainment Separator. AIChE Journal. p. 549, 1955.

Chien, S.F., and W. Ibele. Pressure Drop and Liquid Film Thickness of Two Phase Annular and Annular-Mist Flows. ASME Paper. 62-WA170.

Davis, R.F. Proc. Inst.Mech.Engrs. 149: 148, 1940.

Fage, A., and F.C. Johansen. Proc. Roy. Soc. (London). 116A: 170, 1927.

Foust, A.S., L.A. Wenzel, C.W. Clump, L. Maus, and L.B. Andersen. Principles of Unit Operations. Toppan Company. Tokyo. 1959.

Fuchs, N.A. The Mechanics of Aerosols. The Macmillan Company. 1964.

Golovin, M.N., and A.A. Putnam. Ind. Engr. Chem. Fund. 1:264, 1962.

Houghton, J.G., and W.H. Radford. Trans. Am. Inst. of Ch.E. 35: 427, 1939.

Hunt, Hanson, and Wilke. AIChE Journal,1: 441, 1955.

Jackson, S., and S. Calvert. AIChE Journal, 12: 1075, 1966.

Jashnani, I.L. Coalescence and HTU in Foam Fractionation Columns. Ph.D. Dissertation, U. of Cincinnati. 1971.

Jones and Pyle. Chemical Engineering Progress. 51: 424, 1955.

Kitchener, J.A. Foams and Free Liquid Films in Recent Progress in Surface Science. Academic Press. New York. 1964.

Lane, W.R. Shatter of Drops in Streams of Air. Ind.Engr. Chem. 43: 1312, 1951.

Leith, D., and W. Licht. The Collection Efficiency of Cyclone Type Particle Collectors - A New Theoretical Approach. Paper presented at San Francisco meeting of AIChE. December 1971.

Mercer, T.T., and H.Y. Chow. J. of Coll. and Interface Sci. 27: 75-83, 1968.

Nukiyama, S., and Y. Tarrasawa. Trans. Soc. of Mech. Engr. (Japan). 4, 5, 6, 1938-1940.

Perry, J.H. Chemical Engineering Handbook. 4th Edition. McGraw-Hill. New York. 1963.

Perry, J.H. Chemical Engineering Handbook. 5th Edition. McGraw Hill. New York. 1963.

Poppelle, E.W. Master Thesis. Newark College of Engineering, (1958).

Roberts, D.C., and D.E. Hartley. A Correlation of Pressure Drop Data for Two Phase Annular Flows in Vertical Channels. Queen Mary College. (London). Nuclear Research Memorandum, No. Q6.

Satsangee, P.D. Master's Thesis. Polytechnic Institute of Brooklyn. 1948.

Shepherd, C.B., and C.E. Lapple. IEC Chem. 31, 1246, 1940.

Sherwood, T.K., and R.L. Pigford. Adsorption and Extraction. McGraw-Hill. New York. 265, 1952.

Sherwood, T.K., G.H. Shipley, and F.A.L. Holloway. Ind. Engr. Chem. 30, 765, 1938.

Schurig, W.F. D.Ch.E. Dissertation. Polytechnic Institute of Brooklyn. 1946.

Stearman, F. and G.J. Williamson. Spray Elimination in Processes for Air Pollution Control. Nonhebel, 2nd ed., CRC Press, Cleveland, 1972.

Steen, D.A., and G.B. Wallis. The Transition from Annular to Annular-Mist Cocurrent Two-Phase Down Flow. NYO-3114-2, 1964.

Taheri, M. and S. Calvert. APCA Journal. 18, 240, 1968.

Uno, H., and S. Tanaka. Adhesion of Suspension Particles on the Wall Surface of the Container. Kolloid-Z. U.Z. Polymere 242, 1186-1195, 1970.

Wallis, G.B. The Onset of Droplet Reentrainment in Annular Gas-Liquid Flow. General Electric Report No. 62 GL127, 1962.

York, O.H. Performance of Wire Mesh Demisters. Chem. Engr. Prog. Vol. 50, No. 8, 421, 1954.

York, O.H., and E.W. Poppelle. CEP. 59, 45, 1963.

Zhivaiking, L.Y. Liquid Film Thickness in Film Type Units. Int. Chem. Engr. 2, 237, 1962.